Diffusion-tensor MRI methods to study and evaluate muscle architecture

Secondulfo, L.

Publication date
2023
Document Version
Final published version

Diffusion-Tensor MRI methods to study and evaluate muscle architecture.

Laura Secondulfo

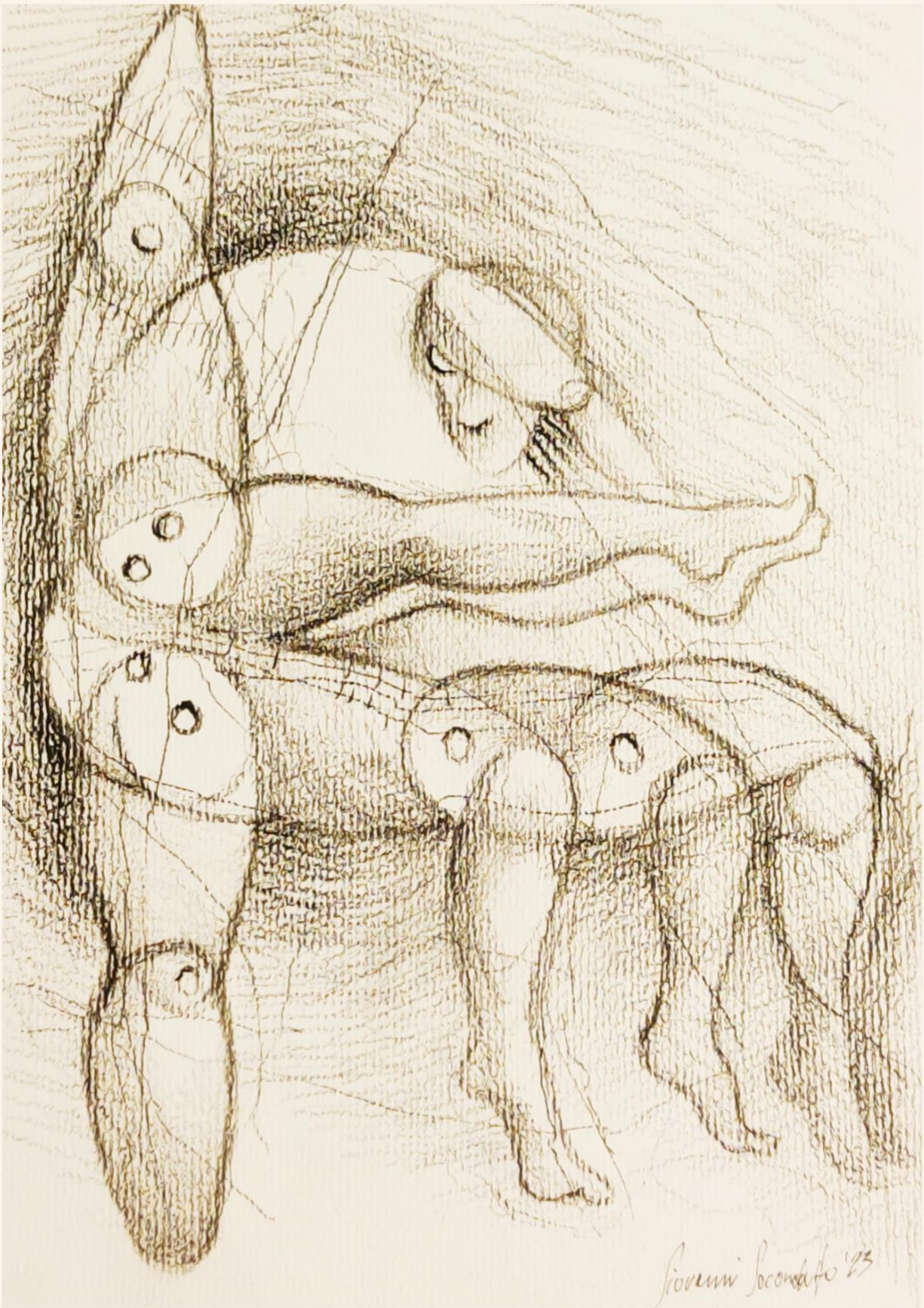

Diffusion-tensor MRI methods to study and evaluate muscle architecture.

Laura Secondulfo

The research described in this thesis was performed at the Department of Biomedical Engineering and Physics, the Department of Radiology and Nuclear Medicine and the Department of Orthopedic Surgery and Sports Medicine at the Amsterdam UMC, Location AMC.

Financial support by the Dutch Technology Foundation TTW (DIMASK 15500) for the publication of this thesis is gratefully acknowledged. Additional financial support was kindly provided by the Sportinnovator grant of The Netherlands Organization for Health Research and Development, ZonMw (50-53800-98).

Charcoal drawing by: Giovanni Secondulfo
Printed by: ProefschriftMaken

Diffusion-tensor MRI methods to study and evaluate muscle architecture

ACADEMISCH PROEFSCHRIFT

ter verkrijging van de graad van doctor
aan de Universiteit van Amsterdam
op gezag van de Rector Magnificus
prof. dr. ir. P.P.C.C. Verbeek
ten overstaan van een door het College voor Promoties ingestelde commissie,
in het openbaar te verdedigen in de Agnietenkapel
op donderdag 28 september 2023, te 10.00 uur

door Laura Secondulfo
geboren te Latina

Promotiecommissie

Promotores:	prof. dr. ir. G.J. Strijkers	AMC-UvA
	prof. dr. ir. A.J. Nederveen	AMC-UvA
Copromotores:	dr. M.T. Hooijmans	AMC-UvA
Overige leden:	prof. dr. H.A. Marquering	AMC-UvA
	prof. dr. J.L. Tol	AMC-UvA
	dr. J.J. Prompers	UMC Utrecht
	prof. dr. N. van der Velde	AMC-UvA
	dr. H.E. Kan	LUMC
	prof. dr. R.T. Jaspers	Vrije Universiteit Amsterdam

Faculteit der Geneeskunde

Table of Contents

CHAPTER 1

Introduction

Introduction

Muscle strain injuries

The Problem

Hamstring injuries are among the most frequently occurring injuries in recreational and professional athletes.[1,2,3,4,5,6,7] For example, they account for as much as 15% of all football related injuries.

Mild forms of muscle damage consist of mild swelling, minor discomfort and delayed onset muscle soreness (DOMS).[8,9] Severe muscle strains result in intra and intermuscular hematoma.[10,11,12]

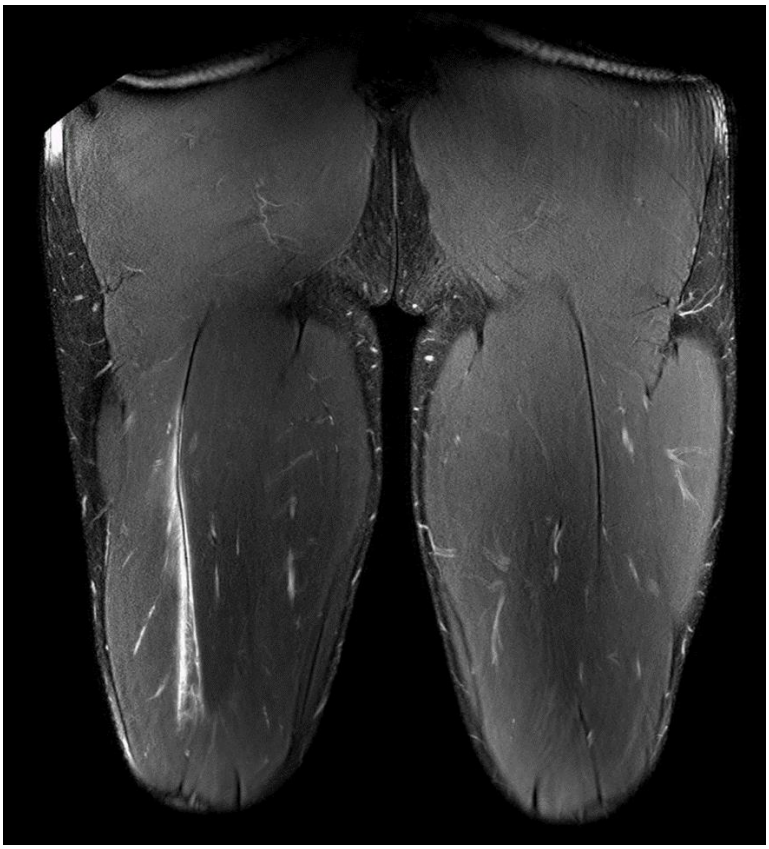

Figure 1: *Coronal T2-weighted MRI image of the upper leg, showing a muscle tear in the Biceps Femoris. Image courtesy of Jithsa Monte, Amsterdam UMC.*

Magnetic Resonance Imaging (MRI) is routinely used for diagnosis. However, MRI and other diagnostic techniques are lacking sufficient sensitivity and/or specificity to inform clinical decisions on the recovery process which would guide a safe moment of return to play (RTP). Therefore, there is an unmet need for new technologies, such as quantitative MRI and ultrasonography, to provide improved readouts of muscle tissue injury and recovery.[13,14]

Over the last decade the interest in training programs to prevent muscle injury significantly grew.[15,16,17,18,19,20] The idea behind such programs is to design a training regime that changes the muscle architecture in such a way that the target muscle becomes less prone to injury. While some training has proven effective in reducing the incidence of hamstring injuries,[10, 11] it has proven difficult to unravel the mechanisms behind their success due to the lack of suitable techniques to visualize and quantify 3D muscle architectural changes with training. Thus, there exists a need for imaging technologies, based on for example MRI or ultrasound, to assess changes in muscle architecture non-invasively over time.

The Hamstrings

The Hamstring muscle group comprises the Biceps Femoris Long Head (BFLH) and Short Head (BFSH), the Semitendinosus (ST) and the Semimembranosus (SM). The proximal attachment point (orego) of the BFLH, ST and SM is the ischial tuberosity. The BFLH and the ST have a conjoined tendon. The distal insertion point of the ST and SM is at the antero-medial side of the tibia at the pes anserinus. The BFLH and BFSH distal insertion point is at the proximal fibula. The Hamstrings muscle group acts both as hip extensor and knee flexor. The BFSH only acts as knee flexor because it only crosses the knee joint. It is assumed that the most common cause for Hamstrings injuries is excessive eccentric loading, which is the muscle loading during stretch that occurs during the extension of the knee and flexion of the hip. The BFLH undergoes the highest stretch during high-speed running, which might explain the reason of most injuries occurring in the BFLH.[21]

Previous research based on clinical and imaging findings reported large variability in days to RTP.[22] And even after return to play athletes have an increased risk of recurrent injury.[23,24] For the treatments of acute Hamstrings injuries there is no consensus on criteria-based progressive rehabilitation programs and the time of return to play after injury. In clinical practice the full range of motion, full strength and functional sport specific activities are assessed in order to evaluate prognosis and monitoring recovery

after injury.[17,25,26] A validated assessment tool using objective criteria would be needed to more accurately determine the moment of RTP, which may reduce the re-injury rates.

Muscle Fiber Architecture

Skeletal muscle consists of multiple fascicles which are surrounded by the perimysium and contain multiple fibers. The fibers are enclosed by the endomysium and are filled with sarcoplasm, ribosomes, mitochondria and protein filaments (myofibrils), with contractile or structural function, which are organized in sarcomeres in series surrounded by the endoplasmic reticulum. The layers of connective tissue are interconnected and transfer the force to the tendon that, in turn, applies it to the skeleton.

Muscle fibers architecture is closely linked to muscle function. The most important parameters which describe muscle architecture are physiological cross-sectional area (PCSA), fiber length, axis of force generation and pennation angle.[27]

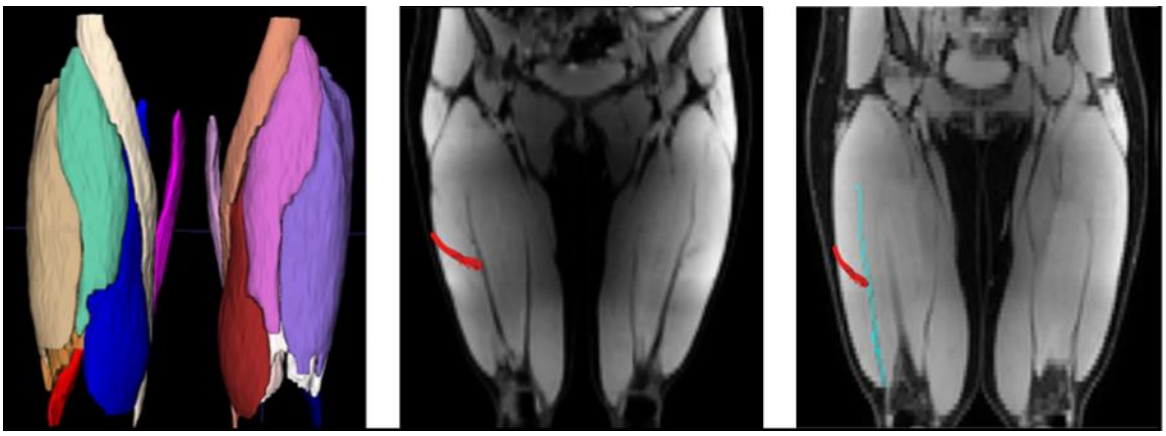

Figure 2: *Muscle architecture parameters: volume, fiber length, and pennation angle. The image shows the volumes of the upper thigh muscles (left) as obtained in chapter 2 of this thesis, a fiber fascicle in red (middle) relative to the deep aponeurosis of the Vastus Lateralis muscle in light blue (right). The pennation angle is defined as the angle between the fiber fascicle and the deep aponeurosis plane.*

The PCSA is the total muscle physiological cross-sectional area which is perpendicular to the muscle fibers[27] and can be calculated as the ratio between the muscle volume and the fiber length:

$$PCSA = \frac{Vmuscle}{\mathrm{L}fiber}$$

Where $Vmuscle$ is the muscle volume and $Lfiber$ is the fiber length.

This measure is important because it showed to be directly proportional to the exertable force.[12] Multiple definitions for the axes of force generation exist, depending on the muscle of interest and the number of dimensions involved in the measurement. In 2D it is often defined as the tendon,[28] whereas in 3D as the line between the insertion and origin of the muscle[29] or as the line through the centroids of the muscle along the muscle length.[30] The pennation angle is the angle between the axis of force generation and the fibers. Muscle fiber length determines the shortening distance of a muscle and the contraction velocity.[27] In elite athletes, both ultrasound and MRI are increasingly used to diagnose and to get prognostic information added about the muscle physiology and injury.[1]

Medical Imaging Techniques

Quantitative Magnetic Resonance Imaging

Magnetic resonance imaging (MRI) is a medical imaging technique that uses a high magnetic field (typically 3T) and the magnetic properties of the hydrogen nuclei (protons), present in mainly water and lipids in biological tissues, to make images of the human body. Apart from the concentration of hydrogen nuclei, which is referred to as proton density (PD), the signal intensity in MR images can be (made) dependent on a variety of other tissue properties to increase contrast between healthy and diseased tissue, improving its diagnostic value. The most used types of contrast are based on tissue differences in the T1 and T2 relaxation times, or longitudinal and transversal relaxation times, respectively.

The T1 relaxation time is the time constant of the exponential relaxation process for spins to return to the equilibrium state from a non-equilibrium state. T1 represents the recovery time of the nuclear magnetization after excitation by the radio-frequency pulses and its value is influenced by the tumbling rate of water and lipids in tissue. Typically, an MR imaging protocol with a short repetition time (TR), which is the timeframe between successive pulse sequences applied to the same slice, is sensitive to tissue differences in the T1 relaxation time generating so-called T1-weighted image contrast.

The T2 relaxation rate is the time constant which determines the rate at which excited protons go out of phase with each other. T2 represents the decrease of the nuclear magnetization after excitation by the MRI radio-frequency pulses. An MR imaging protocol with a long echo time (TE), which is the time at which the electrical signal induced by the spinning protons is measured, is sensitive to tissue differences in the T2 relaxation time generating so-called T2-weighted image contrast. The shorter TE is, the lower is the electrical signal which is measured. The T2 values are highly dependent on the presence of water in tissue and therefore tissue edema is generally accompanied by long T2 relaxation times and high signal intensity on T2 weighted images.

Processes of inflammation and edema typical of muscle strain and certain pathologies of the skeletal muscle result in changes of T2 relaxation time, measured with single voxel proton spectroscopy (1H MRS)[31,32,33] or Multi Spin Echo (MSE),[34,35] in combination with fat suppression techniques or advanced post-processing to avoid overestimation of the T2 relaxation time.[36] Reduced water T2 values in skeletal muscle have been associated with fibrosis.[37,38]

Clinical examinations of muscular diseases with MRI usually assess also the fat fraction in a volumetric manner with chemical shift based water fat imaging (DIXON).[39] Dixon is a quantitative imaging technique which uses the difference between precessional frequencies of protons in water and fat to separate these components. In the 2-point-DIXON method firstly two images are acquired with a spin echo sequence, in the first one with water and fat signals in-phase (IP) and the second one out-of-phase (OP). The fat and the water images are obtained by subtracting and summing these IP and OP images, respectively. In the 3-point-DIXON algorithm the measurements are more reliable because the imprecisions due to the B0 inhomogeneities, which is static noise due to the static magnetic field, are corrected thanks to the contribution of individual fat spectral peaks.

Moreover, it is important to consider the confounding effects on fat estimation of three factors. Firstly, the T1 relaxation, causing fat fraction overestimation, can be minimized with the optimization of sequence parameters. Secondly, single fat peak models have shown to underestimate the fat fraction. Finally, the T2* relaxation effect, which is due to signal relaxation between echoes in presence of macroscopic field inhomogeneities and which could cause fat overestimations in low fat ranges. This can be avoided by measuring more echoes and account for the T2* relaxation time in the fitting process. In this thesis the DIXON sequence images, more specifically the water and the out-of-phase images, were used as anatomical references to delineate the tendons, aponeurosis, and muscle contours.

Diffusion-Tensor MRI

Diffusion

Diffusion is the movement of particles like molecules and ions. Generally, diffusion follows the concentration gradient, according to Fick's law of diffusion, from regions at high concentration to regions at low concentration. In absence of a concentration gradient, diffusion follows the Brownian motion of particles. Self-diffusion depends on viscosity and temperature, and it is described by the diffusion coefficient. The presence of physical barriers like biological membranes or intracellular proteins in biological tissues reduces the diffusion coefficient. Then the diffusion is commonly referred to by the apparent diffusion coefficient (ADC).

In some tissues, like in the human brain and in the muscle tissue, diffusion is anisotropic. Diffusion tensor imaging (DTI) allows to describe mathematically the anisotropic characteristics of diffusion of water molecules in biological tissue microstructure in vivo and enables its quantification. DTI therefore allows for a noninvasive in vivo volumetric assessment of muscle architecture and microstructure.[31,40,41]

Diffusion Weighted Imaging

Diffusion weighted images in skeletal muscle are commonly acquired with single shot spin-echo planar imaging sequences (SE-EPI). In some studies, stimulated echo[42,43,44,45,46] or twice-refocused spin echo sequences[47] have been used.

In diffusion weighted imaging the image is generally obtained by measuring the signal loss due to diffusing spins under the influence of two intense and brief (G) gradient pulses placed symmetrically around the 180° RF pulse and separated in time (Δ). These gradient pulses have a different effect on spins that are stationary, flowing, or diffusing.

The pulsed gradient will have no net effect on stationary spins, as phase accumulation during the first gradient pulse of length δ will be compensated during the second gradient pulse. For flowing spins, the coherent movement during the time Δ between the gradient pulses will result in incomplete phase compensation and a net phase accumulation which is proportional to the spin velocity.

Since diffusing spins move randomly in time and direction, phase accumulation will be random as well, resulting in net zero phase accumulation. However, because of the random phase, the net magnetization will be lower proportional to the diffusion coefficient.

The diffusion-weighted signal equals

$S_b = S_0 e^{(-b\,\mathbf{g}^T \mathbf{D}\,\mathbf{g})}$,

where S_b is the diffusion weighted signal, S_0 is the signal intensity without diffusion weighting, **D** is the diffusion tensor, b is the b-value indicating the strength of the diffusion weighting, and **g** is a vector indicating the pulsed gradient direction. The b value is equal to $\gamma^2 G^2 \delta^2 (\Delta - \delta/3)$, where G is the pulse gradient amplitude, δ is the pulse gradient duration, γ is the gyromagnetic ratio of the nucleus and Δ is the duration between the gradient pulses.[48]

DTI

In DTI diffusion-weighting gradients are applied in a minimum of 6 non-collinear directions to describe diffusion by a 3 x 3 diffusion tensor **D**. A diffusion weighted signal is measured in each direction **g**. The choice of the b-value determines the desired contrast between non-weighted and weighted images.

Considerations on DTI Acquisitions

The image quality achievable in skeletal muscle with DTI is affected by the sequence parameters, field inhomogeneities, susceptibility artifacts, the presence of fat, patient motion or image blurring due to T2* decay during the echo.[49]

Because of the short T2 relaxation time of skeletal muscle (~30 ms), it is challenging to achieve enough diffusion weighting within reasonable echo time before the magnetization is lost due to T2 decay.[50,51] Therefore, the TE must be as short as possible to retain sufficient signal-to-noise (SNR) and the choice of the b-value is often a compromise between diffusion-weighting and SNR.[52,53] In the majority of muscle diffusion studies, a b-value in the range of 300 and 800 s/mm^2 is used. In this thesis a b-factor of

450 s/mm^2 was used, because previous simulation studies in muscle showed an optimal value around 400 - 500 s/mm^2.[54]

In DTI data acquisition the recommended number of gradient directions is at least 6, however in practice the number of directions used in different studies varied between 6 and 48 directions.[57] Theoretically, more gradient directions are preferred, but practically it is equally important to have high SNR per diffusion direction.[58] For robust and rotation invariant tensor calculation, in previous studies at least 12 gradient directions were recommended.[57] Moreover, we use a strict criterium that SNR should be at least 25.[2]

Due to the multiple directions of acquisition, the acquisition of DTI sequences is time-consuming. Consequently, in order to limit the acquisition time, the spatial resolution is generally low. Higher resolution would be needed to quantify diffusion in smaller sized muscles. Moreover, EPI readout is sensitive to susceptibility artifacts, like Eddy currents, which results in image distortion. During the acquisition, image distortion can be prevented by shimming and corrective gradients. Besides the effect of low signal to noise and field inhomogeneities, contamination of fat signals should be avoided in Diffusion Tensor Imaging.[1,2,12]

Fat Suppression Techniques

Fat suppression is relevant for a correct estimation of parameters in DTI because the diffusion coefficient of fat is two orders of magnitude lower than that of water[38] and muscles tissue is generally surrounded by fat tissue. In 3T MRI the dominating lipid frequencies resonate in the range 0.5-2.75 ppm and the main aliphatic peak resonates at 1.3 ppm. The aliphatic group includes the methyl and methylene fat peaks.[6] The lipid frequency which resonates on the opposite side of the water signal at 5.3 ppm constitute the olefinic fat peak.

The first fat suppression techniques used in this thesis targets the methylene and methyl fat peaks. The Spectrally Adiabatic Recovery (SPAIR) is based on chemical selective pre-saturation inversion recovery pre-pulses. Part of the aliphatic peak, the methylene and methyl fat peak, is suppressed. This is a robust technique which is insensitive to B1 inhomogeneities across the imaging volume, which can be particularly useful for imaging large regions of the body.

Secondly, we have used the slice selective gradient reversal (SSGR) technique to suppress the aliphatic fat peak.[55,56] SSGR is based on the notion that due to chemical shift, fat is excited by the 90° pulse in a slice that is displaced with respect to the water slice. By reversing the polarity of the 180° pulse slice selection gradient, the displacement turns in opposite direction. If both slices are sufficiently separated no fat spins will experience both excitation and refocusing pulses, resulting in no MRI signals from fat in the image. This technique can provide good fat suppression at high field strengths and in the presence of magnetic field inhomogeneities.

For the suppression of the olefinic fat peak, a SPIR pulse can be applied with center on the olefinic peak. With this approach the lipid magnetization is flipped to the transverse plane while the water magnetization remains along the longitudinal axis. Before the image is acquired, the inverted magnetization of the fat signal is dephased with spoiler gradients, whereas the water magnetization is left along the longitudinal axis.[7]

In this thesis a combination of the SPAIR, the SSGR, and the SPIR pulse techniques was used for the DTI measurements to suppress the signal from both the olefinic and aliphatic fat peaks and to achieve uniform fat suppression. This is particularly important in musculoskeletal MRI, as B1 inhomogeneities caused by high magnetic susceptibility of bone and other tissues can lead to field distortions that affect DTI data, which relies on precise gradients and radiofrequency pulses to manipulate water molecule diffusion properties.

DTI Indices

In every voxel the acquired diffusion data are used to reconstruct the tensor with Linear Least squares (LLS), Weighted Linear Least squares (WLLS) or Non-Linear Least Squares (NLS). The tensor is decomposed in three orthogonal eigenvectors (v_1, v_2, v_3) and corresponding eigenvalues (λ_1, λ_2, λ_3). The direction of the first eigenvector v_1 corresponds to the direction of the fibers of the skeletal muscle fascicle with respect to the scanner coordinate system. The second eigenvector v_2 and the third eigenvector v_3 point orthogonally to the first eigenvector and their average, the radial diffusivity, is thought to be the DTI index most sensitive to damages in muscle fibers as it reflects the diffusion of water molecules perpendicular to fiber orientation.[13]

Mean Diffusivity (MD) and Fractional Anisotropy (FA) can be derived from the eigenvalues. The mean diffusivity (MD) reflects the average diffusion in tissue, whose value in skeletal muscle is approximately 1.6 $x10^{-3}$ mm^2/s.[54] The fractional anisotropy (FA) is a dimensionless scalar index between 0 and 1 that reflects the level of diffusion directional anisotropy.[40]

DTI fiber tractography is derived from the principal diffusion directions (eigenvector 1, v_1) and the fractional anisotropy (FA) by using deterministic and probabilistic algorithms. In musculoskeletal applications three-dimensional muscle fiber tractography is used to assess muscle architecture parameters,[57,58,59] whereas the diffusion indices, such as MD and FA, can be used to evaluate muscle tissue microstructure.[30]

The DTI indices can vary due to exercise,[60] injury[61] and disease.[62] Therefore, Diffusion weighted MRI (DWI) and DTI have been used to assess the effect of exercise, like mild and severe muscle damage. Previous studies showed correlation between the T_2 relaxation time and diffusion[65] and an increase of T_2 relaxation time, MD, λ_2, and λ_3 directly after exercise.[66] Whereas, the FA, which is sensitive to diffusion anisotropy, showed increased values when loads were applied.

DTI Post-processing

DTI parameter estimation can be subject to errors due to the presence of fat signal, low SNR and artefacts.[54] Some errors can be addressed in post-processing.[67] In the case of low SNR, the three eigenvalues and the MD could be underestimated whereas the FA could be overestimated.[54] Based on previous simulation studies, SNR of the non-weighted diffusion imaging should be at least 20 for accurate estimations of diffusion indices and fiber orientations. In many studies noise suppression techniques are applied.[68,69] Imaging denoising methods include spatial domain filtering or transform domain filtering. In this thesis the denoising was obtained with a Rician noise model and principal component analysis. Subsequently, the SNR map and the average SNR value in the muscle, reported as the ratio of S_0 and the standard deviation of the Rician noise, was used as cut-off.[54]

In post-processing the deformations and the susceptibility artifacts which are caused by field inhomogeneities can be corrected by using B_0-field maps[54,68] with the registration of diffusion-weighted images to the non-weighted images (b-value = 0 s/mm^2).[54] Moreover, the diffusion images are registered to the anatomical references in which the muscles are segmented. Due to the eddy-current induced

deformation of the muscle tissue, registration of the diffusion weighted images to non-diffusion-weighted or anatomical images can be challenging. In this thesis, registration consisted of a combination of rigid, affine, and b-spline registration steps. The manual segmentation of many muscles on the anatomical images is a time-consuming process. Therefore, several automatic and semi-automatic segmentation algorithms were introduced (see Chapter 2).

AIM OF THIS THESIS

The aim of this thesis was to develop different approaches to measure muscle architectural parameters with Diffusion Tensor MR Images (DTI) which can be applied to study changes in muscle architecture after an injury prevention program.

Chapter 1 provided a brief introduction to the topics of the thesis with a preamble on the need for evidence-based clinical decisions in Hamstrings injuries. An overview of the MRI techniques used in this thesis to assess muscle architectural parameters was presented, with a primary focus on Diffusion Tensor Imaging (DTI).

The first part of this thesis addresses improvement in the analysis of skeletal muscle MRI and specifically DTI data to extract relevant muscle architectural parameters. In Chapter 2 a supervised framework is introduced to speed up the segmentations of upper leg muscles for the evaluation of diffusion tensor indices. This approach consisted of a transversal propagation of few manually segmented slices and the longitudinal propagation of different time points.

In Chapter 3, I propose a diffusion tensor-based method to facilitate a volumetric assessment of fiber fascicle orientations (or 'fiber angles') and changes therein in leg muscle without the need for performing manual and labor-intensive fiber-tractography. The feasibility of this method was shown for both the upper- and lower-leg muscles.

In Chapter 4, we presented a method to measure the pennation angle with fiber tractography and compared it with a 3D-US based method in the Vastus Lateralis muscle.

The second part of this thesis focuses on the application of the presented technique for the measurement of fiber fascicle orientations (or 'fiber angles') in a relevant application. To this end, in Chapter 5 we compared the effects of two different injury prevention programs on basketball players. Changes in fiber fascicle orientations of the full muscle volume and fiber length in the hamstring muscles obtained with DTI were the primary outcome parameters.

Finally, Chapter 6 concludes the thesis with a summary, discussion of the findings and future perspectives.

References

1. Silvers-Granelli H, Zachazewski J, Li B, et al. HAMSTRING INJURIES IN MAJOR AND MINOR LEAGUE BASEBALL: ARE THEY PREVENTABLE? *Br J Sports Med*. 2017;51(4). doi:10.1136/bjsports-2016-097372.267
2. Zachazewski J, Silvers HJ, Li B, et al. Hamstring Injuries in Major and Minor League Baseball. *Orthop J Sport Med*. 2016;4(7_suppl4). doi:10.1177/2325967116s00182
3. Cornelissen M, Kemler E, Verhagen E, Gouttebarge V. A systematic review of injuries in recreational field hockey: From injury problem to prevention. *J Sports Sci*. Published online 2020. doi:10.1080/02640414.2020.1764898
4. Crema MD, Jarraya M, Engebretsen L, et al. Imaging-detected acute muscle injuries in athletes participating in the Rio de Janeiro 2016 Summer Olympic Games. *Br J Sports Med*. 2018;52(7). doi:10.1136/bjsports-2017-098247
5. Roe M, Murphy JC, Gissane C, Blake C. Time to get our four priorities right: An 8-year prospective investigation of 1326 player-seasons to identify the frequency, nature, and burden of time-loss injuries in elite Gaelic football. *PeerJ*. 2018;2018(7). doi:10.7717/peerj.4895
6. Martínez-Silván D, Wik EH, Alonso JM, et al. Injury characteristics in male youth athletics: A five-season prospective study in a full-time sports academy. *Br J Sports Med*. 2021;55(17). doi:10.1136/bjsports-2020-102373
7. Edouard P, Branco P, Alonso JM. Muscle injury is the principal injury type and hamstring muscle injury is the first injury diagnosis during top-level international athletics championships between 2007 and 2015. *Br J Sports Med*. 2016;50(10). doi:10.1136/bjsports-2015-095559
8. Armstrong RB. Mechanisms of exercise-induced delayed onset muscular soreness: A brief review. *Med Sci Sports Exerc*. 1984;16(6).
9. 69. Cheung K, Hume PA, Maxwell L. Delayed onset muscle soreness: Treatment strategies and performance factors. *Sport Med*. 2003;33(2). doi:10.2165/00007256-200333020-00005
10. Clarkson, Priscilla M.; Hubal MJ. Exercise-Induced Muscle Damage in Humans : American Journal of Physical Medicine & Rehabilitation. *Am J Phys Med Rehabil Novemb 2002 - Vol 81 - Issue 11 - p S52-S69*. 2002;81(11).
11. Järvinen TAH, Järvinen M, Kalimo H. Regeneration of injured skeletal muscle after the injury. *Muscles Ligaments Tendons J*. 2013;3(4). doi:10.11138/mltj/2013.3.4.337
12. Järvinen TAH, Järvinen TLN, Kääriäinen M, et al. Muscle injuries: optimising recovery. *Best Pract Res Clin Rheumatol*. 2007;21(2). doi:10.1016/j.berh.2006.12.004
13. Kruse RC, Whipple MT, Schmidt E, Wilz L. Role of Ultrasound in Managing Hamstring Muscle Injuries. *Curr Phys Med Rehabil Reports*. 2021;9(4). doi:10.1007/s40141-021-00330-7
14. Thierfelder KM, Gerhardt JS, Gemescu IN, Notohamiprodjo S, Rehnitz C, Weber MA. Imaging of hip and thigh muscle injury: a pictorial review. *Insights Imaging*. 2019;10(1). doi:10.1186/s13244-019-0702-1
15. Fournier-Farley C, Lamontagne M, Gendron P, Gagnon DH. Determinants of Return to Play after the Nonoperative Management of Hamstring Injuries in Athletes. *Am J Sports Med*. 2016;44(8). doi:10.1177/0363546515617472
16. Rudisill SS, Kucharik MP, Varady NH, Martin SD. Evidence-Based Management and Factors Associated With Return to Play After Acute Hamstring Injury in Athletes: A Systematic Review. *Orthop J Sport Med*. 2021;9(11). doi:10.1177/23259671211053833
17. Pickett B, Bytomski JR, Zafonte RD. Evidence based management of sports related concussion. *J Osteopath Med*. 2021;121(5). doi:10.1515/jom-2021-0058

18. Root HJ, Bay RC, DiStefano LJ. INFLUENCE OF PREVENTIVE TRAINING PROGRAM FEEDBACK COMPLEXITY ON ATHLETE INJURY RISK. *Orthop J Sport Med*. 2020;8(4_suppl3). doi:10.1177/2325967120s00272
19. Paszkewicz J, Webb T, Waters B, McCarty CW, Van Lunen B. The effectiveness of injury-prevention programs in reducing the incidence of anterior cruciate ligament sprains in adolescent athletes. *J Sport Rehabil*. 2012;21(4). doi:10.1123/jsr.21.4.371
20. Root HJ, Frank BS, Denegar CR, et al. Application of a preventive training program implementation framework to youth soccer and basketball organizations. *J Athl Train*. 2019;54(2). doi:10.4085/1062-6050-375-17
21. Chumanov ES, Heiderscheit BC, Thelen DG. Hamstring musculotendon dynamics during stance and swing phases of high-speed running. *Med Sci Sports Exerc*. 2011;43(3). doi:10.1249/MSS.0b013e3181f23fe8
22. Askling CM, Tengvar M, Saartok T, Thorstensson A. Acute first-time hamstring strains during high-speed running: A longitudinal study including clinical and magnetic resonance imaging findings. *Am J Sports Med*. 2007;35(2). doi:10.1177/0363546506294679
23. De Visser HM, Reijman M, Heijboer MP, Bos PK. Risk factors of recurrent hamstring injuries: A systematic review. *Br J Sports Med*. 2012;46(2). doi:10.1136/bjsports-2011-090317
24. Cruz J, Mascarenhas V. Adult thigh muscle injuries—from diagnosis to treatment: what the radiologist should know. *Skeletal Radiol*. 2018;47(8). doi:10.1007/s00256-018-2929-1
25. Willits K, Amendola A, Bryant D, et al. Operative versus nonoperative treatment of acute achilles tendon ruptures: A multicenter randomized trial using accelerated functional rehabilitation. *J Bone Jt Surg - Ser A*. 2010;92(17). doi:10.2106/JBJS.I.01401
26. Chang JS, Kayani B, Plastow R, Singh S, Magan A, Haddad FS. Management of hamstring injuries: Current concepts review. *Bone Jt J*. 2020;102(10). doi:10.1302/0301-620X.102B10.BJJ-2020-1210.R1
27. Lieber RL, Fridén J. Functional and clinical significance of skeletal muscle architecture. *Muscle and Nerve*. 2000;23(11). doi:10.1002/1097-4598(200011)23:11<1647::AID-MUS1>3.0.CO;2-M
28. Randhawa A, Wakeling JM. Multidimensional models for predicting muscle structure and fascicle pennation. *J Theor Biol*. 2015;382. doi:10.1016/j.jtbi.2015.06.001
29. Lee D, Li Z, Sohail QZ, Jackson K, Fiume E, Agur A. A three-dimensional approach to pennation angle estimation for human skeletal muscle. *Comput Methods Biomech Biomed Engin*. 2015;18(13). doi:10.1080/10255842.2014.917294
30. Hiblar T, Bolson EL, Hubka M, Sheehan FH, Kushmerick MJ. Three dimensional ultrasound analysis of fascicle orientation in human tibialis anterior muscle enables analysis of macroscopic torque at the cellular level. In: *Advances in Experimental Medicine and Biology*. Vol 538. ; 2004. doi:10.1007/978-1-4419-9029-7_56
31. Willcocks RJ, Forbes SC, Finanger EL, et al. P.13.5 Magnetic resonance imaging and spectroscopy detect changes with age, corticosteroid treatment, and functional progression in DMD. *Neuromuscul Disord*. 2013;23(9-10). doi:10.1016/j.nmd.2013.06.599
32. Arpan I, Willcocks RJ, Forbes SC, et al. Examination of effects of corticosteroids on skeletal muscles of boys with DMD using MRI and MRS. *Neurology*. 2014;83(11). doi:10.1212/WNL.0000000000000775
33. Willcocks RJ, Arpan IA, Forbes SC, et al. Longitudinal measurements of MRI-T2 in boys with Duchenne muscular dystrophy: Effects of age and disease progression. *Neuromuscul Disord*. 2014;24(5). doi:10.1016/j.nmd.2013.12.012
34. Fullerton GD, Cameron IL, Hunter K, Fullerton HJ. Proton magnetic resonance relaxation behavior of whole muscle with fatty inclusions. *Radiology*. 1985;155(3). doi:10.1148/radiology.155.3.4001376

35. Carlier PG. Global T2 versus water T2 in NMR imaging of fatty infiltrated muscles: Different methodology, different information and different implications. *Neuromuscul Disord*. 2014;24(5). doi:10.1016/j.nmd.2014.02.009
36. Williams SE, Heemskerk AM, Welch EB, Li K, Damon BM, Park JH. Quantitative effects of inclusion of fat on muscle diffusion tensor MRI measurements. *J Magn Reson Imaging*. 2013;38(5). doi:10.1002/jmri.24045
37. McCully K, Posner J. Measuring exercise-induced adaptations and injury with magnetic resonance spectroscopy. In: *International Journal of Sports Medicine*. Vol 13. ; 1992. doi:10.1055/s-2007-1024621
38. Damon BM, Gregory CD, Hall KL, Stark HJ, Gulani V, Joan Dawson M. Intracellular acidification and volume increases explain R2 decreases in exercising muscle. *Magn Reson Med*. 2002;47(1). doi:10.1002/mrm.10043
39. Glover GH, Schneider E. Three-point dixon technique for true water/fat decomposition with B0 inhomogeneity correction. *Magn Reson Med*. 1991;18(2). doi:10.1002/mrm.1910180211
40. Basser PJ, Pierpaoli C. Microstructural and physiological features of tissues elucidated by quantitative-diffusion-tensor MRI. *J Magn Reson*. 2011;213(2). doi:10.1016/j.jmr.2011.09.022
41. Iima M, Yano K, Kataoka M, et al. Quantitative Non-Gaussian Diffusion and Intravoxel Incoherent Motion Magnetic Resonance Imaging. *Invest Radiol*. 2015;50(4). doi:10.1097/rli.0000000000000094
42. Steidle G, Eibofner F, Schick F. Quantitative diffusion imaging of adipose tissue in the human lower leg at 1.5 T. *Magn Reson Med*. 2011;65(4). doi:10.1002/mrm.22699
43. Karampinos DC, King KF, Sutton BP, Georgiadis JG. Intravoxel partially coherent motion technique: Characterization of the anisotropy of skeletal muscle microvasculature. *J Magn Reson Imaging*. 2010;31(4). doi:10.1002/jmri.22100
44. Karampinos DC, King KF, Sutton BP, Georgiadis JG. Myofiber ellipticity as an explanation for transverse asymmetry of skeletal muscle diffusion MRI in vivo signal. *Ann Biomed Eng*. 2009;37(12). doi:10.1007/s10439-009-9783-1
45. Hiepe P. Functional Muscle MRI in Human Calf Muscle using IVIM. *Ismrm*. 2013;44(12).
46. Hiepe P, Güllmar D, Ros C, et al. Functional DTI in Voluntary Contracted Human Calf Muscles Using an MR Compatible Ergometer. In: *Proc Intl Soc Mag Reson Med 20*. ; 2012.
47. Gaige TA, Benner T, Wang R, Wedeen VJ, Gilbert RJ. Three dimensional myoarchitecture of the human tongue determined in vivo by diffusion tensor imaging with tractography. *J Magn Reson Imaging*. 2007;26(3). doi:10.1002/jmri.21022
48. Yablonskiy DA, Sukstanskii AL. Theoretical models of the diffusion weighted MR signal. *NMR Biomed*. 2010;23(7). doi:10.1002/nbm.1520
49. Karampinos DC, Banerjee S, King KF, Link TM, Majumdar S. Considerations in high-resolution skeletal muscle diffusion tensor imaging using single-shot echo planar imaging with stimulated-echo preparation and sensitivity encoding. *NMR Biomed*. 2012;25(5). doi:10.1002/nbm.1791
50. Gold GE, Han E, Stainsby J, Wright G, Brittain J, Beaulieu C. Musculoskeletal MRI at 3.0 T: Relaxation times and image contrast. *Am J Roentgenol*. 2004;183(2). doi:10.2214/ajr.183.2.1830343
51. Stanisz GJ, Odrobina EE, Pun J, et al. T1, T2 relaxation and magnetization transfer in tissue at 3T. *Magn Reson Med*. 2005;54(3). doi:10.1002/mrm.20605
52. inha S, Sinha U, Edgerton VR. In vivo diffusion tensor imaging of the human calf muscle. *J Magn Reson Imaging*. 2006;24(1). doi:10.1002/jmri.20593
53. Saupe N, White LM, Sussman MS, Kassner A, Tomlinson G, Noseworthy MD. Diffusion tensor magnetic resonance imaging of the human calf: Comparison between 1.5 t and 3.0 t-

preliminary results. *Invest Radiol*. 2008;43(9). doi:10.1097/RLI.0b013e31817e909f
54. Froeling M. *DTI of Human Skeletal Muscle. From Simulation to Clinical Implementation.*; 2012.
55. Fernando D, Karampinos DC, King KF, et al. Removal of olefinic fat chemical shift artifact in diffusion MRI. *Magn Reson Med*. 2011;65(3). doi:10.1002/mrm.22670
56. Kuroda K, Oshio K, Mulkern R V., Jolesz FA. Optimization of chemical shift selective suppression of fat. *Magn Reson Med*. 1998;40(4). doi:10.1002/mrm.1910400402
57. Oudeman J, Mazzoli V, Marra MA, et al. A novel diffusion-tensor MRI approach for skeletal muscle fascicle length measurements. *Physiol Rep*. 2016;4(24):1-12. doi:10.14814/phy2.13012
58. Anneriet M. Heemskerk, Bruce M. Damon. Diffusion Tensor MRI Assessment of Skeletal Muscle Architecture. *Curr Med Imaging Rev*. 2007;3(3). doi:10.2174/157340507781386988
59. Galbán CJ, Maderwald S, Uffmann K, de Greiff A, Ladd ME. Diffusive sensitivity to muscle architecture: A magnetic resonance diffusion tensor imaging study of the human calf. *Eur J Appl Physiol*. 2004;93(3):253-262. doi:10.1007/s00421-004-1186-2
60. Oudeman J, Nederveen AJ, Strijkers GJ, Maas M, Luijten PR, Froeling M. Techniques and applications of skeletal muscle diffusion tensor imaging: A review. J Magn Reson Imaging. 2016;43(4). doi:10.1002/jmri.25016
61. Froeling M, Oudeman J, Strijkers GJ, et al. Muscle changes detected with diffusion-tensor imaging after long-distance running. Radiology. 2015;274(2). doi:10.1148/radiol.14140702
62. Zaraiskaya T, Kumbhare D, Noseworthy MD. Diffusion tensor imaging in evaluation of human skeletal muscle injury. J Magn Reson Imaging. 2006;24(2). doi:10.1002/jmri.20651
63. Qi J, Olsen NJ, Price RR, Winston JA, Park JH. Diffusion-weighted imaging of inflammatory myopathies: Polymyositis and dermatomyositis. J Magn Reson Imaging. 18 2008;27(1). doi:10.1002/jmri.21209
64. Damon BM, Froeling M, Buck AKW, et al. Skeletal muscle diffusion tensor-MRI fiber tracking: rationale, data acquisition and analysis methods, applications
65. Ababneh ZQ, Ababneh R, Maier SE, et al. On the correlation between T2 and tissue diffusion coefficients in exercised muscle: Quantitative measurements at 3T within the tibialis anterior. *Magn Reson Mater Physics, Biol Med*. 2008;21(4). doi:10.1007/s10334-008-0120-8
66. Okamoto Y, Mori S, Kujiraoka Y, Nasu K, Hirano Y, Minami M. Diffusion property differences of the lower leg musculature between athletes and non-athletes using 1.5T MRI. *Magn Reson Mater Physics, Biol Med*. 2012;25(4). doi:10.1007/s10334-011-0294-3
67. Hooijmans MT. *Quantitative MR in Dystrophic Muscle*.; 2017.
68. Froeling M, Nederveen AJ, Heijtel DFR, et al. Diffusion-tensor MRI reveals the complex muscle architecture of the human forearm. *J Magn Reson Imaging*. 2012;36(1). doi:10.1002/jmri.23608
69. Sinha S, Sinha U. Reproducibility analysis of diffusion tensor indices and fiber architecture of human calf muscles in vivo at 1.5 Tesla in neutral and plantarflexed ankle positions at rest. *J Magn Reson Imaging*. 2011;34(1). doi:10.1002/jmri.22596

CHAPTER 2

Supervised segmentation framework for evaluation of diffusion tensor imaging indices in skeletal muscle

Laura Secondulfo

Augustin C. Ogier

Jithsa R. Monte

Vincent L. Aengevaeren

David Bendahan

Aart J. Nederveen

Gustav J. Strijkers

Melissa T. Hooijmans

NMR in Biomedicine, 2020

Abstract

Diffusion tensor imaging (DTI) is becoming a diagnostic tool map muscle recovery processes following physical activity, like mild and severe muscle damage, and to understand muscle disease progression. Segmenting many individual leg muscles on the anatomical images is necessary for quantification, but it is still a time-consuming manual process.

The purpose of this chapter is to illustrate a study that we performed on the impact of a supervised segmentation framework on the quantification of DTI indices in individual upper leg muscles, which would facilitate significantly the application of MRI to study longitudinal changes in muscle architecture in large cohorts.

Longitudinally acquired MRI datasets (baseline, post-marathon and follow-up) of the upper legs of 11 subjects, consisting of a DTI and Dixon acquisition, were used in this study. Supervised segmentations for the upper leg muscles were performed first in each single subject at baseline which was developed by Ogier et al. using the out-of-phase Dixon images. These segmentations were longitudinally propagated for the post-marathon and follow-up time points.

In parallel, for validation purposes manual segmentations were performed on the water image of the Dixon for each of the time points. Dice similarity coefficients (DSCs) were calculated to compare the manual and semi-automatic segmentations. Bland-Altman and regression analyses were performed, to evaluate the impact of the two segmentation methods on mean diffusivity (MD), fractional anisotropy (FA) and the third eigenvalue (λ_3). The average DSC for all analyzed muscles over all time points was 0.92 ± 0.01, ranging between 0.48 and 0.99. Bland-Altman analysis showed that the 95% limits of agreement for MD, FA and λ_3 ranged between 0.5% and 3.0% for the transversal propagation and between 0.7% and 3.0% for the longitudinal propagations. Similarly, regression analysis showed good correlation for MD, FA and λ_3 ($r = 0.99$, $p < 0.0001$).

In conclusion, the supervised segmentation framework successfully quantified DTI indices in the upper-leg muscles compared with manual segmentation while only requiring manual input of 30% of the slices, resulting in a threefold reduction in segmentation time.

Abbreviations

- **BFLH**
  biceps femoris long head muscle
- **BFSH**
  biceps femoris short head muscle
- **CNN**
  convolutional neural network
- **DSC**
  Dice similarity coefficient
- **DTI**
  diffusion tensor imaging
- **FA**
  fractional anisotropy
- **G**
  gracilis muscle
- **IVIM**
  intra-voxel incoherent motion
- **LoA**
  limits of agreement
- **MD**
  mean diffusivity
- **RF**
  rectus femoris muscle
- **S**
  sartorius muscle
- **SM**
  semimembranosus muscle
- **SNR**
  signal-to-noise ratio
- **SPAIR**
  spectral attenuated inversion recovery
- **SPIR**
  spectral pre-saturation with inversion recovery
- **SSGR**
  slice selective gradient reversal
- **ST**
  semitendinosus muscle
- **VI**
  vastus intermedius muscle
- **VL**
  vastus lateralis muscle
- **VM**
  vastus medialis muscle
- λ_3
  eigenvalue 3

Introduction

MRI is extensively used in clinical evaluations of skeletal muscle to assess the location, extent and severity of several pathological conditions.[1, 2] The common contrast mechanisms in clinical skeletal muscle scans consist of T_1-weighted contrast to assess muscle anatomy and fat infiltration, and sequences that employ T_2-weighted contrast to characterize muscle edema. Over the years, advances in MRI techniques and post-processing have expanded the MRI toolbox for assessing healthy and diseased muscle composition, architecture, perfusion and function in a quantitative manner, leading to what is known as quantitative MRI.

Diffusion tensor imaging (DTI) is a quantitative MRI technique which has received considerable attention and that was introduced in the previous chapter. The orientational dependence of DTI, which is due to the isotropic self-diffusivity of water in tissue, allows for three-dimensional reconstructions of muscle fiber architecture.[3, 4] As it was explained in the previous chapter, quantitative DTI-derived indices are heavily dependent on tissue integrity and have been shown to change in a variety of skeletal muscle pathologies and injuries.[5, 6] Furthermore, in sport medicine, DTI has shown promise as a relevant tool to understand the muscle recovery process that follows physical activity and after injury.[7, 8]

For instance, our group investigated changes in DTI indices in the upper leg muscles during recovery after a marathon.[9, 10] Distinct changes in DTI indices were detected in muscles that appeared normal on T_2-weighted images, demonstrating the added value of DTI as a sensitive readout of muscle integrity.

The analysis of DTI acquisitions requires many post-processing steps for calculation of the DTI indices, which have been almost entirely automated—for more details see reference.[11] However, segmentation of all the leg muscles, necessary for quantification, is a time-consuming manual process, in which the accuracy and reproducibility may be operator dependent.[12] Therefore, there is great need for (semi-) automatic segmentation tools in the context of quantitative imaging of skeletal muscle. Recently, some (semi-) automatic approaches have been proposed for skeletal muscle[12-20] and showed good correspondence, reflected by high Dice similarity coefficient (DSC) values, with manual segmentation. However, these approaches only focused on either a partial volume of the muscles or entire muscle groups rather than the full volume of individual muscles.

Moreover, so far little is known about the impact that (semi-) automatic segmentation approaches may have on quantification of imaging outcome measures in skeletal muscle, especially on DTI analysis.

The purpose of the study reported in this chapter is to evaluate a supervised muscle segmentation framework, previously developed by Ogier *et al.,*[21, 22] for the quantification of DTI indices in individual muscles. Using this tool, we aimed to assess the accuracy, feasibility and impact on the quantification of DTI indices considering manual segmentation as the ground truth. Also, we aimed to assess the corresponding reduction in work load compared with manual segmentation.

Methods

Participants and study set-up

The study set-up and the MRI protocol of the study are reported in detail by Hooijmans *et al.*[10] For this study we included 11 subjects who competed in the marathon in Amsterdam (The Netherlands) on 15 October 2017. The participants were 51 ± 6-year-old males of average fitness level. MRI examinations were obtained at three time points: (1) baseline (1 week prior to the marathon), (2) post-marathon (24-48 h after the marathon) and (3) follow-up (2 weeks after the marathon). The study was approved by the local medical ethics committee and all participants signed written informed consent.

MRI protocol

Participants received an MRI examination of both upper legs on a 3T MR scanner (Ingenia, Philips, Best, The Netherlands) using a 16-element anterior body receive coil and a 12-channel table top coil. Subjects were positioned in a feet-first supine position in the scanner. The data were acquired in three transversal stacks with 30 mm overlap, covering 498 mm proximal to distal with a field of view (FOV) of 480 × 276 mm^2. The total duration of the scan protocol was 48 min and included diffusion-weighted spin-echo Echo-planar imaging for DTI parameter estimations (SE-EPI, bandwidth = 31 Hz/pixel, T_R = 5,000 ms, T_E = 57 ms, matrix = 160 × 92, voxel size = 3 × 3 × 6 mm^3, number of slices = 31, SENSE = 1.9, *b*-values (s/mm^2)/no. of directions = 0/1, 1/6, 10/3, 25/3, 100/3, 200/6, 400/8 and 600/12, fat suppression: combination of a spectral pre-saturation inversion recovery (SPIR) pulse, spectral attenuated inversion recovery (SPAIR) pulse and slice selective gradient reversal (SSGR)). A

combination of the three suppression techniques was used to suppress the signal from both the olefinic and aliphatic fat peaks. The signal from the olefinic fat peak at 5.3 ppm was suppressed with a non-selective SPIR pulse, whereas the aliphatic main peak at 1.3 ppm was suppressed using a combination of SPAIR and SSGR.[23-25] In the SSGR consecutive opposite slice selective gradients are applied on consecutive radiofrequency pulses, which are centered on the water section, resulting in a reduction of the excited fat section and consequently of the fat signal intensity.[26] For anatomical reference a four-point mDIXON fast field echo sequence was used (MS-FFE, bandwidth = 434 Hz/pixel, T_R = 210 ms, T_E = 2.60, 3.36, 4.12 and 4.88 ms, matrix = 320 × 184, voxel size = 1.5 × 1.5 × 6 mm^3, number of slices = 31, SENSE = 2), a noise map to calculate signal-to-noise ratios (SNRs) (SE-EPI without diffusion weighting, T_R = 5000 ms, T_E = 57 ms, matrix = 160 × 160, voxel size = 3 × 3 × 6 mm^3, number of slices = 31, SENSE = 1.9, SPIR/SPAIR/SSGR), as well as a multi-turbo spin-echo sequence for quantitative water T_2-mapping and a fat-suppressed T_2-weighted scan to assess acute muscle damage. For the purpose of this study, the diffusion-weighted spin-echo EPI, noise scan and Dixon acquisitions were considered.

DTI parameter estimations

MR images were analyzed using QMRITools for Wolfram Mathematica (https://mfroeling.github.io/QMRITools). Diffusion data were de-noised using a principal component analysis (PCA) noise algorithm, and corrected for motion and eddy currents using affine registration (elastix: http://elastix.isi.uu.nl). Second, the diffusion data were registered to the anatomical space using sequential rigid and B-spline registration to correct for EPI distortions. The diffusion tensor was calculated using an intra-voxel incoherent motion (IVIM)-based iterative weighted linear least squares algorithm (iWLLS).[27] By using IVIM correction, an anisotropic pseudo-diffusion component was modeled in addition to the standard diffusion tensor, to remove the perfusion biases in the diffusivity estimation,[28] as explained in the study by Hooijmans *et al.*.[10] The third eigenvalue (λ_3), mean diffusivity (MD) and fractional anisotropy (FA) were used as outcome parameters and shown as mean values over the full muscle volume. Previous studies[10] have shown that λ_3 is the most sensitive DTI parameter to training, whereas MD and FA show the highest and the lowest repeatability respectively.[29] SNR was defined as the mean of the signal in a muscle region of interest divided by the standard deviation of the noise (σ). Muscles with an SNR value below 15 were excluded from the Bland-Altman and linear regression analyses.

Manual segmentation

Manual segmentation was considered the ground truth for the comparisons with the results of the supervised segmentations. Manual segmentations of 10 muscles in both upper legs, i.e. biceps femoris short head (BFSH), biceps femoris long head (BFLH), semitendinosus (ST), semimembranosus (SM), gracilis (G), sartorius (S), vastus medialis (VM), vastus lateralis (VL), vastus intermedius (VI) and rectus femoris (RF) muscles were performed by two experts in muscle anatomy (MH, JM) on the out-of-phase Dixon images in ITK-SNAP (www.itksnap.org). These segmentations were done for all subjects at baseline and the two post-marathon time points. Delineation of the muscles was done avoiding fascia and subcutaneous fat tissue. Additionally, they were eroded by one pixel to avoid partial volume effects due to fat tissue. The segmentations were subsequently registered (elastix: http://elastix.isi.uu.nl) to the DTI acquisitions to correct for misalignments between the Dixon and the lower-resolution diffusion scans. The time required for the manual segmentation of one dataset including the whole set of muscles in two legs for a single time point was on average 420 min.

Supervised segmentation

Segmentation of the muscles was performed on the out-of-phase Dixon images, as schematically illustrated in Figure 1. The first step of the supervised segmentation started with a manual segmentation of the muscles in a limited number of slices within the full muscle volume, whereas in the study by Ogier *et al.*[21] muscles were delineated in the muscle belly in two slices 10 cm above the knee and 10 cm below the hip, respectively. Additional manual segmentations were performed in slices for which the muscle changes drastically in size by more than 30 pixels, and at the muscle's origin and insertion. Subsequently, an N4 bias correction algorithm[30] was used on all data sets. After this, the segmentation was automatically completed based on a propagation algorithm, named transversal propagation, which uses both shape information from the initial manual segmentations and grayscale anatomical information to follow the anatomical variations of muscles along the leg, as described by Ogier *et al.*.[21] Because of the differences in size and shape between the 10 upper-leg muscles and between subjects, the number of manually segmented slices differed between muscles and subjects (see Section 3). We refer to the segmentation of the muscles in a single subject as the transversal propagation step. For the post-marathon and follow-up time points, the manual segmentation of selected slices could be omitted. Instead, both post-marathon and follow-up segmentations were obtained by automatic propagation of the baseline segmentation. This so-called longitudinal propagation step, implemented with the ANTs library,[21] as described by Ogier *et al.*,[22] consisted of a robust registration process with rigid and affine optimized transformations, followed by a diffeomorphic multi-level registration with B-spline regularization ρ. The registration

parameters were: multi-resolution levels = 4, gradient step = 0.1, shrink-factors = 6 × 4 × 2 × 1, smoothing sigmas = 3 × 2 × 1 × 0 voxels, number of iterations per level = 100 × 70 × 50 × 10, convergence threshold = 10^{-6}, window size = 10 iterations. The knot spacing for the B-spline smoothing was set at 26 mm at the base resolution level of the update displacement field and it was reduced by a factor of two for each succeeding multi-resolution level. The described regularization ρ was applied at all dataset time points in order to correct for muscle shape deformations between two acquisition sessions, typically caused by difference in positioning and eddy currents. After the registration was completed, nearest-neighbor interpolation was applied to restore the original integer values of the segmentation labels. All the computations were performed by means of an Intel Xeon E5-2620 v4 processor.

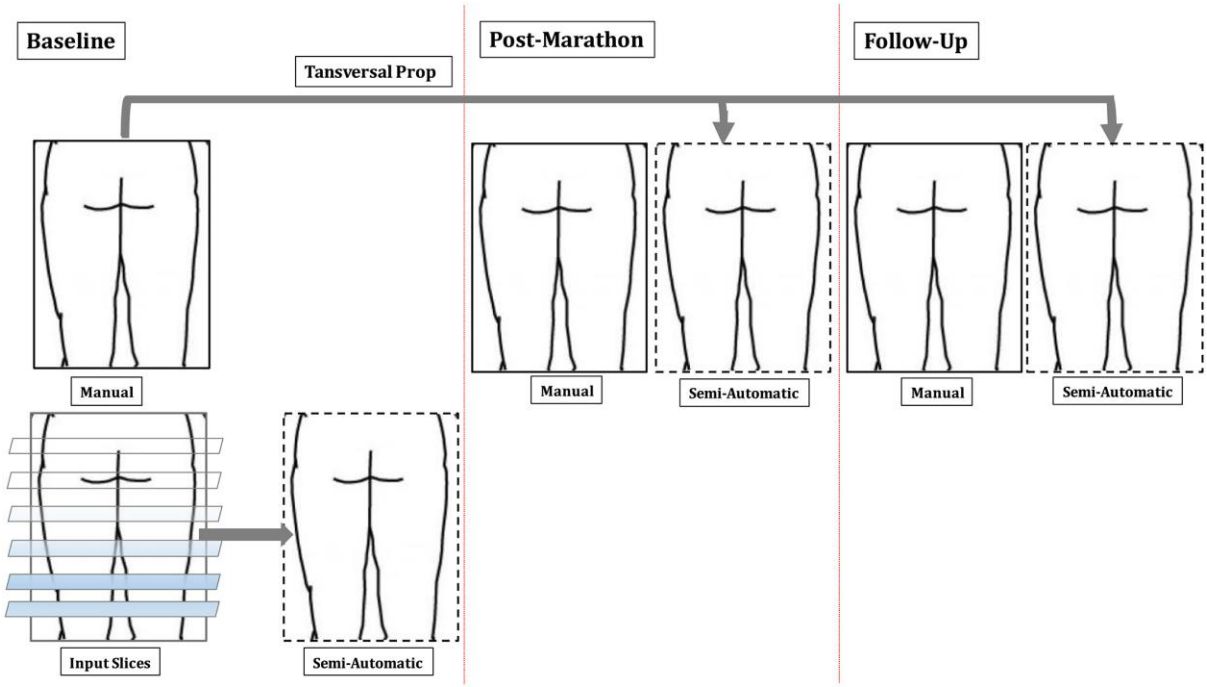

Figure 1: *Schematic of the study set-up. DTI measurements were performed at 3 time points, i.e. at baseline, 24-48 hrs. post-marathon and at a 2 weeks follow-up. Manual segmentations were performed for 10 muscles in both upper legs at all 3 time points. At baseline, a supervised semi-automatic segmentation was performed based on a selected set of manually segmented slices (transversal propagation). For the post-marathon and the follo-up time points the segmentation was automatically propagated without further manual input (longitudinal propagation)*

Validation

To rate the quality of the supervised segmentation for the extraction of DTI indices, we considered several metrics. The volume similarity was assessed for each muscle in each dataset via the DSC[31] for the propagated regions only, thus excluding the manually segmented slices used for input. To assess

differences between manual and supervised automatic segmentations on the quantification of DTI indices, we focused on MD, FA and λ_3. These DTI indices were calculated for all upper leg muscles using (i) the manual segmentations, (ii) the supervised automatic segmentations excluding the manually delineated slices and (iii) the full supervised automatic segmentations. The latter two were used to evaluate both the impact of the automatic propagation on DTI parameter estimations, as well as to consider the final complete supervised segmentation in comparison to the manual gold-standard segmentation. Differences between manual and automatic segmentations were assessed by Bland-Altman analysis and linear regression of the DTI indices.

Segmentation time

Individual muscles differ in their anatomical shape, aponeurosis locations, amounts of connective tissue and intra- and inter-muscular fat. The muscle delineation complexity therefore varied between different muscles and between different subjects. In the transversal propagation, the operator performed the manual segmentations in a selected number of slices, as described above. Consequently, the time required for segmentation differed between muscles and was calculated from the number of slices that were manually delineated compared with the total number of slices in a given muscle. The mean values and the standard error of the time saved as a percentage are reported for each muscle.

Results

The transversal and longitudinal supervised segmentations were successfully executed for all 11 subjects. A transversal and longitudinal propagation of the segmentations of a representative subject are visualized in Figure 2, also indicating the manually segmented slices used as input for the transversal propagation. Figure 3 shows the comparison of the changes of the DTI indices between manual and supervised segmentations of three muscles for a representative subject at baseline, post-marathon and follow-up time points. Visual assessment of the graphs showed excellent correspondence for the DTI indices between manual and supervised automatic segmentations.

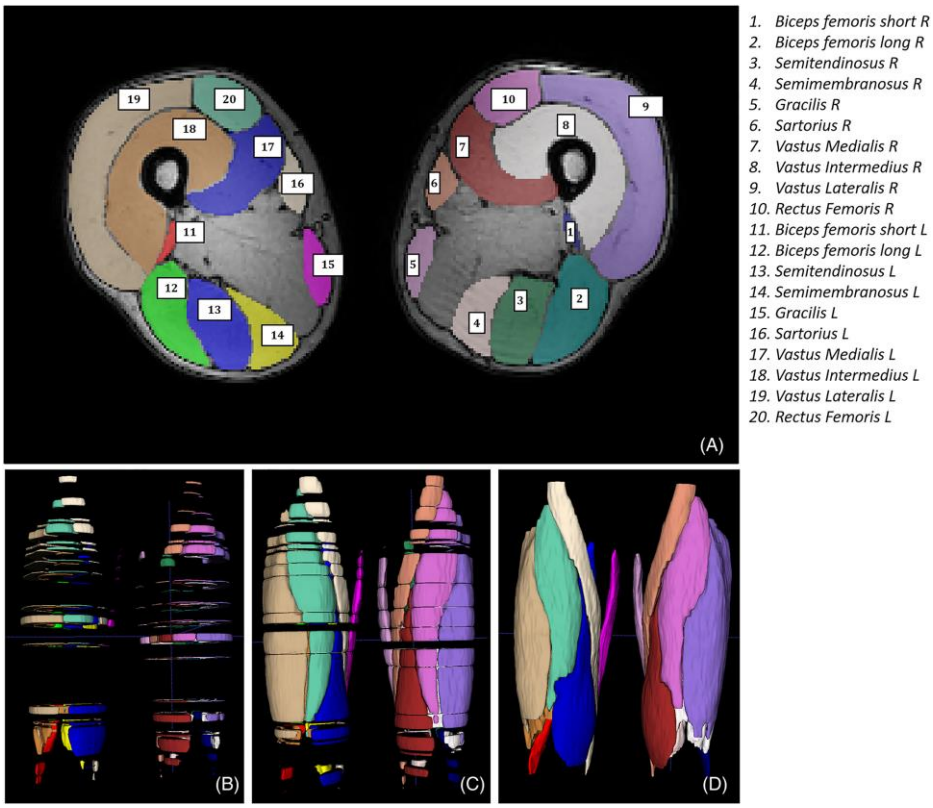

Figure 2: *Anterior view of upper leg muscle segmentations, where knees are at the bottom and hips at the top of the image. (A) Transversal slice, approximately halfway between knee and hip, showing segmentations of the 10 muscles considered in this study in both legs, for example, 21 slices for the BFLH muscle in this subject. (B) Longitudinal views of the upper legs with an example of input segmentations at baseline. Adjacent slices were selected as input when muscle shape changed. (C) Propagations resulting from the transversal propagation step. (D) The full volumes obtained with the transversal propagation step*

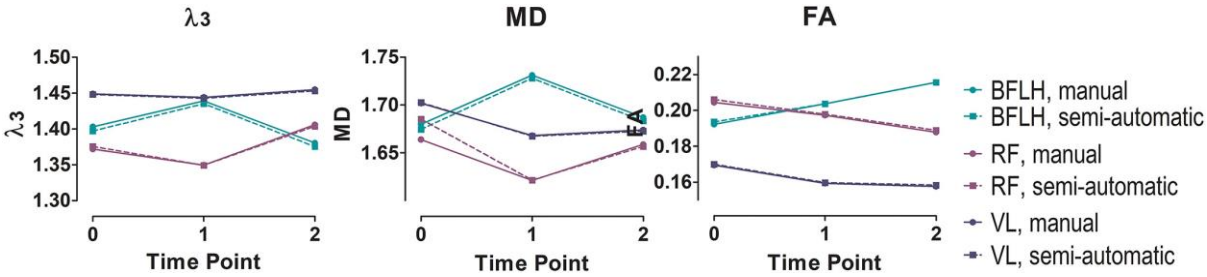

Figure 3: *Comparison of the manual and supervised semi-automatic segmentations of the mean values of λ_3, MD and FA for the BFLH, RF and VL muscles of a representative subject at baseline, post-marathon and follow-up time points*

DSC values

DSC values calculated for the comparison between manual segmentation and the supervised segmentations of all analyzed muscles, excluding the manually segmented slices, for the three time points are shown in Figure 4. For the transversal propagation step, the DSC values for different subjects and muscles ranged between 0.62 and 0.95 (Figure 4 left), with 70% of the DSC values above 0.90. The DSC values for the volumes obtained through the longitudinal registration process ranged between 0.48 and 0.98 (with 68% above 0.90) for the post-marathon time point and between 0.59 and 0.99 (with 76% above 0.90) at follow-up (Figure 4 middle, right). In the transversal propagation the muscles that scored the highest and lowest DSC values were VI (0.94 ± 0.01) and G (0.87 ± 0.07) respectively. Similarly, in the longitudinal propagations the muscles with the highest and lowest DSC values were VI (post-marathon 0.95 ± 0.03, follow-up 0.96 ± 0.03) and G (post-marathon 0.82 ± 0.16, follow-up 0.88 ± 0.11).

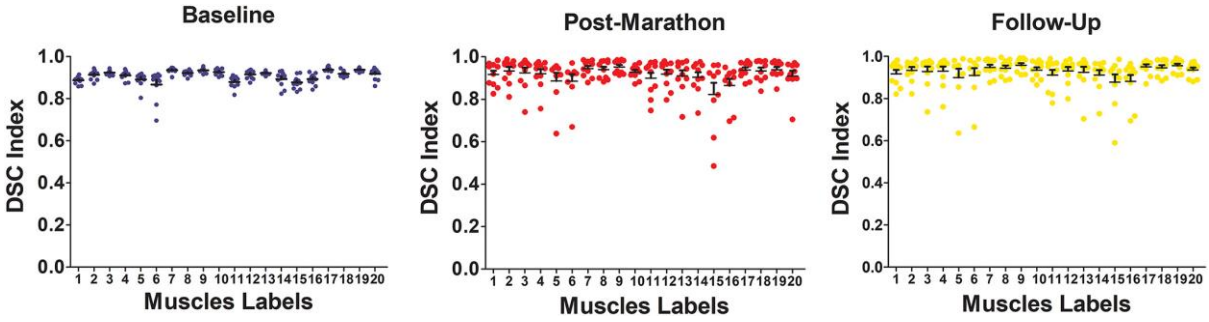

Figure 4: *DSCs for the supervised segmentations compared with the manual segmentations for the baseline (4A in blue), post-marathon (4B in red) and follow-up (4C in yellow) time points for all the segmented muscles. The numbers correspond to the muscles listed in Figure 2. Each dot reflects an individual subject and the group mean and standard deviation are shown in black*

Linear regression analysis

The G and S muscles were excluded from this part of the analysis because of low SNR (<15) in the diffusion images. The linear regression of mean λ_3, MD and FA in the 16 muscle volumes (two legs, eight muscles each) obtained with supervised automatic segmentation versus the values obtained with manual segmentation, excluding the S and G muscles, resulted in r^2 values of 0.99 and $p < 0.0001$ for all indices at all time points (Figure 6 top, baseline; Figure 7 top, post-marathon; Figure 8 top, follow-up). By including the muscles with low SNR (S and G muscles) r^2 values were lower, 0.98 (λ_3), 0.91 (MD) and 0.99 (FA) at baseline, respectively ($p < 0.0001$), whereas at post-marathon r^2 values were 0.96 (λ_3), 0.91 (MD) and 0.94 ($p < 0.0001$) and at follow-up r^2 values were 0.95 (λ_3), 0.95 (MD) and 0.99 (FA) ($p < 0.0001$).

Bland-Altman analysis

Bland-Altman analysis were carried out for the three different time points separately by considering the mean values of MD, FA and λ_3 of each segmented muscle with sufficient SNR of each participant. The derived 95% limits of agreement (LoAs) are reported in Table 1. At baseline, the 95% LoA ranged between 0.5% and 1.5% in the full volumes and between 0.7% and 3% excluding manual segmentations (Figure 6 bottom). The bias ranged between −0.0008 and 0.0010. At post-marathon and follow-up, the LoA ranged between 0.7% and 3.1% (Figure 7 bottom and Figure 8 bottom) with the bias between −0.0005 and 0.0016. The best agreement was presented by λ_3. At baseline, some distinct outliers were observed in the Bland-Altman plots (Figure 7). Outliers in λ_3 corresponded to the BFLH right leg. Some outliers in MD were generated by the right and left SM and the left RF. When including the manually segmented slices no outliers were observed.

Table 1: *95% LoAs, the LoA percentage with respect to the mean resulting from the Bland-Altman analysis and the bias of the DTI parameters of the supervised and manual muscle segmentations at the THREE time points*

DTI parameter	Baseline full volume			Baseline excluding manual segmentations			Post-marathon			Follow-up		
λ_3 ($10^{-3}mm^2/s$)	[−0.008 0.008]	0.5%	0.0003	[−0.016 0.020]	0.7%	0.0010	[−0.016 0.019]	0.7%	0.0016	[−0.012 0.014]	0.7%	0.0011
MD ($10^{-3}mm^2/s$)	[−0.023 0.023]	1.2%	−0.0008	[−0.030 0.031]	1.8%	0.0002	[−0.026 0.031]	1.7%	0.0023	[−0.032 0.034]	1.8%	−0.0003
FA (—)	[−0.003 0.003]	1.5%	−0.0003	[−0.006 0.005]	3.0%	−0.0004	[−0.006 0.005]	3.0%	−0.0005	[−0.006 0.005]	3.1%	0.0007

Input slices and segmentation time

The percentage of slices for which manual segmentation was required at baseline, prior to transversal and longitudinal propagation, is shown in Figure 5. On average only 30% of the slices needed to be manually segmented at baseline, thus resulting in more than three times faster segmentations at baseline and 10 times faster for the three time points. The BFSH of the right leg required the most manual segmented slices, the BFLH of the left leg the fewest. Figure 5 shows that the numbers of manually segmented slices of the same muscle in the right and left legs are in the same range.

Furthermore, for the longitudinal segmentation the reduction in time is even greater, as these required no additional manual segmentations.

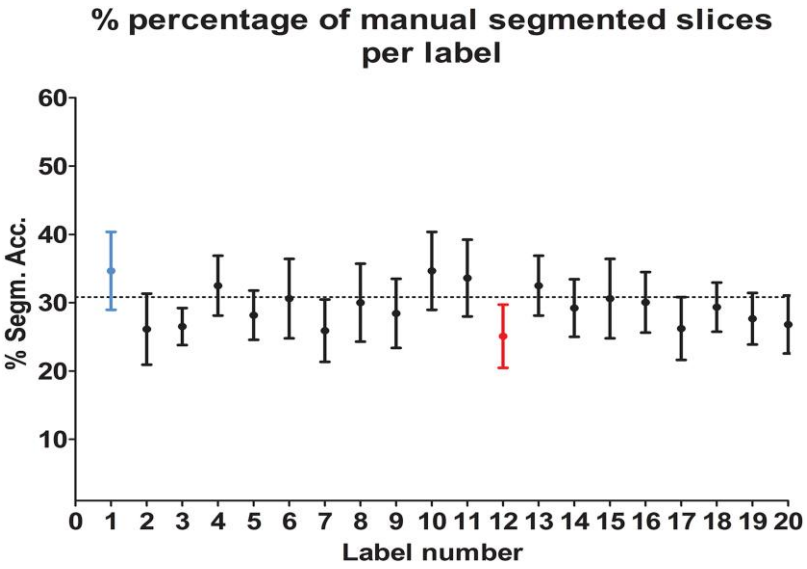

Figure 5: *Percentage of segmented slices used for transversal propagation at baseline for the individual muscles. The BFSH of the right leg (blue) required the most manual segmented slices; the BFLH of the left leg (red) the fewest. Each point represents the mean and the range of the segmentation acceleration. The dotted line represents the average acceleration time.*

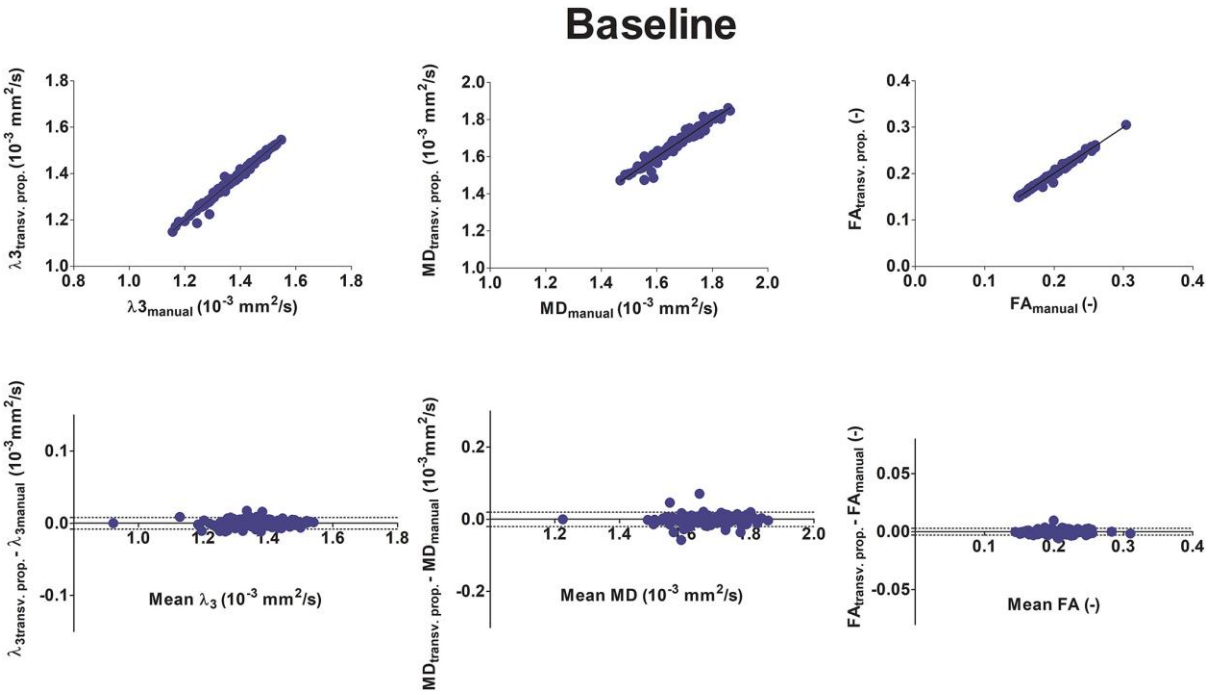

Figure 6: *Linear regression analysis (top) and Bland-Altman plot (bottom) at baseline of diffusion indices λ_3 (10^{-3}mm^2/s), MD (10^{-3} mm^2/s) and FA (—) comparing manual segmentation with those resulting from the transversal propagations.*

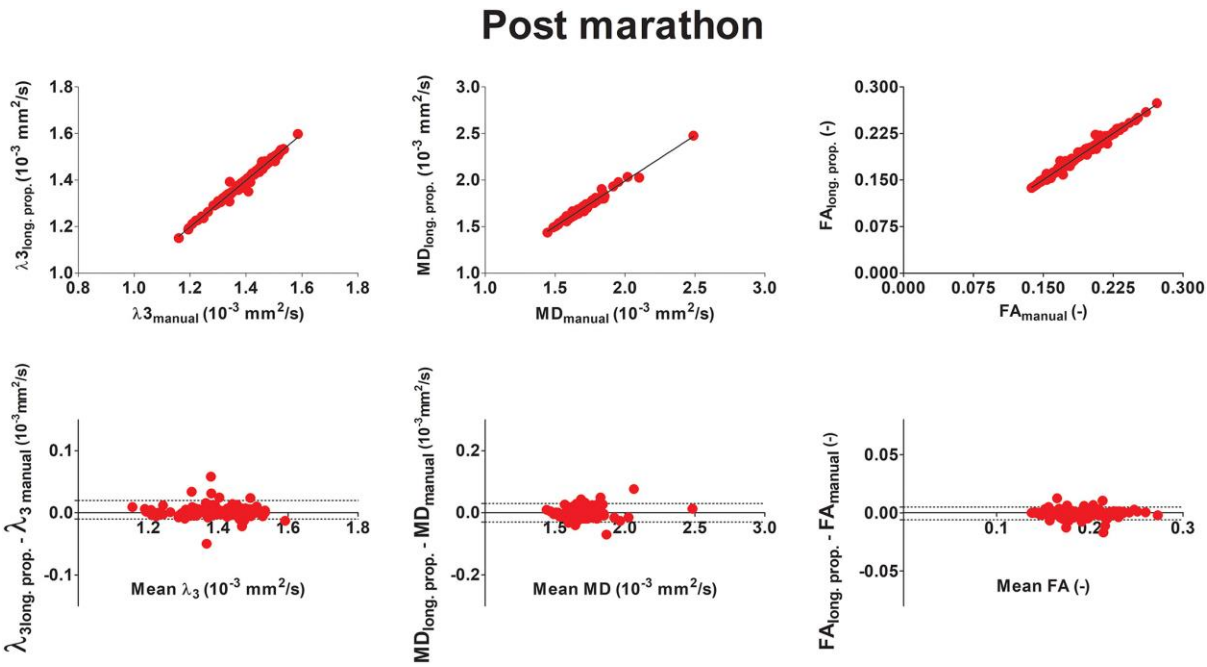

Figure 7: *Linear regression analysis (top) and Bland-Altman plot (bottom) post-marathon of diffusion indices λ_3 (10^{-3}mm^2/s), MD (10^{-3} mm^2/s) and FA (—) comparing manual segmentation with those resulting from the longitudinal propagations*

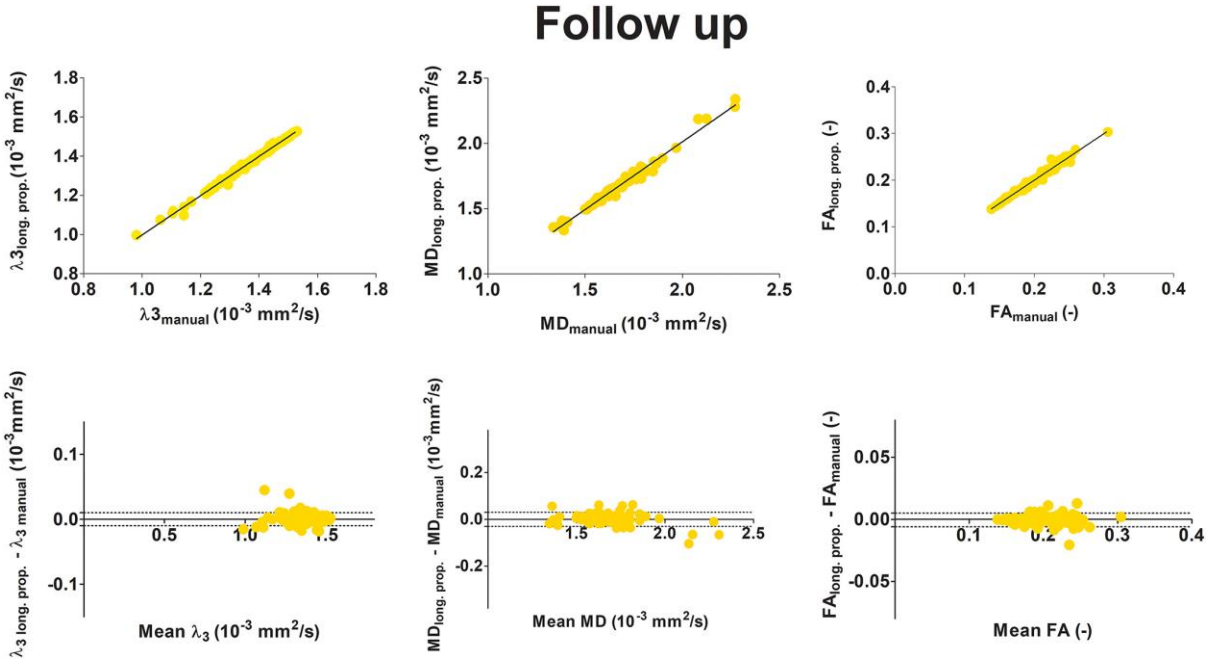

Figure 8: *Linear regression analysis (top) and Bland-Altman plot (bottom) at follow-up of diffusion indices λ_3 (10^{-3}mm^2/s), MD (10^{-3} mm^2/s) and FA (—) comparing manual segmentation with those resulting from two longitudinal propagation steps*

Discussion

DTI is becoming increasingly popular to study muscle injury and disease, as the diffusion indices provide a direct window into muscle fiber integrity and architectural organization.[4, 5] For quantitative analysis of changes in diffusion values, segmentation of individual muscles is required. Such segmentations are often performed manually,[12] which is a time-consuming, laborious and an operator-dependent process. This study aimed to evaluate the impact of a supervised semi-automatic segmentation framework on the quantification of DTI indices in the upper leg muscles. Compared with the conventional manual segmentation approach, similar DTI indices were found using this supervised semi-automatic segmentation framework, as represented by high LoAs and r^2 values. Furthermore, this study showed that the segmentation time of the entire muscle volume can be three times faster for a single time point without significant impact on the quantification of DTI indices, which we believe is an important step to more widespread application of DTI to study muscle injury and disease. In addition, the time saving for multiple time points is even larger (10-fold for three time points), given that no further manual delineations are needed.

The Dice similarity coefficient was, with a few outliers, consistently high when comparing manual and supervised segmentations. These results agree with the previous results that were obtained by Ogier *et al.,*[22] who reported a DSC of 0.91 for the transversal propagation and 0.88 for the longitudinal propagation. Interestingly, for most of our muscles, with the exception of the smaller muscles with a more changeable cross-sectional area in the proximal-distal direction (S and G muscles), even better similarity indexes were found. We have not yet characterized with certainty the reasons why some muscles are less well propagated at post-marathon and follow-up in comparison with baseline, but the factors that might have influenced the results are the differences in the semi-automatic and automatic segmentation methods applied, the muscle shape deformation between two acquisition sessions and the muscle size, because both G and S, the two smallest muscles in the upper leg, showed the lowest Dice coefficient. However, more importantly, in this longitudinal study we also evaluated the impact of automatic segmentation on the quantification of the muscle DTI indices. The Bland-Altman analysis resulted in excellent LoA values (maximum of 3% for FA) and low bias (maximum of 0.4% for FA in the transversally propagated volumes). These ranges can be compared with the changes in muscle DTI parameters that are normally expected in muscle injury and disease. For example, changes in DTI indices reported after physical activity, such as a triathlon[8] or a marathon,[9] are generally larger than the 95% LoAs reported above. Also, the changes in DTI indices

observed in the presence of musculoskeletal diseases, as shown in the study by Maggi *et al.*[7] in patients with muscular dystrophy (FA varies by 8.4%), are larger than the 95% LoA found in our work. In the study by Sigmund *et al.*[6] in dermatomyositis patients, MD in the quadriceps muscles varied by 1.7%, which is smaller than the 95% LoA we found over all analyzed muscles. However, in our work the quadriceps muscles showed the best correspondence with manual segmentation. Consequently, when considering our LoA for quadriceps muscles only, even these changes could be quantified. However, this would not be the case for the other muscle groups. This indicates that by using the proposed semi-automatic segmentation method the changes in DTI indices that are due to physical activity and certain diseases, such as muscular dystrophy, remain detectable, whereas smaller changes due to other pathologies, such as dermatomyositis, cannot be detected in all muscle groups.

It is furthermore interesting to review some of the input requirements and time savings using this supervised semi-automatic segmentation framework. At baseline, only 30% of the slices were required as input for the supervised segmentation compared with the full manual segmentation, reducing the time spent for manual delineation of muscle outlines for a full segmentation of 10 muscles in both upper legs from 840 min to 140 min. Furthermore, the segmentations of the post-marathon and follow-up time points were obtained directly from the baseline, without additional need of manual delineation of the muscles. This makes the segmentation process in larger cohort studies much more manageable, especially in longitudinal studies. However, for this comparison, we did not include the computer processing time for the transversal and longitudinal propagation steps that can be executed without further user interaction in the background. These steps do require time, which strongly depends on the computer processor (ie of the order of 120 min for the transversal propagation and 300 min for the longitudinal propagation using an Intel Xeon E5-2620 v4 processor). For the transversal propagation at baseline it was important that a sufficient number of slices were manually segmented in those regions with large changes in muscle cross-section, typically at the muscle origin and insertion. The selection of these slices based on muscle shape variations is a subjective factor in the transversal segmentation process that could lead to user-dependent performance. In fact, in comparison with the study by Ogier *et al.*[22], for the sake of robustness we segmented a higher percentage of slices manually than strictly necessary, leading to less reduction in segmentation time (70% in our study as compared with 85% by Ogier *et al.*). This difference is mainly due to the fact that in this study the supervised semi-automatic segmentation framework was applied to segment the full muscle volume, while in the study by Ogier *et al.* the most distal muscle regions (10 cm above the knees) were not segmented.

Over the past years, some other semi-automatic and fully automated segmentation methods for skeletal muscle have been proposed. These methods use non-rigid multi-atlas registration or convolutional neural networks (CNNs) and have primarily focused on specific locations in the upper leg muscles[13-15] rather than full volumetric analysis.[16] Furthermore, these methods have also been used to determine muscle volume and to extract fat fractions. One of these previous studies, by Kemnitz *et al.*,[14] compared active shape model (ASM) and active contour model (ACM) approaches at mid-thigh level and showed that the precision of the technique was higher for the quadriceps muscles (DSC values of 0.93 and 0.94) than for the hamstring muscles (DSC values of 0.87 and 0.89) and lowest for the S muscle (DSC values of 0.74 and 0.82). These findings are in agreement with our results, where we found high DSC values for the quadriceps and hamstring muscles and lowest for the G and S muscles. The CNN approach proposed by Kemnitz *et al.*[13, 15] proved to be the fastest approach, less than 1 s per slice, and was also very precise (average DSC value 0.98). However, it is important to note that both methods described above have been trained only for a particular anatomical location rather than for the segmentation of the full volume of individual muscles; moreover, no volumetric analysis was reported. Another approach that has been used is the AMRA automatic segmentation technique developed at Linköping University. This approach is based on non-rigid multi-atlas registration on water fat Dixon images[18] and was used to evaluate automatic quantification of fat fraction and volume increases in the quadriceps muscle group[16]. This study[18] showed very good correlation with the manual segmentation of the estimated volumes of the quadriceps muscles, with $r = 0.98$ and $p < 0.0001$. These values are in the same range as what we found for the DTI indices determined in individual muscles rather than in a muscle group. Unfortunately, no information is given concerning other muscle groups or individual muscles.

This study has some limitations. First, the manual segmentation of the input slices was performed only once, by two albeit expert observers, because the manual segmentation is very time consuming and laborious, and requires quite some experience and anatomical knowledge. Therefore, the intra-observer reproducibility was not tested at this point. Second, thus far, we have only focused on the impact of supervised segmentation on DTI quantification using whole muscle segmentations. The impact of semi-automatic segmentation on quantification could vary along the proximo-distal muscle axis and therefore affect more localized assessments in a different manner. Additionally, in this work only healthy muscle tissue has been evaluated. Pathophysiological changes due to injury or disease alter image contrast and could impact the performance of the supervised semi-automatic segmentation framework. Future studies will include localized muscle damage to evaluate how well the propagation algorithms perform under these circumstances.

Conclusion

The purpose of the present study was to evaluate a supervised muscle segmentation framework developed by Ogier *et al.*,[21, 22] for the quantification of DTI indices in individual muscles of the thighs. Using this tool, we assessed the accuracy, feasibility and impact on the quantification of DTI indices in comparison with manual segmentation as well as the reduction in work load compared with manual segmentation. Linear regression and the Bland-Altman analysis of the DTI indices showed good agreement between the results obtained with manual segmentation and the results obtained with the supervised muscle segmentation framework. The work load and segmentation time were reduced threefold at baseline compared with manual segmentation and the segmentation of post-marathon and follow-up time points was completely automated. The proposed semi-automatic segmentation method for the detection of changes in DTI indices that are due to physical activity and diseases proved fast, feasible, accurate, reproducible and less operator dependent.

References

1. Saifuddin A, Tyler P, Hargunani R. *Musculoskeletal MRI*. CRC Press; 2016.
2. de Mello R, Ma Y, Ji Y, Du J, Chang EY. Quantitative MRI musculoskeletal techniques: an update. *Am J Roentgenol*. 2019; 213(3): 524- 533.
3. Damon BM, Froeling M, Buck AK, et al. Skeletal muscle diffusion tensor-MRI fiber tracking: rationale, data acquisition and analysis methods, applications and future directions. *NMR Biomed.*2017; 30(3):e3563.
4. Froeling M, Nederveen AJ, Heijtel DF, et al. Diffusion-tensor MRI reveals the complex muscle architecture of the human forearm. *J Magn Reson Imaging*. 2012; 36(1): 237- 248.
5. Hooijmans MT, Damon BM, Froeling M, et al. Evaluation of skeletal muscle DTI in patients with Duchenne muscular dystrophy. *NMR Biomed.* 2015; 28(11): 1589- 1597.
6. Sigmund EE, Baete SH, Luo T, et al. MRI assessment of the thigh musculature in dermatomyositis and healthy subjects using diffusion tensor imaging, intravoxel incoherent motion and dynamic DTI. *Eur Radiol.* 2018; 28(12): 5304- 5315.
7. Maggi L, Moscatelli M, Frangiamore R, et al. Quantitative muscle MRI protocol as possible biomarker in Becker muscular dystrophy. *Clin Neuroradiol*. 2020; 30(1): 875– 885. https://doi.org/10.1007/s00062-019-00875-0
8. Keller S, Yamamura J, Sedlacik J, et al. Diffusion tensor imaging combined with T2 mapping to quantify changes in the skeletal muscle associated with training and endurance exercise in competitive triathletes. *Eur Radiol*. 2020; 30: 2830- 2842.
9. Froeling M, Oudeman J, Strijkers GJ, et al. Muscle changes detected with diffusion-tensor imaging after long-distance running. *Radiology*. 2015; 274(2): 548- 562.
10. Hooijmans MT, Monte JR, Froeling M, et al. Quantitative MRI reveals microstructural changes in the upper leg muscles after running a marathon. *J Magn Reson Imaging*. 2020; 52(2): 407- 417.
11. Charles JP, Suntaxi F, Anderst WJ. In vivo human lower limb muscle architecture dataset obtained using diffusion tensor imaging. *PLoS ONE* 2019; 14(10):e0223531. https://doi.org/10.1371/journal.pone.0223531
12. Barnouin Y, Butler-Browne G, Voit T, et al. Manual segmentation of individual muscles of the quadriceps femoris using MRI: a reappraisal. *J Magn Reson Imaging*. 2014; 40(1): 239- 247.
13. Kemnitz J, Baumgartner CF, Ruhdorfer A, et al. Clinical validation of fully automated segmentation of thigh muscle and adipose tissue cross sectional areas using machine learning with a convolutional neural network. *Osteoarthr Cartil*. 2019; 27: S383- S384.
14. Kemnitz J, Eckstein F, Culvenor AG, et al. Validation of an active shape model-based semi-automated segmentation algorithm for the analysis of thigh muscle and adipose tissue cross-sectional areas. *Magn Reson Mater Phys Biol Med*. 2017; 30(5): 489- 503.
15. Kemnitz J, Baumgartner CF, Eckstein F, et al. Clinical evaluation of fully automated thigh muscle and adipose tissue segmentation using a U-Net deep learning architecture in context of osteoarthritic knee pain. *Magn Reson Mater Phys Biol Med*. 2020; 33(4): 483- 493. https://doi.org/10.1007/s10334-019-00816-5
16. Mandić M, Rullman E, Widholm P, et al. Automated assessment of regional muscle volume and hypertrophy using MRI. *Sci Rep*. 2020; 10: 2239– 2246. https://doi.org/10.1038/s41598-020-59267-x
17. Gyftopoulos S, Lin D, Knoll F, Doshi AM, Rodrigues TC, Recht MP. Artificial intelligence in musculoskeletal imaging: current status and future directions. *Am J Roentgenol*. 2019; 213(3): 506- 513.
18. Thomas MS, Newman D, Leinhard OD, et al. Test-retest reliability of automated whole body and compartmental muscle volume measurements on a wide bore 3T MR system. *Eur Radiol*. 2014; 24(9): 2279- 2291.

19. Mesbah S, Shalaby A, Stills S, et al. A novel automatic segmentation method to quantify the effects of spinal cord injury on human thigh muscles and adipose tissue. In: M Descoteaux, L Maier-Hein, A Franz, P Jannin, DL Collins, S Duchesne, eds. *Medical Image Computing and Computer-Assisted Intervention—MICCAI 2017*. Vol 10434. Cham, Switzerland: Springer; 2017: 703- 711.
20. Gadermayr M, Li K, Müller M, et al. Domain-specific data augmentation for segmenting MR images of fatty infiltrated human thighs with neural networks. *J Magn Reson Imaging*. 2019; 49(6): 1676- 1683.
21. Ogier A, Sdika M, Foure A, Le Troter A, Bendahan D. Individual muscle segmentation in MR images: a 3D propagation through 2D non-linear registration approaches. In *2017 39th Annual International Conference of the IEEE Engineering in Medicine and Biology Society (EMBC). IEEE* 2017: 317- 320. https://doi.org/10.1109/EMBC.2017.8036826
22. Ogier AC, Heskamp L, Michel CP, et al. A novel segmentation framework dedicated to the follow-up of fat infiltration in individual muscles of patients with neuromuscular disorders. *Magn Reson Med*. 2020; 83(5): 1825- 1836.
23. Williams SE, Heemskerk AM, Welch EB, Li K, Damon BM, Park JH. Quantitative effects of inclusion of fat on muscle diffusion tensor MRI measurements. *J Magn Reson Imaging*. 2013; 38(5): 1292- 1297. https://doi.org/10.1002/jmri.24045
24. Lee W, Lim SL, Ho JXM, Rumpel H. Fat-suppressed magnetic resonance imaging—how to do it perfectly. *MAGNETOM Flash.* 2019;(74): 43- 51.
25. Visser F. Application tip. Optimizing SPIR and SPAIR fat suppression. *Philips NetForum Community.* 2004. http://clinical.netforum.healthcare.philips.com (Accessed June 20, 2020).
26. Nagy Z, Weiskopf N. Efficient fat suppression by slice-selection gradient reversal in twice-refocused diffusion encoding. *Magn Reson Med*. 2008; 60(5): 1256- 1260. https://doi.org/10.1002/mrm.21746
27. De Luca A, Bertoldo A, Froeling M. Effects of perfusion on DTI and DKI estimates in the skeletal muscle. *Magn Reson Med*. 2017; 78(1): 233- 246.
28. Shlaffke L, Rehmann R, Rohm M, et al. Multi-center evaluation of stability and reproducibility of quantitative MRI measures in healthy calf muscles. *NMR Biomed.* 2019; 32(9):e4119.
29. Monte JR, Hooijmans MT, Froeling M, et al. The repeatability of bilateral diffusion tensor imaging (DTI) in the upper leg muscles of healthy adults. *Eur Radiol.* 2020; 30(3): 1709- 1718. https://doi.org/10.1007/s00330-019-06403-5
30. Tustison NJ, Avants BB, Cook PA, et al. N4ITK: improved N3 bias correction. *IEEE Trans Med Imaging.* 2010; 29(6): 1310- 1320.
31. Dice LR. Measures of the amount of ecologic association between species. *Ecology*. 1945; 26(3): 297- 302. https://doi.org/10.2307/1932409

CHAPTER 3

A diffusion tensor-based method facilitating volumetric assessment of fiber orientation in skeletal muscle

Laura Secondulfo

Melissa T. Hooijmans

Jozef J. M. Suskens

Valentina Mazzoli

Mario Maas

Johannes L. Tol

Aart J. Nederveen

Gustav J. Strijkers

PLoS One, 2022

Abstract

The purpose of this chapter is to illustrate a DTI-based method which was developed to quantitatively assess fiber angles (or 'fiber fascicle orientations') and changes therein in leg muscles without the need for performing manual and labor-intensive fiber-tractography, to facilitate longitudinal studies on muscle fiber architectural adaptations in healthy subjects. Please note that in this thesis the terms 'fiber angles' and 'fiber fascicle orientations' are used interchangeably.

The upper legs of five volunteers were scanned twice on the same day. The right lower legs of five volunteers were scanned twice with the ankle in three positions, i.e. -15° dorsiflexion, 0° neutral position, and 30° plantarflexion. The MRI protocols consisted of a noise scan, a 3-point mDixon scan and a DTI scan. Fiber-angle color maps were generated for four muscles in the upper legs and two muscles in the lower leg. Voxel-wise fiber angles (θ) were calculated from the angle between the principal eigenvector of the diffusion tensor and a reference line defined between the origo and insertion points of each muscle. Bland-Altman analysis, intraclass correlation coefficient (ICC), coefficient of variation (CV%), minimal detectable change (MDC), standard error (SE) and Friedman test were used for assessing the feasibility of this method and in order to have an indication of the repeatability and the sensitivity.

Bland-Altman analysis showed good repeatability (CV%<10 and 0.7≤ICC≤0.9) with exception of the Tibialis Anterior (TA) muscle in dorsiflexion position(CV%: 12.2) and the Semitendinosus (ST) muscle (left leg) (CV%: 11.4). The best repeatability metrics were found for the Soleus (SOL) muscle in neutral position (CV%: 2.6). Changes in average θ in TA and SOL with ankle positions were observed in accordance with expected agonist and antagonist functions of both muscles. For example, for the anterior left compartment the change in fiber angle Δθ with respect to the neutral position Δθ = -1.6° ± 0.8° and 2.2 ± 2.8° (p = 0.008), for dorsiflexion and plantarflexion, respectively.

Our method facilitates fast inspection and quantification of muscle fiber angles in the lower and upper leg muscles in rest and detection of changes in lower-leg muscle fiber angles with varying ankle angles.

Introduction

Muscle fiber architecture is a dominant determinant of muscle functioning in terms of tension, exertable force, response to physical exercise, as well as vulnerability to muscle injury and disease.[1] Biomechanical metrics for muscle force prediction include muscle contractile volume, fiber length and fiber angles (pennation angles). The study of changes in muscle architecture following intervention, training and response to therapy allows for a better understanding of the relationship between muscle architectural adaptations and function.[2,3]

In clinical practice, the most commonly used definition of pennation angle is the two dimensional (2D) pennation angle between the muscle fascicles and the aponeurosis or tendon[4] in a specific location of the muscle. Another used definition of pennation angle in 2D is the angle between the muscle fascicles and the line of action of the tendon.[4] This definition is useful but it lacks three-dimensional information of the full muscle volume. A quantitative volumetric assessment is needed when there is no a priori knowledge concerning the location of expected changes in muscle architecture due to training or response to treatment. Less common in clinical practice but very useful in biomechanics for the estimation of muscle force are the definitions of pennation angle in three-dimensional volume, in which the pennation angle is defined between the muscle fascicles and the line of action of the muscle[5] which in turn can be subject to different definitions.

Traditional 2D ultrasound presents technical limitations which impede a straightforward volumetric assessment of the muscle architecture. In the last decade newer techniques have been introduced in order to obtain 3D muscle images of muscle fibers such as three-dimensional ultrasonography (3D-US)[5-7] and diffusion tensor imaging (DTI) in magnetic resonance imaging (MRI).[8]

Magnetic resonance imaging (MRI) and particularly diffusion tensor imaging (DTI) allows for a non-invasive quantification of muscle macro- and microstructural parameters.[8] Especially, in sport medicine, DTI has shown promise as a relevant tool to understand the muscle recovery process that follows physical activity and after injury.[9] Moreover, the inherent 3D nature of MRI facilitates the assessment of muscle fiber architecture in a volumetric way, for the majority of the body's muscles.

DTI has been used previously for the quantification of muscle fiber angles according to different definitions. These studies showed congruity between the direction of the first eigenvector of the diffusion tensor ε_1 and histology-defined fiber angles in skeletal[10-13] and cardiac muscle.[14-16] Over the past decade various studies focused on estimating pennation angles in individual muscles based on

DTI-based fiber tractography, different line of action definitions and manual aponeurosis delineation.[16-18] Fiber tractography is a non-invasive 3D modeling technique used to investigate the muscle microstructure, local collagen fiber alignment, and the 3D collagen network. It is obtained from DTI by combining the main diffusion direction ε_1 and the fractional anisotropy FA of adjacent voxels in order to obtain tracts representing the muscle fibers and based on both deterministic and probabilistic algorithms generally relying on assumptions concerning the muscle physiology that translates in stopping criteria like the step size, the turning angle, the FA range, tract density and the maximum tract length. However, accurate and reproducible aponeurosis delineation on MR images is difficult[19] and fiber tractography outcomes are promising but subject to variability due to different algorithms and the stopping criteria. Furthermore, these stopping criteria and tracking settings often require optimization for individual subjects, muscles[16,20,21] and locations within the muscle which is a time-consuming process. This hampers reproducibility of the pennation angle measurements, particularly needed in longitudinal studies. Consequently, there is a need for a simple, semi-automated and robust method to quantify pennation angle in skeletal muscle. Ideally, such a method should be independent on the positioning of the subject in the MRI scanner, easily applicable, objective and based on non-deformable anatomical structures. Such a method will specifically facilitate longitudinal studies on muscle fiber architectural adaptations due to training and response to treatment.

The purpose of this study was to develop and evaluate the feasibility of a DTI-based method to quantitatively assess fiber angles and changes therein in whole leg muscle volumes in a straightforward manner, without the need to perform fiber tractography or tendon delineation, in order to facilitate longitudinal studies on muscle fiber architectural adaptations due to training or response to treatment.

Methods

Study design

We evaluated the repeatability and sensitivity of the method in the upper (experiment 1) and lower leg (experiment 2) muscles. The study was approved by the local institutional research board IRB and the medical research committee of the Amsterdam UMC and written informed consent was provided by all subjects prior to the study.

Experiment 1 (Upper leg)

The upper legs of five (N = 5) healthy volunteers (3 male, 2 female, age range 20 to 40) were scanned twice on the same day with a 3T Philips Ingenia MRI scanner (Philips Healthcare, Best, the Netherlands), using a 16-channel anterior coil and the 10-channel table posterior coil. Subjects were positioned in feet-first supine position. The data were acquired in three transverse stacks with 30 mm overlap, covering 498 mm proximal to distal with a field of view (FOV) of 480 x 276 mm^2. The MRI protocol consisted of a noise map to calculate signal-to-noise ratios (SNR) (SE-EPI without diffusion weighting, T_R = 4630 ms, T_E = 53 ms, matrix = 160 × 160, voxel size = 3 × 3 × 6 mm^3, number of slices = 31, SENSE = 1.5), a 3-point mDixon scans as anatomical reference (sequence = FFE, TR = 8.0 ms, TE1/ΔTE = 1.33/1.1 ms, voxel size = 1.5 x 1.5 x 3.0 mm^3) and a DTI scan for diffusion parameter estimation (sequence = SE-EPI, TR = 4630 ms, TE = 53 ms, voxel-size = 3 x 3 x 6 mm^3, SENSE = 1.5, number of gradient directions = 48, diffusion b-value = 450 s/mm^2). Slice-selection gradient reversal (SSGR) and spectrally adiabatic inversion recovery (SPAIR) were used for fat suppression.[22] The scan time per stack was 7 min for the DTI scan, 2 min for the Dixon scan and 30 s for the Noise scan. The participants were taken out of the MRI scanner in between the two sessions for about 15 minutes to rest.

Experiment 2 (Lower leg)

The right lower legs of five (N = 5) male healthy volunteers (age range: 21–43) were scanned with a 3T Philips Achieva MRI scanner (Philips Healthcare, Best, the Netherlands) using a 16-channel torso coil. A custom-built device was used to place the ankle in three different positions, *i.e*. -15° dorsiflexion, 0° neutral, and 30° plantarflexion, to induce passive lengthening and shortening of the muscles in the lower leg. MRI measurements of the lower leg for the three ankle positions were performed in one examination. The MRI protocol consisted of a 3-point mDixon scan (sequence = FFE, TR = 7.7 ms, TE1/ΔTE = 2.1/1.7 ms, voxel-size = 1.0 x 1.0 x 2.5 mm^3, FOV = 192x156 mm^2), the DTI scan (sequence = SE-EPI, TR = 11191 ms, TE = 51.63 ms, voxel-size = 3 x 3 x 5 mm^3, SENSE acceleration factor = 1.5, number of gradient directions = 12, diffusion b-value = 400 s/mm^2, FOV = 192x156 mm^2) and a noise scan obtained by repeating the DT-MRI scan with a single volume and setting the power of the RF to zero. Slice-selection gradient reversal (SSGR) and spectrally adiabatic inversion recovery (SPAIR) were used for fat suppression.[22] The scan time for each ankle position was 11 min. Example anatomical reference and diffusion images for the lower leg are shown in Figure 1. Each volunteer was examined on the same day in two separate scanning sessions, with at least 30 min in between. The dataset was also used to assess fiber length by Mazzoli *et al*..[23]

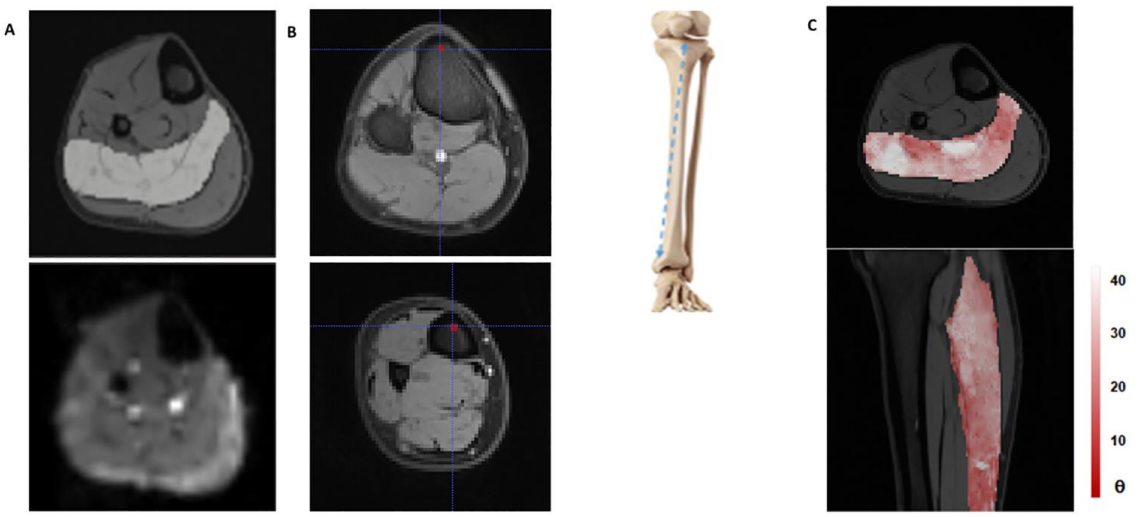

Figure 1: *Graphical representation of steps to create 3D angle (ϑ) color maps. (A) An mDixon scan (top) was used as anatomical reference to segment the muscles. Example diffusion-weighted image (bottom) with b-value = 450 s/mm^2. DTI was used for voxel-wise calculation of the principal diffusion direction, corresponding to the muscle fiber direction. (B) Reference points and schematical drawing of the reference line. The fiber angle was defined as the angle of the principal diffusion direction with the reference line, which in this example was defined by manually drawing points to anatomical landmarks (indicated by the blue crosshair and red points) on the tibia bone on the mDixon images. (C) Axial and longitudinal cross sections of the lower leg with the fiber angles of the SOL muscle as a color-coded overlay.*

DTI post-processing

The DTI data were analyzed with QMRITools for Wolfram Mathematica (Wolfram Research, Inc., Mathematica, Version 12, Champaign, IL).[24] Data processing consisted of 1) noise suppression, with Principal Component Analysis algorithm (PCA), 2) affine registration of the diffusion-weighted images to the non-weighted diffusion images to correct for eddy current-induced image distortions 3) b-spline registration to the mDixon water anatomical images to correct for susceptibility induced deformations.[25] Directional diffusion data were fitted to a tensor model with an iterative weighted linear least square algorithm (iWLLS).[26] The principal eigenvector ε_1 of the diffusion tensor in each voxel, corresponding to the muscle fiber angles, was calculated by an eigen decomposition. The SNR was calculated as the mean of the signal in a muscle ROI divided by the standard deviation of the noise (σ) as calculated from the noise scan. Datasets with SNR below 25 were excluded from further analysis.[26]

Segmentation

In the lower leg, to facilitate segmentations, the mDixon out-of-phase images were re-sampled to a resolution of 1 x 1 x 1 mm^3. Manual delineation of the muscles was done in the resulting 25 slices using ITK-SNAP [27] on the images obtained with the ankle in neutral position. The segmentations were then transferred to all six datasets (three positions x two measurements) by registering the down-sampled mDixon images to full resolution out-of-phase mDixon images using rigid registration followed by non-linear b-spline registration, as previously described by Mazzoli *et al*..[23]

For the upper leg, we segmented the biceps femoris long head (BFLH) and the semitendinosus (ST) muscles. Additionally, the maps of the upper legs were divided in 5 proximal to distal sub-regions of equal length, *i.e*., 0–20%, 20–40%, 40–60%, 60–80%, and 80–100% of the muscle length by using Matlab R2016b (MathWorks, Natick, MA, USA). For the lower leg, the Soleus (SOL) and the Tibialis Anterior (TA) muscles were selected, because these are antagonist muscles and we expect differences in fiber angles with different ankle positions. Figure 1 illustrates the segmentation of the SOL with the ankle in neutral position. For a more detailed regional analysis of muscle fiber angles in a multi-pennate muscle, the SOL muscle was further segmented into four compartments, *i.e*., two anterior bi-pennate compartments and two posterior uni-pennate compartments, following anatomical landmarks such as tendon sheets and muscle borders. The segmentation was manually executed by LS (four years of experience) in the upper legs muscles and in the compartments of the lower leg. The full muscle volumes of the lower leg muscles were manually drawn by VM (seven years of experience). The manual delineation took about three hours per muscle.

Fiber angle color maps

To calculate fiber angles and generate color maps of the fiber angles (θ) in the full muscle volume, the following strategy was applied. First, a reference line was defined in ITK-SNAP based on two anatomical landmarks identified in the out-of-phase images by a trained person according to a muscle specific definition, as schematically illustrated in Figure 1. For the upper leg (experiment 1), two reference lines were defined between the origo and insertion points of the BFLH and the ST, respectively (Figure 1A), according to the definition of line of action of a muscle by Delp *et al*. [28] For the lower leg (experiment 2), a single reference line was defined for both the SOL and the TA muscles by a point on the tibia plate and the most distal and posterior point of the diaphysis (Figure 1B). The intra-observer variability of the fiber angle maps deriving from the placement of the reference line was evaluated.

The voxel-wise fiber angles (θ) were subsequently calculated in MATLAB R2016b (The MathWorks Inc., Natick, MA, USA) from the direction of the principal eigenvector of the diffusion tensor ε_1 and the vector describing the direction of the reference line A using $\theta = acos\left(\frac{A\,\varepsilon 1}{|A|\,|\varepsilon 1|}\right)$, with the constraint of $\theta < 90°$ in order to ensure unique angles.

Statistical analysis

Bland-Altman analysis, the Coefficient of Variation (CV%) and the Intraclass Correlation Coefficient (ICC) were used to represent and to assess the repeatability of the fiber angles maps quantified with our analysis method and expressed as mean value for the full muscle volumes of twenty and thirty individual upper and lower leg muscles respectively. The CV% is defined as the standard deviation divided by the mean.[29] An intra-subject CV% < 10 was considered an index of good repeatability. The ICC is defined as the variance of intra-subjects measurements divided by the total variance of inter-subjects and intra-subjects measurements and in this study for test-retest reliability it was calculated with a two-way random effects, with measures of absolute agreement.[30] Values of ICC between 0.6 and 0.75 were considered moderately good, 0.75≤ICC≤0.9 was considered very good, ICC>0.9 was judged very good, and ICC = 0.9 was rated excellent. The Bias is calculated as the mean of the errors between the two measurements. In this context the bias does not represent the trueness of the method in respect to a gold-standard,[31] but it is intended as a measure of the repeatability of the method. The coefficient of repeatability CR can be calculated as 1.96 (or 2) times the standard deviation of the differences between the two measurements, it is a precision measure which represents the value below which the absolute difference between two repeated test results may be expected to lie with a probability of 95%. Additionally also the Standard Error of the estimate (SE) and the Minimal Detectable Difference (MDD) were calculated in order to compare with other studies. The SE is calculated by taking the standard deviation and dividing it by the square root of the sample size,[32] it indicates how large the prediction errors of the estimates is for the dataset.[33] MDD is measured as the standard error of measurement multiplied by 1.96 and √2.[30] The MDD indicates the smallest change that can be detected statistically.

Fiber angle maps and distribution plots are used to evaluate the ability of the method to assess differences in fiber angles between the three ankle positions in the full volumes of the SOL and the TA muscles and in the four muscle compartments of the SOL muscle. Furthermore, Friedman tests were used to assess differences in fiber angles between the three ankle positions in the four muscle compartments of the SOL muscle. Post-hoc analysis with Wilcoxon signed ranks test was used to determine which of the compartments differed in fiber angles. All statistical analysis were performed

in SPSS (IBM SPSS Statistics for Windows, Version 26 Armonk, NY: IBM Corp) and the significance level was corrected for multiple comparisons and set at p = 0.017.

Results

All scans were successfully completed and all DTI datasets had signal to noise ratio SNR > 25, to allow for accurate tensor calculations.[26] The average SNR in the muscles in the non-diffusion-weighted images in experiment 1 (upper legs) was above 25 (range 25–70), whereas for experiment 2 (lower legs) it was above 30 (range 30–70). The fiber angle color maps were calculated and Figure 1C shows representative cross-sections of the lower leg with overlays of the SOL muscle, color-coded according to the fiber angle (θ) to illustrate the 3D nature of our approach.

The intra-observer variability for placing the reference line in the BFLH, ST and lower leg were 1.0±0.4 voxels and 0.4±0.6 voxels respectively.

The Bland-Altman analysis of the whole-muscle mean fiber angle (θ) in the ST and BFLH of the right and left upper legs and the TA, SOL and anterior right, anterior left, posterior right and posterior left compartments of the SOL muscle in the lower leg are shown in Figure 2. The mean angle, the Bland-Altman analyses on the full muscle volumes and on the SOL anatomical compartments, the bias and SD, the CR, the mean CV%, MDD, ICC and SE are listed in Tables 1 and 2. For experiment 1 (upper leg muscles), the bias was -0.6 ± 2.9° in the right leg BFLH and -0.9 ± 1.7° in the left leg BFLH, with Coefficient of Repeatability (CR) ±5.7 and ±7, respectively. For the ST, the bias was -1.6 ± 2.8° for the right leg and -1.8 ± 3.7° for the left leg, with CR ±5.5 and ±7.1 for right and left, respectively (Table 1). For the SOL muscle in experiment 2, the bias between the two measurements in neutral, dorsiflexion, and plantarflexion position was 0.8 ± 0.8°, 0.3 ± 1.4°, and 0.6 ± 2.0° with CR ±1.8, ±1.5, and ±3.9 (Table 2). For the TA muscle, the bias was 2.1 ± 1.8°, 3.5 ± 3.6°, 1.0 ± 0.6° with CR between ±7.0, ±3.6, ±1.2, for neutral, dorsiflexion and plantarflexion positions, respectively (Table 2).

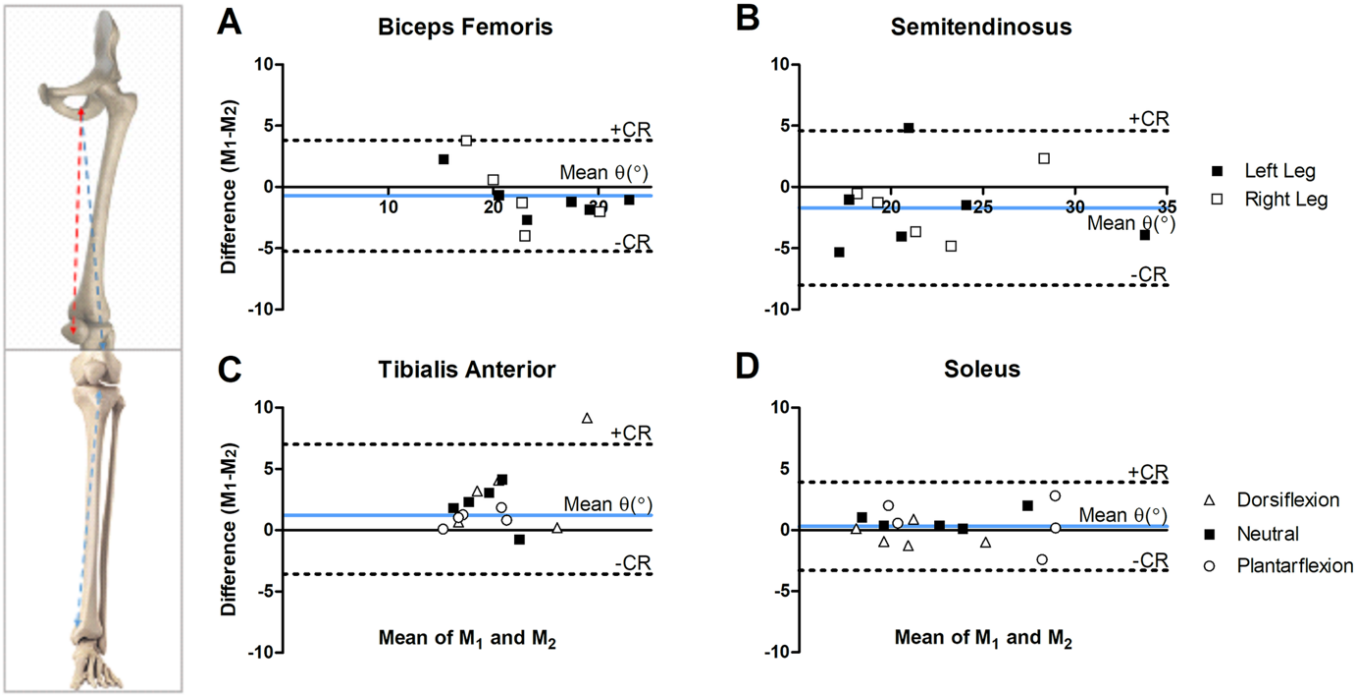

Figure 2: *Bland-Altman analysis for the repeated measurements M1 and M_2 of the whole volume average fiber angles ϑ_{M1} and ϑ_{M2} for (A) Biceps Fermoris, (B) Semitendinosus, (C)Tibialis Anterior, and (D) Soleus muscles. ϑ_{M1} and ϑ_{M2} are the repeated measurements. The light blue line indicates the bias and the dashed lines indicate the Bias±Coefficient of Repeatability (CR),* i.e., *±1.96 x standard deviation (SD).*

Table 1: *Quantitative results of Bland-Altman analysis of repeated measurements of fiber angles ϑ (°).*

	BFL Right	BFL Left	ST Right	ST Left
Angle θ	22.7±4.7	25.0±6.7	22.1±4.1	20.1±3.3
Bias±SD	-0.6 ± 2.9	-0.9 ± 1.7	-1.6 ± 2.8	-1.8 ± 3.7
CR	±5.7	±7	±5.5	±7.1
Mean CV%	7.7	5.1	7.8	11.4
ICC	0.9	0.9	0.9	0.8
MDD	7.5	11.5	8.2	11.5
SE	2.7	4.1	2.9	4.1

The mean and standard deviation (SD) of the bias, the coefficient of repeatability (CR) and the CV% are shown for the left and right Biceps Femoris Long Head (BFL).

Table 2: *Quantitative results of Bland-Altman analysis of repeated measurements of fiber angles ϑ (°).*

		TA	SOL	SOL ANT RIGHT	SOL ANT LEFT	SOL POST RIGHT	SOL POST LEFT
Dorsiflexion	**Angle θ**	20.0 ±4.4	21.4±1.7	15.3±2.0°	19.4±3.1°	24.6±2.1°	20.2±1.6°
	Bias±SD	1.5 ± 1.8	0.3 ± 1.4	0.5±1.4	2.6±3.1	0.6±3.1	1.2±1.9
	CR	±7.0	±1.8	±2.7	±6.1	3.9	±3.8
	Mean CV%	12.2	3.0	4.8	11.8	6.4	5.3
	ICC	0.7	0.8	0.9	0.5	0.03	0.4
	MDD	13.1	2.5	3.7	10.6	5.3	5.9
	SE	4.7	0.9	1.3	3.8	1.9	2.1
Neutral	**Angle θ**	17.4±2.2	21.7±1.6	15.9±1.9°	18.8±3.3°	24.7±1.7°	20.2±2.1°
	Bias±SD	1.2 ± 1.8	0.1 ± 1.0	0.3±1.3	0.8±1.9	0.8±1.3	0.7±0.3
	CR	±3.6	±1.5	±2.5	±3.8	±1.5	±0.6
	Mean CV%	10.4	2.6	4.7	6.3	3.0	2.4
	ICC	0.7	0.9	0.9	0.9	0.9	0.9
	MDD	7.4	2.9	3.2	5.3	2.9	2.0
	SE	2.7	1.0	1.2	1.9	1.0	0.7
Plantarflexion	**Angle θ**	16.6±2.1	23.8±2.9	17.57±3.4°	21.1±4.6°	26.0±5.2°	22.1±4.5°
	Bias±SD	1.0 ± 0.6	0.6 ± 1.5	1.0±3.6	2.4±3.7	-0.4±3.8	1.6±3.2
	CR	±1.2	±3.9	±7.1	±6.1	±1.8	±6.3
	Mean CV%	4.4	4.9	10.2	7.7	12.4	9.4
	ICC	0.9	0.8	0.7	0.8	0.7	0.8
	MDD	3.2	5.3	9.4	10.6	2.6	9.1
	SE	1.1	1.9	3.4	3.8	0.9	3.3

The mean and standard deviation (SD) of the bias, the coefficient of repeatability (CR), the CV% the ICC and the SE are shown for the left and right Semitendinosus (ST), the Tibialis anterior (TA), and the Soleus (SOL) muscle.

The ability of the method to detect differences in muscle fiber angles along the length of the muscle was assessed in the ST muscle. Fiber angle color maps of the ST muscles overlayed on the anatomical MR image together with the mean fiber angles in the 5 proximal to distal sub-sections are shown in Figure 3. The average measured fiber angle for the ST was 22.1 ± 4.1°. The muscle fiber angle distribution along the muscle length was highly subject dependent, with one subject having particularly high fiber angles in the medial portion (40–60%) of the ST muscle. Nevertheless, an average fiber angle distribution of the ST muscle was determined for all subjects, showing a parabolic curved angle distribution (Figure 3).

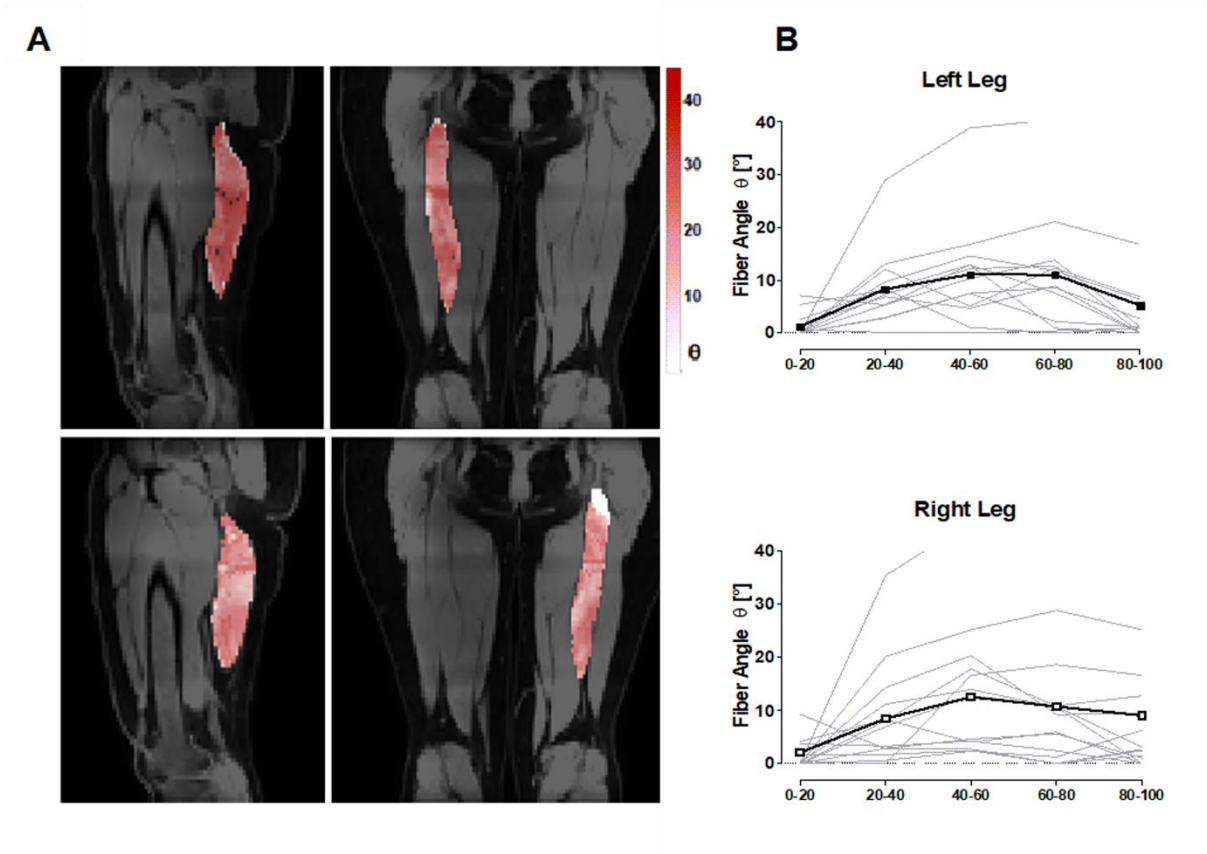

Figure 3: *(A) 3D fiber angle color maps of the right (top) and left (bottom) semitendinosus (ST) muscles in sagittal and transversal views. (B) The mean fiber angle ϑ of the left and right ST muscles in five evenly distributed regions proximally to distally along the muscle length and normalized to the lowest value. The black curve represents the mean angle of the 10 measurements (5 subjects measured twice).*

The evaluation of the method's ability to detect small changes in fiber angles due to different ankle position using the fiber angle color maps and fiber angle distribution plots in the full muscle volumes of the TA and SOL muscles and in the four sub-compartments (two anterior (left & right) and two posterior (left & right)) of the SOL muscle is shown in Figure 4 and Figure 5, respectively. Figure 4 shows, in line with the agonist and antagonist function of the TA and SOL muscles, that the fiber angle distribution of the full muscle volumes shift to higher θ for the TA muscle (20.0°) and lower θ for the SOL muscle (21.4°) in dorsiflexion position, whereas the distribution shifts to lower θ for the TA muscle (16.0°) and higher θ for the SOL muscle (23.8 ± 2.9°) in plantarflexion position. Furthermore, regional differences in θ between ankle positions are visible in the fiber angle color maps for both the TA and the SOL muscles. For example, the anterior and posterior compartments of the SOL muscle become more distinctly visible during contraction (plantarflexion) as white and red patchy areas. Because of the complex multi-pennate architecture of the SOL muscle, we performed a detailed

assessment of the changes in fiber angles with ankle position for the four sub-compartments. In nine out of ten measurements, the fiber angle distribution of the left compartments shifted to higher fiber angles with changing ankle position from dorsiflexion to plantarflexion, whereas the fiber angle distributions of the right compartments remained largely the same (Figure 5).

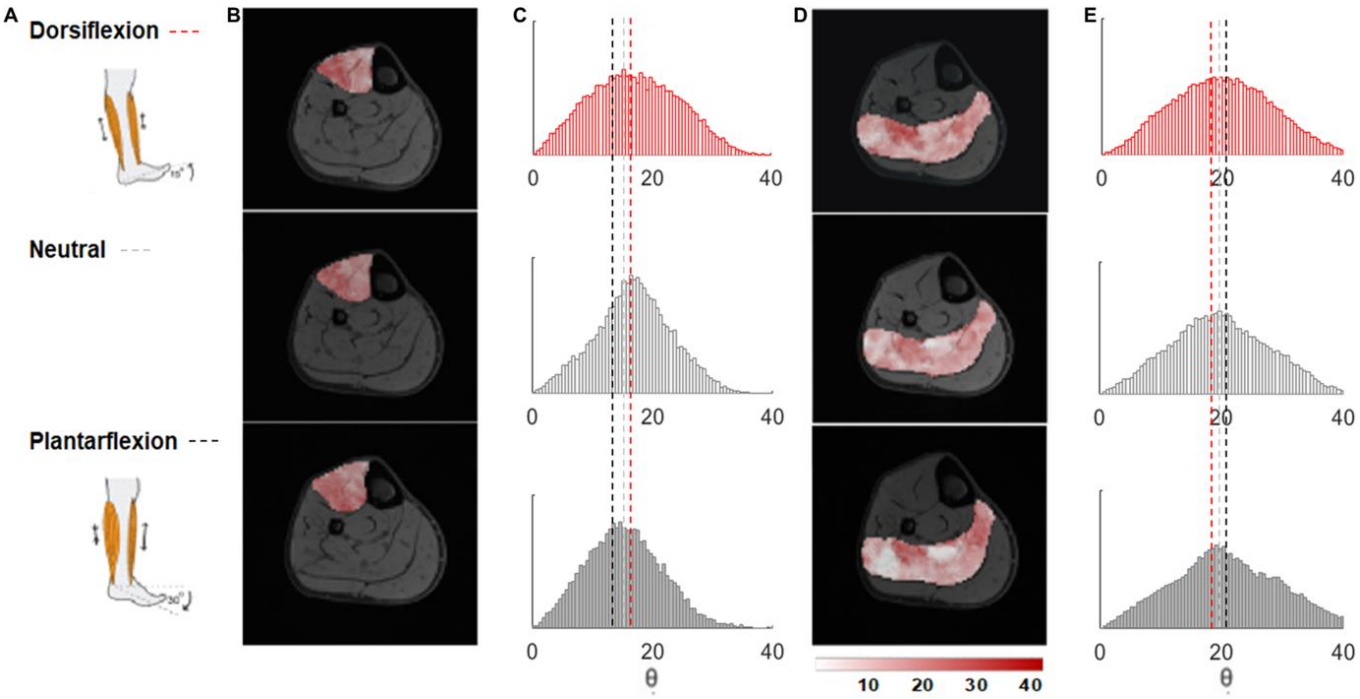

Figure 4: *Fiber angle distributions of the TA and SOL muscles with different foot positions and fiber angle color maps for a representative subject. (A) Schematic drawing of dorsiflexion and plantarflexion position of the foot (B) Fiber angle color maps of the TA muscle overlayed on a mid-belly slice of the Dixon water image for the three foot.*

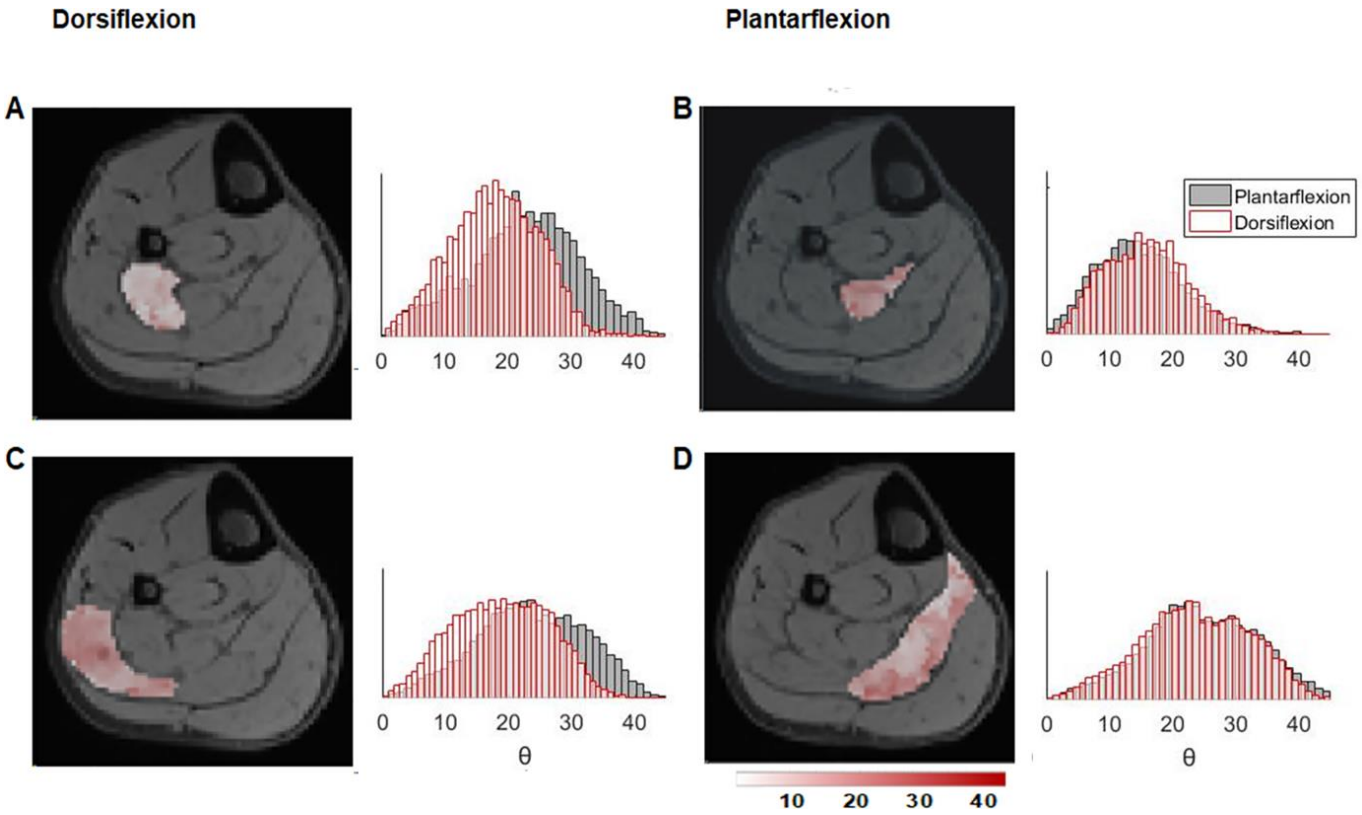

Figure 5: *Fiber angle distributions of the SOL muscle with dorsiflexion and plantarflexion foot positions for a representative subject. The SOL muscle is segmented in 4 volumes with (A) the left anterior, (B) the right anterior, (C) the left proximal, and (D) the right proximal compartments. Color maps of the fiber angles are shown as overlays on a mid-muscle belly water Dixon image.*

The normalized changes of the mean fiber angles Δθ for dorsiflexion and plantarflexion with respect to the neutral position are summarized for the four compartments of the SOL muscle in Figure 6. The anterior and posterior left sub-compartments of the SOL muscle showed statistical difference between the three ankle positions, with the lowest angles in dorsiflexion position and highest angles in plantarflexion position. Table 3 shows the mean angle θ, the mean angle change Δθ and the p-value of the Friedman and Wilcoxon test in dorsiflexion and plantarflexion for 10 subjects in the four sub-compartments of the SOL muscle (anterior right, anterior left, posterior right, and posterior left).

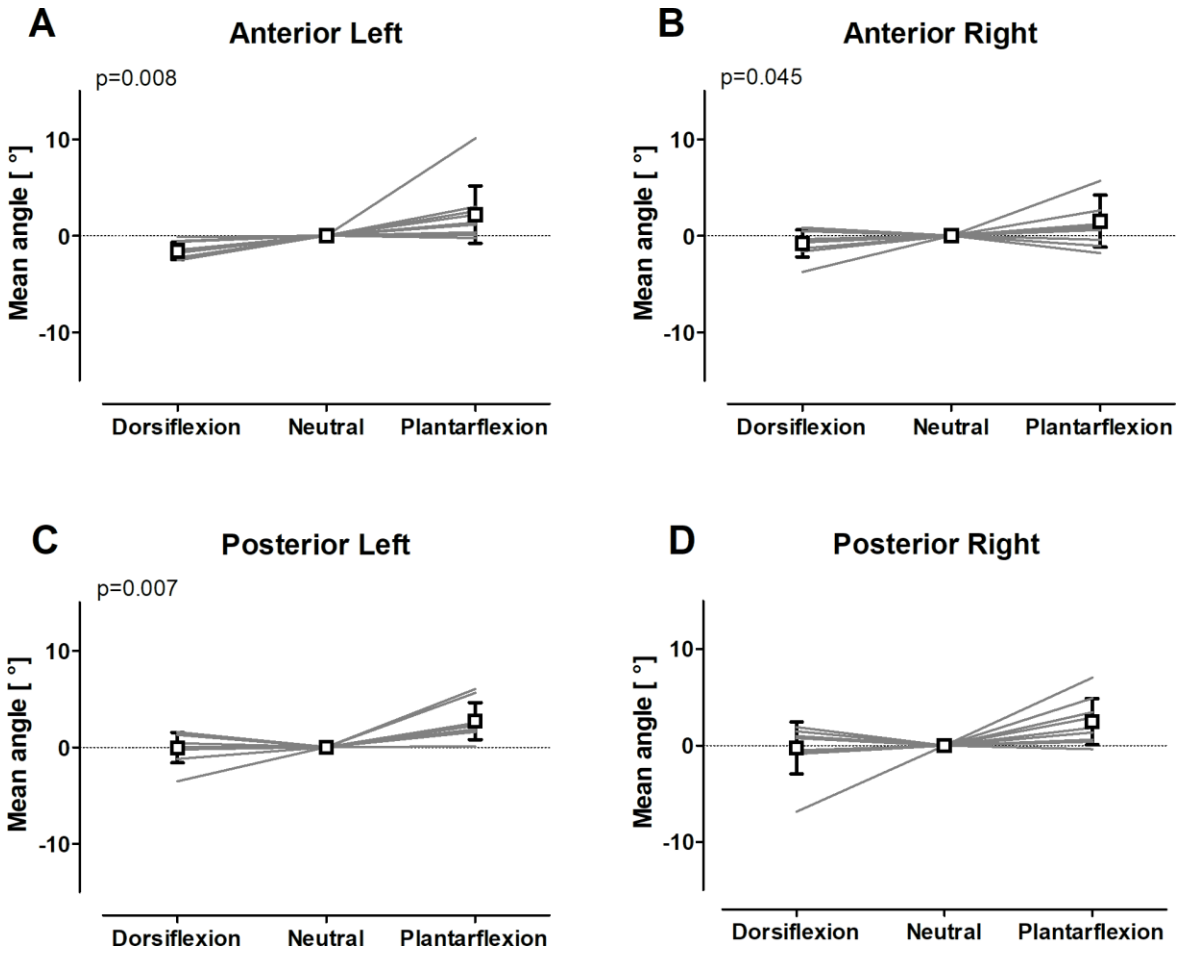

Figure 6: *Mean fiber angles ϑ in the four sub-compartments of the SOL muscle as function of foot position. The fiber angles are shown for the (A) left anterior, (B) right anterior, (C) left posterior, and (D) right posterior compartments. Gray solid lines are the data for the individual subjects, whereas the open square symbols are group averaged and standard deviation.*

	Ankle Position	Anterior		Posterior	
		Right	Left	Right	Left
Angle θ	Dorsiflexion	15.3±2.0°	19.4±3.1°	24.6±2.1°	20.2±1.6°
	Neutral	15.9±1.9°	18.8±3.3°	24.7±1.7°	20.2±2.1°
	Plantarflexion	17.57±3.4°	21.1±4.6°	26.0±5.2°	22.1±4.5°
Change Δθ	Dorsiflexion	-0.8± 1.3°	0.6± 0.8°	-0.2± 2.5°	-0.0 ± 1.5°
	Plantarflexion	1.5± 2.6°	2.2± 2.8°	2.5± 2.2°	2.7±1.8°
p-value	Friedman Test	0.045	0.008	0.06	0.007
	Wilcoxon test		0.009		

Table 3: *The mean measured fiber angle (ϑ) in three ankle positions (dorsiflexion, neutral and plantarflexion), the mean change of angle (Δϑ) in dorsiflexion and plantarflexion normalized in respect to the neutral position and the p-value of the Friedman Test and the post-hoc correction are reported among 10 subjects in the four compartme.*

The changes were statistically significant in the anterior and posterior left compartments ($p = 0.008$ and $p = 0.007$) and in the anterior right compartment ($p = 0.045$) of the SOL muscle. The more detailed post-hoc analysis showed significant differences $\Delta\theta = 2.2 \pm 2.8°$ in fiber angles between the neutral and the plantarflexion positions in the anterior left sub-compartment of the SOL muscles ($p = 0.009$), in which the bias was $0.1 \pm 1.0°$ and $0.6 \pm 1.5°$, whereas the CR was ±1.5 and ±3.9, suggesting that plantarflexion position contributed majorly to this main effect.

Discussion

In this study we presented a DTI-based method to quantitatively assess fiber angles and changes therein in whole leg muscle volumes. We found that our method for quantification of fiber angle is feasible in the mean angle of the full volumes of both the lower and upper leg muscles. Furthermore, we showed that our method is sensitive to detect fiber angle differences along the length of the muscle and between different ankle positions.

Key to our method is that we defined the fiber angle in 3D and with respect to a reference line. This approach differs from the definition of 2D pennation angle which is the acute angle between the fascicles and the muscle aponeurosis or tendon.[34] The reference line is determined using two points, which are systematically defined on the basis of well visible anatomical landmarks, such as bones and tendons. The definition of the anatomical landmarks is set for each muscle, in the upper legs they were at the origo and insertion points, according to a simple definition of the line of action of the muscles,[28,35] whereas in the lower leg the reference line was based on the tibia bone. Consequently the reference line is rotationally invariant, which guarantees its high correspondence in a longitudinal follow up of the same subject, even in cases with severe remodeling.

The measurement of the pennation angle in the BFLH and the ST muscles are in line with previous ultrasound studies that reported a pennation angle of $20.74 \pm 2.53°$ as average of N = 8 locations in the BFLH muscle[36] and 18.07° in the ST muscle for control subjects at rest.[34]

Moreover, the ultrasound and cadaver study by Tosovic *et al.*[37] reported the same muscle angle curved distribution as the one we reported for the BFLH and the ST muscles.

Our calculated fiber angles showed good repeatability in both the upper legs and the lower leg muscles because presented CV<10 and ICC ≥0.7, with exception of the ST (left leg) and the TA muscle

in dorsiflexion. The results are comparable to the repeatability reported in other DTI and US studies. In fact, in previous validation studies differences of 3.0 ± 7.3° between 2D ultrasound and human dissection in BFLH were not considered significant, while changes of 6° were observed with knee and hip rotations of up to 90°.[38] Moreover, we believe that the goodness of the repeatability depends on the expected changes in the specific clinical application of the method. For instance, previous ultrasound studies in the BFLH muscle after intervention reported a difference in the pennation angle in the BFLH between re-injured and non-reinjured subjects of only 1.4° at the halfway point between the ischial tuberosity and the knee joint fold.[39] We think the ability to measure such change with and MRI-based method would be difficult. A possible improvement can be achieved by dividing the muscle length evenly and measuring the mean angle in the medial regions of the muscle length.

Of all analyzed muscles and positions, the muscle in the right upper leg and the TA in the dorsiflexion ankle position showed the largest CR. This might be due to the fact that there are shading artifacts in the left upper leg due to B1 inhomogeneity with the 3T wavelength. The lower repeatability of the TA muscle in dorsiflexion could be due to the fact that this ankle position was not well tolerated by all subjects resulting in some difficulty to control ankle position during and between measurements.

Froeling *et al*.[26] and Heemskerk *et al*.,[21] in the assessment's study of the reproducibility of DTI indices, identified as causes of lower repeatability multiple factors like the variations in anatomy (arms, legs) and muscles, repositioning, SNR and inclusion of non-muscle tissue, such as adipose tissue and blood vessels.

The good repeatability of our method is in line to the repeatability presented in studies on other fiber tractography based methods to quantify muscle pennation angle.[16-18] Previous studies have shown that the tractography repeatability is not optimal yet and that differences in the stopping criteria and the algorithm can influence the pennation angle calculation.[39,40,41,42]

Recent work by Bolsterlee and colleagues[16,17] showed that anatomically constrained tractography can deal with some of the variations introduced by fiber tractography. To the best of our understanding, the exclusion of the fiber tracts was done on the basis of specific criteria such as the fiber length. Therefore, only a certain ratio of seeds, which was different for each muscle, led to successfully tracked fibers.[17] Furthermore, Bolsterlee *et al*. fitted fiber tracts to different polynomial orders, which resulted in minor mean absolute differences of the pennation angle between 0.5° and 1.9°. In two different studies by Bolsterlee and colleagues the angles in the individual compartments of the SOL muscle have been measured according to two different definitions.

In the first study,[17] the angles were measured with respect to the long axis of the muscle, defined as a line connecting a proximal and a distal point on the anterior surface of the muscle between medial-anterior and lateral-anterior compartment. In the medial-anterior, lateral-anterior, medial-posterior and lateral-posterior the measured angles were 22°, 27°, 38°, 34° in plantarflexion with ankle angle 69 ± 12° and 17°, 18°, 24°, 24° in dorsiflexion with ankle angle of 108 ± 7°. The pennation angles were larger in muscle plantarflexion than in dorsiflexion, like in our study. The difference with our measurements in the posterior compartments of the SOL muscle is due to the different degrees of flexion of the ankle, which varied between 19° and 56° instead of 45°.

In the second study by Bolsterlee and colleagues,[16] the pennation angle was defined as 90° minus the mean angle between a vector parallel to the endpoint's slope and the normal vectors of all triangles of the surface model within a radius of 1.5 mm around the endpoint. The pennation angle was the mean of the angles that the fascicle made with the deep and superficial aponeuroses. In this study the left foot was placed in neutral position with ankle angle 87 ± 3° with respect to the horizontal plane by mean of an MRI compatible foot plate. This study reported very similar results to the ones we measured: 19.0°, 20.0°, 24.6°, 21.2° in the medial posterior, medial anterior, lateral posterior and lateral anterior compartments.

This anatomically constrained method showed a good intra-class correlation coefficient (ICC) between 0.8 and 1 for pennation angle in the gastrocnemius muscle, but lower than in our study for the TA muscle with ICC of 0.6 and the anterior compartments of the SOL muscle in neutral position with ICC of 0.91, 0.14, 0.93, 0.60 in the medial-posterior, medial-anterior, lateral-posterior and lateral-anterior compartments. The lower repeatability in the TA muscle and anterior compartment of the SOL muscle compared to the other muscles is in line with our findings in the Bland Altman analysis. Even though the method with anatomical constraints proved repeatable and relatively insensitive to tracking parameters in the gastrocnemius muscle, it was not equally repeatable in the other muscles and several seed points (60%) and voxels of the full volume were excluded in order to obtain anatomically correct fibers.

In another study by Fouré and colleagues, a different fiber tractography based method was used[18,40] and they defined 3D pennation angles between the principal axis of each muscle and the local muscle fiber direction. The principal axis was determined via a principal component analysis on the three-dimensional coordinates of each muscle segmentation mask. The local muscle fiber direction was taken from the first and last points of a fiber-tract in the muscle. Finally, the pennation angles were weighted over all fiber tracts within each voxel.[39] The calculated angle for the SOL muscle in eight

young healthy subjects in 15°-20° plantarflexion was 43 ± 3° and 29 ± 6° for the superficial and deep compartments, respectively, which is around double of the value we found. These values are difficult to compare firstly because the SOL muscle was divided only in two compartments instead of four compartments, secondly because the change in angle between different positions was not assessed and finally, because in our experiment we used a reference line based on the tibia bone instead of the centroid of the muscle mask segmentation. Nevertheless, the difference between the superficial and deep compartment is comparable to the difference we found between the anterior right and the posterior right compartments of the SOL muscle in plantarflexion.

Furthermore, this method showed good reproducibility, reflected by low coefficient of variances between two measurements.[18] The mean CV% = 5.5 and 6.6 for the superficial (posterior) and the deep (anterior) SOL muscle and mean CV% = 8.4 for the TA.

The study investigated changes in pennation angle due to gender but not changes due to the effect of ankle position.

In our study, the evaluation of the effect of ankle positions on fiber angles showed significant differences in fiber angles between the neutral and the plantarflexion positions in the anterior left sub-compartment of the SOL muscles, suggesting that plantarflexion position contributed majorly to the statistical difference between the three ankle positions.

Our observations in the full volumes of both lower leg muscles are in agreement with biomechanical predictions. The fiber angle is expected to decrease during passive lengthening and to increase during passive shortening.[43,44] Previous work by Sinha *et al.*, using a method based on the first eigenvector with polar coordinates in respect to the magnet z-axis on six healthy subjects, reported changes in the fiber angles of the SOL muscle medialis up to 48° and 41° respectively in the anterior and in the posterior sub compartments between neutral (ankle angle 90°) and plantarflexion (ankle angle 120°).[45] This change is much larger than we measured and is probably due to the different definition of pennation angle used and the area analyzed.

In contrast, changes in fiber angles between ankle positions in the sub-compartments of the SOL muscle we report here compare very well to those reported by Bolsterlee *et al*. who found changes in pennation angles in the range of approximately 5° to 14° for the different compartments of the SOL muscle.[16] Previous studies showed that architectural patterns during muscular shortening can be heterogeneous in the muscle and between subjects[43,44] and that changes in muscle architecture due to ankle position may not follow a linear relationship.[46,47]

Our approach used the definition of pennation angles in the 3D volume of upper leg muscles with respect to a simple definition of the muscle's line of action in the upper legs with extended legs and in respect to the tibia bone in the lower leg. This measurement can be used to calculate the muscle force[28,35] as well as to monitor global or local changes of muscle fiber angles following, training or therapeutic intervention.

On the other hand, if a 2D definition of pennation angle would be desired instead in a specific region of the muscle the method here presented allows fast calculation of fiber angles with respect to new reference lines or planes conforming to other pennation angle definitions.

A limitation to our study is that we did not provide direct comparison with an independent technique like ultrasound, which can be considered the most established technique for the determination of fiber angles in skeletal muscle.

Conclusions

In this study we have presented a method to assess fiber angles in skeletal muscle and changes therein. Our study indicated that fiber angle quantification in full 3D volumes and in specific muscle compartments of individual muscles is feasible with this method. Additionally, this method is sensitive enough to detect fiber architecture changes in lower leg muscles due to different foot positions. These results warrant the application of our method to longitudinally monitor changes in fiber angles following training intervention.

References

1. Zatsiorsky V. M. & Prilutsky B. I. Biomechanics of Skeletal Muscles. (2012).
2. Lieber RL, Friden J. Functional and clinical significance of skeletal muscle architecture. Muscle Nerve 2000; 23(11): 1647–1666. pmid:11054744
3. Lieber RL, Friden J. Clinical significance of skeletal muscle architecture. Clin. Orthop. Relat. Res. 2001; 383: 140–151. pmid:11210948
4. Randhawa Avleen, and Wakeling James M. "Multidimensional models for predicting muscle structure and fascicle pennation." *Journal of theoretical biology* 382 (2015): 57–63. pmid:26073723
5. Lee Dongwoon, Li Z., Sohail Q. Z., Jackson K., Fiume E., & Agur A. "A three-dimensional approach to pennation angle estimation for human skeletal muscle." *Computer Methods in Biomechanics and Biomedical Engineering*. 2015;18(13): 1474–1484. pmid:24849037
6. Hiblar T, Bolson EL, Hubka M, Sheehan FH, Kushmerick MJ. Three dimensional ultrasound analysis of fascicle orientation in human tibialis anterior muscle enables analysis of macroscopic torque at the cellular level. In Molecular and Cellular Aspects of Muscle Contraction.
7. Kurihara T, Oda T, Chino K, Kanehisa H, Fukunaga T. Use of three-dimensional ultrasonography for the analysis of the fascicle length of human gastrocnemius muscle during contractions. Int. J. Sport Health Sci. 2005; 3: 226–234.
8. Damon B. M., Froeling M., Buck A. K. W., Oudeman J., Ding Z., Nederveen A. J., et al. Skeletal muscle diffusion tensor-MRI fiber tracking: rationale, data acquisition and analysis methods, applications and future directions. *Nmr Biomed* 30, e3563 (2017). pmid:27257975
9. Damon B. M., Buck A. K., & Ding Z. (2011). Diffusion-tensor MRI based skeletal muscle fiber tracking. Imaging in medicine, 3(6), 675. pmid:25429308
10. Levin D. I., Gilles B., Mädler B., & Pai D. K. (2011). Extracting skeletal muscle fiber fields from noisy diffusion tensor data. Medical Image Analysis, 15(3), 340–353. pmid:21345716
11. Froeling M., Nederveen A. J., Heijtel D. F., Lataster A., Bos C., Nicolay K., et al. (2012). Diffusion-tensor MRI reveals the complex muscle architecture of the human forearm. Journal of Magnetic Resonance Imaging, 36(1), 237–248. pmid:22334539
12. Van Donkelaar C. C., Kretzers L. J. G., Bovendeerd P. H. M., Lataster L. M. A., Nicolay K., Janssen J. D., et al. (1999). Diffusion tensor imaging in biomechanical studies of skeletal muscle function. Journal of ANATOMY, 194(1), 79–88. pmid:10227669
13. Napadow V. J., Chen Q., Mai V., So P. T., & Gilbert R. J. (2001). Quantitative analysis of three-dimensional-resolved fiber architecture in heterogeneous skeletal muscle tissue using nmr and optical imaging methods. Biophysical journal, 80(6), 2968–2975. pmid:11371469
14. Qin X., Wang S., Shen M., Zhang X., Wagner M. B., & Fei B. (2014, March). Mapping cardiac fiber orientations from high-resolution DTI to high-frequency 3D ultrasound. In Medical Imaging 2014: Image-Guided Procedures, Robotic Interventions, and Modeling (Vol. 9036, p. 90361O). International Society for Optics and Photonics.
15. Wang, L. H., Zhu, Y. M., Yang, F., Liu, W. Y., & Magnin, I. E. (2014, April). Simulation of dynamic DTI of 3D cardiac fiber structures. In 2014 IEEE 11th International Symposium on Biomedical Imaging (ISBI) (pp. 714–717). IEEE.
16. Bolsterlee B., Finni T., D'Souza A., Eguchi J., Clarke E. C. & Herbert R. D. Three-dimensional architecture of the whole human soleus muscle in vivo. *Peerj* 6, e4610 (2018). pmid:29682414
17. Bolsterlee B D'Souza A, Herbert RD. Reliability and robustness of muscle architecture measurements obtained using diffusion tensor imaging with anatomically constrained tractography. J Biomech. 2019 Mar 27;86:71–78. Epub 2019 Jan 30. pmid:30739766.
18. Fouré A., Ogier A. C., Le Troter A., Vilmen C., Feiweier T., Guye M., et al. (2018). Diffusion properties and 3D architecture of human lower leg muscles assessed with ultra-high-field-

strength diffusion-tensor MR imaging and tractography: Reproducibility and sensitivity to sex difference and intramuscular variability. Radiology, 287(2), 592–607. pmid:29381871
19. Handsfield Geoffrey G., et al. "Determining skeletal muscle architecture with Laplacian simulations: a comparison with diffusion tensor imaging." *Biomechanics and modeling in mechanobiology* 16.6 (2017): 1845–1855. pmid:28577041
20. Oudeman Jos, et al. "Techniques and applications of skeletal muscle diffusion tensor imaging: a review." Journal of Magnetic Resonance Imaging 43.4 (2016): 773–788. pmid:26221741
21. Heemskerk A. M., Sinha T. K., Wilson K. J., Ding Z., & Damon B. M. (2010). Repeatability of DTI-based skeletal muscle fiber tracking. NMR in biomedicine, 23(3), 294–303. pmid:20099372
22. Williams SE, Heemskerk AM, Welch EB, Li K, Damon BM, Park JH. Quantitative effects of inclusion of fat on muscle diffusion tensor MRI measurements. J Magn eason Imaging. 2013 Nov;38(5):1292–7. Epub 2013 Feb 15. pmid:23418124; PMCID: PMC3664247.
23. Mazzoli V., Oudeman J., Nicolay K., Maas M., Verdonschot N., Sprengers A. M., et al. (2016). Assessment of passive muscle elongation using Diffusion Tensor MRI: Correlation between fiber length and diffusion coefficients. NMR in Biomedicine, 29(12), 1813–1824. pmid:27862471
24. Froeling Martijn. "QMRTools: a Mathematica toolbox for quantitative MRI analysis." *Journal of Open Source Software* 4.38 (2019): 1204.
25. Luca A. D., Bertoldo A. & Froeling M. Effects of perfusion on DTI and DKI estimates in the skeletal muscle. *Magn eason Med* 78, 233–246 (2016). pmid:27538923
26. Froeling M., Oudeman J., van den Berg S., Nicolay K., Maas M., Strijkers G. J., et al. (2010). Reproducibility of diffusion tensor imaging in human forearm muscles at 3.0 T in a clinical setting. Magnetic resonance in medicine, 64(4), 1182–1190. pmid:20725932
27. Yushkevich, Paul A., Yang Gao, and Guido Gerig. "ITK-SNAP: An interactive tool for semi-automatic segmentation of multi-modality biomedical images." *2016 38th Annual International Conference of the IEEE Engineering in Medicine and Biology Society (EMBC)*. IEEE, 2016.
28. Delp Scott L., et al. "An interactive graphics-based model of the lower extremity to study orthopaedic surgical procedures." IEEE Transactions on Biomedical engineering 37.8 (1990): 757–767. pmid:2210784
29. Andrew F. Siegel, in Practical Business Statistics (Seventh Edition), 2016.
30. Bartko John J. "The intraclass correlation coefficient as a measure of reliability." Psychological reports 19.1 (1966): 3–11. pmid:5942109
31. Vaz Sharmila, et al. "The case for using the repeatability coefficient when calculating test–retest reliability." PloS one 8.9 (2013): e73990. pmid:24040139
32. Lassere M. N., Van der HEIJDE D. É. S. I. R. É. E., and KENT R. Johnson. "Foundations of the minimal clinically important difference for imaging." The Journal of rheumatology 28.4 (2001): 890–891. pmid:11327272
33. Oliveira De, Fernandes Liliam, and Luciano Luporini Menegaldo. "Individual-specific muscle maximum force estimation using ultrasound for ankle joint torque prediction using an EMG-driven Hill-type model." Journal of biomechanics 43.14 (2010): 2816–2821. pmid:20541763
34. Karagiannidis Evagelos, et al. "Semitendinosus muscle architecture during maximum isometric contractions in individuals with anterior cruciate ligament reconstruction and controls." Muscles, ligaments and tendons journal 7.1 (2017): 147. pmid:28717622
35. Herzog W, Read LJ. Lines of action and moment arms of the major force-carrying structures crossing the human knee joint. J Anat. 1993;182 (Pt 2)(Pt 2):213–230. pmid:8376196
36. Kellis Eleftherios, et al. "Muscle architecture variations along the human semitendinosus and biceps femoris (long head) length." Journal of Electromyography and Kinesiology 20.6 (2010): 1237–1243.
37. Tosovic D., et al. "Anatomy of the long head of biceps femoris: an ultrasound study." Clinical Anatomy 29.6 (2016): 738–745.
38. Chleboun Gary S., et al. "In vivo measurement of fascicle length and pennation angle of the human biceps femoris muscle." *Cells Tissues Organs* 169.4 (2001): 401–409. pmid:11490120

39. Calamante Fernando. "Track-weighted imaging methods: extracting information from a streamlines tractogram." Magnetic Resonance Materials in Physics, Biology and Medicine 30.4 (2017): 317–335. pmid:28181027
40. Heemskerk AM, Sinha TK, Wilson KJ, Ding Z, Damon BM. Repeatability of DTI-based skeletal muscle fiber tracking. NMR Biomed. 2010 Apr;23(3):294–303. pmid:20099372; PMCID: PMC4416059.
41. Keller S, Yamamura J, Sedlacik J, et al. Diffusion tensor imaging combined with T2 mapping to quantify changes in the skeletal muscle associated with training and endurance exercise in competitive triathletes. *Eur Radiol*. 2020;30:2830–2842. pmid:31953666
42. Forsting Johannes, et al. "Diffusion tensor imaging of the human thigh: consideration of DTI-based fiber tracking stop criteria." *Magnetic Resonance Materials in Physics*, *Biology and Medicine* 33.3 (2020): 343–355. pmid:31776703
43. Deux J. F., Malzy P., Paragios N., Bassez G., Luciani A., Zerbib P., et al. (2008). Assessment of calf muscle contraction by diffusion tensor imaging. European radiology, 18(10), 2303–2310. pmid:18463875
44. Shin DD, Hodgson JA, Edgerton VR, Sinha S. In vivo intramuscular fascicle-aponeuroses dynamics of the human medial gastrocnemius during plantarflexion and dorsiflexion of the foot. J. Appl. Physiol. 2009; 107(4): 1276–1284. pmid:19608924
45. Sinha U., Sinha S., Hodgson J. A. & Edgerton R. V. Human soleus muscle architecture at different ankle joint angles from magnetic resonance diffusion tensor imaging. *Journal of applied physiology (Bethesda*, *Md*: *1985)* 110, 807–819 (2011). pmid:21164150
46. Kawakami Y., Ichinose Y., & Fukunaga T. (1998). Architectural and functional features of human triceps surae muscles during contraction. Journal of applied physiology, 85(2), 398–404. pmid:9688711
47. Pappas GP, Asakawa DS, Delp SL, Zajac FE, Drace JE. Nonuniform shortening in the biceps brachii during elbow flexion. J. Appl. Physiol. 2002

Supporting Information

Supplementary Table 1: Mean of repeated measurements of fiber angles θ (^{o}) in the BFLH muscle of the right leg.

M1	M2
20.2	19.7
22.1	23.4
29.1	31.1
21.0	25.1
19.3	15.5

Supplementary Table 2: Mean of repeated measurements of fiber angles θ (^{o}) in the BFLH muscle of the left leg.

M1	M2
20.2	20.8
32.4	33.4
26.8	28.0
28.2	30.1
16.4	14.1

Supplementary Table 3: Mean of repeated measurements of fiber angles θ (°) in the ST muscle of the right leg.

M1	M2
17.9	18.4
18.6	19.9
20.8	25.7
19.5	23.1
29.5	27.1

Supplementary Table 4: Mean of repeated measurements of fiber angles θ (°) in the ST muscle of the left leg.

M1	M2
17.2	18.2
18.5	22.6
14.5	19.8
23.3	24.8
23.4	18.5

Supplementary Table 5: Mean of repeated measurements of fiber angles θ (°) in the SOL muscle.

Dors T1	Dors T2	Neu T1	Neu T2	Plant T1	Plant T2
17.4	17.3	18.1	17.0	19.3	18.7
20.1	19.2	21.7	21.6	26.8	24.0
22.1	23.1	25.31	23.3	25.5	25.4
18.8	20.1	20.9	20.5	23.7	26.1
18.0	18.9	18.6	18.2	19.6	17.6

Supplementary Table 6: Mean of repeated measurements of fiber angles θ (°) in the TA muscle.

Dors T1	Dors T2	Neu T1	Neu T2	Plant T1	Plant T2
14.6	14.0	14.8	13.0	13.1	13.0
29.4	20.2	18.9	19.6	18.6	17.8
19.6	15.5	18.3	15.3	15.3	14.0
22.4	22.2	19.9	15.8	18.7	16.9
17.4	14.2	16.3	14.0	14.8	13.8

Supplementary Table 7: Mean of repeated measurements of fiber angles θ (°) in the SOL muscle anterior right compartment.

Dors 1	Dors 2	Neu 1	Neu 2	Plant 1	Plant 2
15.2	16.7	17.3	15.8	16.3	16.6
24.0	18.0	16.6	17.4	16.3	13.7
19.3	15.9	16.7	16.9	17.5	16.3
18.6	21.4	17.6	15.7	15.9	16.2
13.2	13.3	12.0	12.9	11.6	12.3

Supplementary Table 8: Mean of repeated measurements of fiber angles θ (°) in the SOL muscle anterior left compartment.

Dors 1	Dors 2	Neu 1	Neu 2	Plant 1	Plant 2
18.87	18.45	20.58	20.34	22.76	21.71
23.13	19.33	19.37	17.99	29.49	20.55
20.94	21.84	18.61	20.74	21.64	21.9
22	19.31	23.5	20.41	23.26	21.79
19.03	11.89	14.1	12.58	14.2	13.35

Supplementary Table 9: Mean of repeated measurements of fiber angles θ (°) in the SOL muscle posterior right compartment.

Dors 1	Dors 2	Neu 1	Neu 2	Plant 1	Plant 2
23.6	25.7	24.1	23.8	24.7	25.2
26.7	21.1	26.0	28.0	33.0	28.4
28.0	26.6	26.5	25.6	29.4	27.5
23.2	24.1	24.1	22.6	29.0	26.1
22.9	24.0	23.5	22.8	23.2	13.3

Supplementary Table 10: Mean of repeated measurements of fiber angles θ (°) in the SOL muscle posterior left compartment.

Dors 1	Dors 2	Neu 1	Neu 2	Plant 1	Plant 2
19.4	18.8	17.6	17.1	18.9	18.4
28.7	25.4	23.1	22.9	23.1	19.3
22.9	22.5	21.0	20.3	20.9	21.8
24.1	26.6	21.6	20.5	22.0	19.3
19.4	13.3	19.3	18.4	19.0	19.1

CHAPTER 4

On the measurement of the Vastus Lateralis muscle pennation angle and fiber length using 3D ultrasound and diffusion-tensor MRI

Laura Secondulfo

Moritz Eggelbusch

Guido Weide

Richard T. Jaspers

Aart J. Nederveen

Rob C.I. Wüst

Gustav J. Strijkers

Melissa T. Hooijmans

Abstract

Purpose

Traditional muscle classifications have proven inadequate in comprehending the intricate relationship between structure and function in skeletal muscles. To accurately measure muscle parameters, it is necessary to explore alternative techniques. This study aims to assess the agreement between 3D ultrasound (3D-US) and Diffusion-Tensor Imaging (DTI) in measuring muscle fiber pennation angle and fiber length in the Vastus Lateralis muscle (VL). By doing so, this research endeavors to enhance our understanding of the strengths and limitations associated with these techniques.

Methods

On the same day, nine subjects underwent MRI scans of their upper legs and 3D ultrasound (3D-US) acquisitions of the Vastus Lateralis (VL) muscle. The MRI datasets included both Diffusion-Tensor Imaging (DTI) and Dixon acquisitions. The 3D-US acquisitions were performed using a 5-cm linear probe in B-mode at a frequency of 30 Hz. The pennation angle, which refers to the angle between the aponeurosis and the muscle fascicles passing through the central point at two-thirds of the muscle belly in the mid-longitudinal plane, was obtained using both imaging modalities. To compare the pennation angles between the two modalities, Bland-Altman analyses, paired t-tests, and intra-class correlation coefficient (ICC) were employed.

Results

The 3D ultrasound (3D-US) measurements revealed an average pennation angle of 18.7 ± 3.9° and a fiber length of 77.6 ± 15.4 mm. In contrast, the DTI fiber-tractography based approach yielded an average pennation angle of 21.9 ± 5.2° and a fiber length of 59.6 ± 15.4 mm. The t-test analysis for the pennation angle yielded a p-value of 0.11 and an ICC-value of 0.34. For fiber length, the t-test resulted in a p-value of 0.05, and ICC analysis indicated that there was no significant correlation.

Conclusions

There was limited agreement between individual subject measurements of the Vastus Lateralis (VL) muscle's pennation angle and fiber length obtained from 3D ultrasound (3D-US) and Diffusion-Tensor Imaging (DTI).

Introduction

The architectural organization of muscle fibers with respect to the whole muscle volume differs among individual skeletal muscles.[1] One can roughly classify muscles based on their shape and muscle fiber architecture, amongst others into fusiform, unipennate, bipennate, and triangular.[2] However, to understand the details on the structure-function relationship of skeletal muscle in health and disease, such general classifications are often inadequate. For one thing the muscle does not act in isolation as contractile forces are transmitted to bones via muscle-tendon junctions and tendons.[3] Moreover, each person is unique and inter-subject differences in muscle shapes and sizes can be substantial. Therefore, there is a great need for accurate measurements of muscle architectural parameters, such as volumes, fiber orientations, and fiber lengths.

The most frequently used image modality for the assessment of muscle fiber orientations and lengths is 2D B-mode ultrasound imaging. 2D-ultrasound is easy to apply, relatively low cost and it offers excellent temporal resolution. However, it is challenging to align the imaging plane with the line of pull or muscle fiber axis, and it is generally difficult to correctly infer 3D architecture from 2D imaging. Alternatively, both Diffusion-Tensor MR Imaging (DTI) and 3D-ultrasound (3D-US) facilitate a 3D assessment of muscle fiber orientations and lengths.

3D-US technique is based on the acquisition of a series of 2D images of the muscle by mean of a 2D B-mode probe sweeping on the muscle surface, which 3D movement is recorded using an external tracking device. Subsequently, the 2D images are registered to form a 3D image.[4,5,6] 3D-US facilitates scanning of a full volume of superficial muscles in any position or posture.

DTI is a dedicated magnetic resonance imaging technique (MRI) capable of quantifying the self-diffusion of water in tissues. In skeletal muscle tissue diffusion is directionally anisotropic because muscle cells are long and approximately cylindrically shaped. Water diffuses therefore more easily along the axis of a muscle fiber than in a transverse direction. From the directional anisotropy one can infer that the local muscle fiber orientation on a voxel-by-voxel basis and fiber bundles can be reconstructed over longer distances by means of fiber-tractography algorithms.[7,8,9] With DTI one can quantify the architecture of multiple muscles belonging to the same anatomy, for example upper or lower legs, simultaneously in a single scan session. However, the physical confinement of most MRI scanners generally limits examinations to a supine or prone body position.

So far little is known about how muscle architectural parameters assessed with 3D-US and DTI compare and only a few studies have compared 2D-US with DTI.[10,11] The purpose of this study was therefore to determine the muscle fiber pennation angle and fiber length of the Vastus Lateralis (VL) muscle using both techniques. The VL muscle was chosen as a 'model' muscle since this muscle was previously studied and well validated using 3D-US in cadavers.[4]

Methods

Study setup

Nine healthy participants (age range: 22-64 years; 5 males) volunteered to participate in this study. Prior to participation, participants were informed about the experimental procedures of the study and provided written informed consent. The study was conducted according to the principles of the Declaration of Helsinki and was approved by the departmental ethics committee of the Vrije Universiteit, Amsterdam, the Netherlands (VCWE-2020-122). We acquired 3D-US and MRI on the same day in two different institutes (Vrije Universiteit and Amsterdam UMC, Amsterdam, the Netherlands) with average of 10 ± 2 hours in between both scans. Participants were instructed not to perform any physical activity one day prior the examinations.

Data Acquisition

MRI

MRI of the upper legs was performed in supine position with the legs stretched (stretched) at 3T (Philips Ingenia, Philips Healthcare, Best, the Netherlands) using a 16-channel anterior coil and a 10-channel table posterior coil. MRI comprised of the acquisition of 3 stacks in order to cover the legs from knee to hip. The examination consisted of a Dixon scan as anatomical reference (sequence = FFE, SENSE, TR = 8 ms, TE1/ΔTE = 1.33/1.1 ms, FOV = 480x276x186 mm^3, voxel size = 1.5x1.5x3.0 mm^3), a DTI scan (sequence = diffusion-weighted SE-EPI; 48 gradient directions, b-value = 0 and 400 s/mm^2, FOV = 480x276x186 mm^3, voxel size = 3.0x3.0x6.0 mm^3, TR = 4630 ms, TE = 53 ms, fat-suppression = SPAIR and SSGR, number of signal averages (NSA) = 3, SENSE and half scan) and a noise-estimation scan (similar to diffusion scan without RF and gradients).

The 3 stacks of images were joined and further processed using QMRITools for Mathematica.[9] A principal component analysis (PCA) method was used for noise suppression. SNR was defined as the mean of the signal in a muscle region of interest divided by the standard deviation of the noise (σ). Scans with SNR lower than 25 were excluded from further analysis. Subsequently, DTI images were registered to the Dixon scan using rigid, affine, and b-spline steps in Elastix.[12] More details on the processing of the DTI data can be found in several other papers.[13, 14,15] Finally, the diffusion tensor was calculated in each voxel using an iterative weighted linear least squares (iWLLS) method.

3D-ultrasound

3D-US acquisition of the right leg's VL muscle morphology was obtained on the same day as the MR acquisitions, with a hip angle of 90° and a knee angle of 0°. The hip angle here is defined as the angle between the thigh and the torso. To prevent displacement or rotation, the lower leg was strapped and secured to the bench. Images were acquired from the participant's right leg in B-mode (30 Hz) using a 5-cm linear probe attached to an ultrasound machine (Arietta Prologue, Hitachi L-55, Hitachi Ltd., Tokyo). Muscle morphology of the VL was obtained using 3D ultrasound imaging, as described previously.[4] Location and orientation of the ultrasound probe were collected over time using a cluster marker that was connected to the ultrasound probe and a motion capture system (Optotrak Certus; Northern Digital, Waterloo, ON, Canada).[16] Ultrasound sweeps of the VL were collected in longitudinal direction, starting from the lateral border of the muscle and scanning from the distal to proximal end of the muscle with the probe in transverse orientation. Subsequent sweeps were taken medially from the previous sweep with around 1-cm overlap. An external trigger marked the start of each scan and was used to synchronize position data with the ultrasound B-mode images to enable the construction of a 3D voxel array to reconstruct the whole VL muscle using customized 3D image-processing software (Matlab, MathWorks, Natick, MA, USA).

Estimation of the outcome parameters

3D-US

To quantify the pennation angle and the fiber length with 3D-US, the Medical Interaction toolkit (MITK)[17] was used. Firstly, the muscle length was calculated by defining the origin and the distal musculotendinous junction of the VL muscle in the 3D reconstructed images. Subsequently, VL pennation angle was determined at 2/3 of the proximal to distal muscle length in the mid-longitudinal fascicle plane[18] (Figure 1B). The mid-longitudinal fascicle plane describes a theoretical plane that

represents the direction of muscle fibers within a muscle. It is determined by considering the vector from the origin to the distal end of the VL muscle belly, along with a straight line that connects the tangent on the deep aponeurosis to its projection on the muscle's cross-section at two-thirds of the distance between the proximal and distal parts of the muscle (green line in Figure 1A). In this plane fiber fascicles are visible in full length (Figure 1B). The pennation angle was defined as the angle between the fibers running through the center of the muscle and the distal deep aponeurosis. To quantify the fiber lengths, the distance between the insertions of the fibers running through the center of the muscle to the deep and superficial aponeurosis was measured. Both outcomes were the average of five repeated measurements.

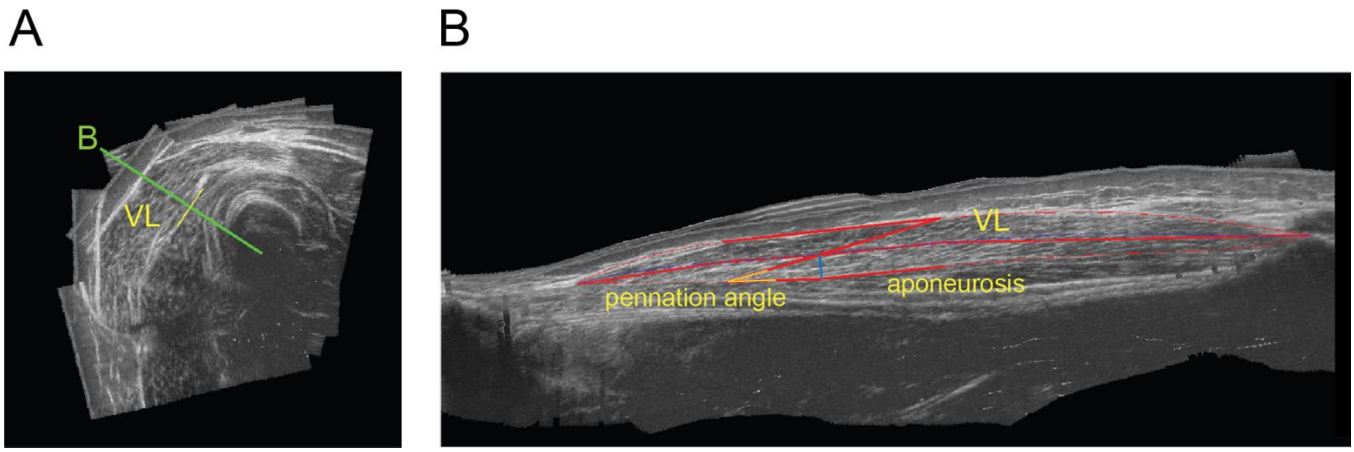

Figure 1*: 3D-US pennation angle quantification. (**A**) Example of a transversal cross section through the 3D-US dataset of the VL muscle. On the transversal plane the longitudinal plane through the muscle center (green line) and its projection on the deep aponeurosis (yellow line) are shown. (**B**) Longitudinal plane through the center of the VL muscle. The pennation angle and the fiber length are determined at 2/3 of muscle length.*

MRI

To quantify the pennation angle and fiber length in MRI we used the muscle DTI toolbox for Matlab developed by Damon *et al.*[8]. Our methodology involved several steps. First, the boundaries of the VL muscle were manually delineated in the DIXON water image. This step was necessary to create a binary image mask that prevented fiber tracts from extending beyond the muscle region. Next, a region of interest (ROI) was manually drawn on the deep aponeurosis of the VL muscle, at a location that corresponds to two-thirds of the muscle's proximal to distal length. This anatomical positioning matched the approach used for the 3D-US measurements (Figure 2A). Once the ROI was established, fiber tracts were propagated from the seed points within the ROI. These tracts reconstructed a

bundle of fibers that extended from the aponeurosis to the lateral border of the muscle (Figure 2B). To mitigate the influence of noise and image artifacts, each fiber was smoothed using a polynomial fit. This smoothing process enabled interpolation of the fiber tract positions at a higher resolution than the original tracts. Following the smoothing step, we quantified the pennation angle and fiber length. The pennation angle was determined as the average angle of the fiber bundle in relation to the aponeurosis (Figure 2C). Additionally, the average fiber length of the bundle was measured. We used the default settings of the software[8] for the selection of the fiber propagation algorithm, ensuring consistency with established conventions.

Muscle thickness is an indicator of muscle strength and power production and it can be used to evaluate the muscle size and the induced training performance of a muscle.[19] In order to assess the impact of errors in measurement of pennation angle and fiber length with the proposed different methods, the equation $thickness = fiber\ length \cdot \sin\vartheta$ was used to calculate VL muscle thickness, where ϑ is the pennation angle.

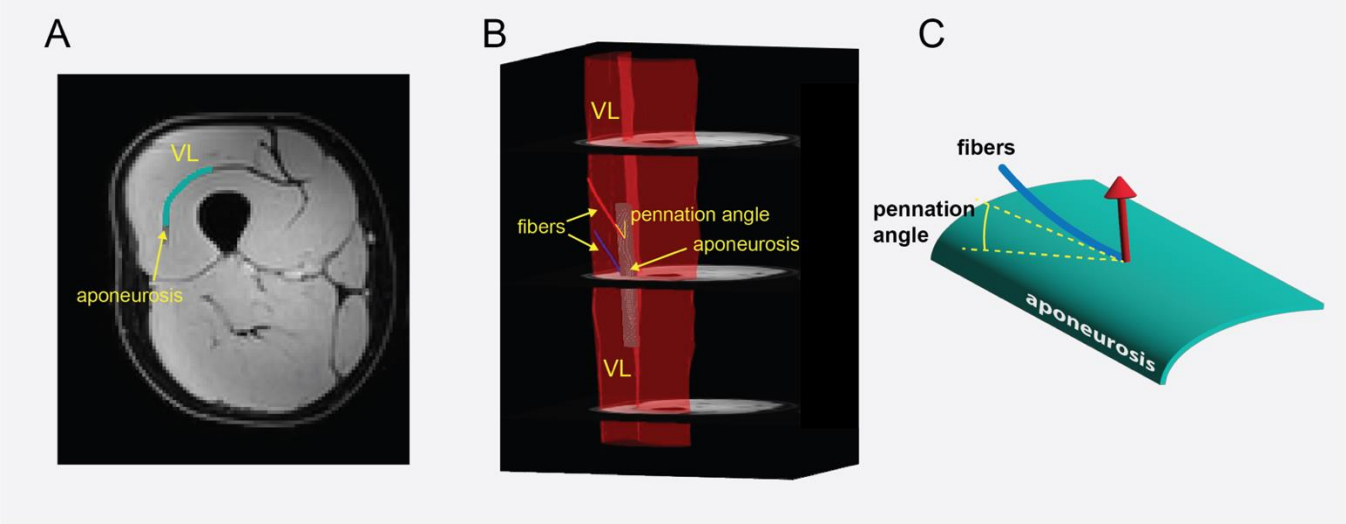

Figure 2*: DTI-based pennation angle and muscle fiber length measurements. (**A**) Transversal cross section of anatomical Dixon image. The VL muscle and the deep aponeurosis in cyan color are indicated. (**B**) Examples of fiber tractography bundles (red and blue fibers) in the mid-belly of the VL muscle at approximately 2/3 of the proximal to distal muscle length. (**C**) Schematic of determination of the pennation angle in the VL muscle using DTI. The pennation angle is defined as the complementary angle between the fiber bundle and the surface normal (red arrow) to the deep aponeurosis (cyan-colored surface).*

Statistical Analyses

Statistical analyses were performed in GraphPad and SPSS (IBM SPSS Statistics for Windows, Version 26 Armonk, NY: IBM Corp). To visualize the distribution of the data, a box plot analysis was performed, in which the median, quartiles and any outliers present in the data were displayed. The bias and paired t-test analysis, the Bland-Altman analysis and the Intraclass correlation coefficient (ICC) were used to represent and to assess the accuracy of the fibertractography-based pennation angle and fiber length with respect to the 3D-US based measurements. The Limits of Agreement (LoAs) of the Bland-Altman analysis were calculated as ±1.96 x standard deviation (SD). The bias was calculated as the mean of the errors between the two measurements.[20]

The ICC is defined as the variance of intra-subjects' measurements divided by the total variance of inter-subject and intra-subject measurements. For reliability it was calculated with a two-way random effect, with measures of absolute agreement.[20, 21] Values of ICC below 0.50 were considered poor, between 0.50 and 0.75 was considered moderate, between 0.75 and 0.90 good, and above 0.9 excellent. Negative values of the ICC indicate no correlation and are reported here as 0.

Results

The nine subjects completed the MRI and 3D-US sessions successfully. All DTI datasets had a signal to noise ratio (SNR) greater than 25, above the criterium for accurate tensor calculations.[22,23]

Figure 3A illustrates the comparisons of VL pennation angles between 3D-US and DTI based on individual measurements and distributions. The average pennation angle measured with 3D-US was 18.7 ± 3.9°, exhibiting a right-skewed data distribution. Conversely, the average pennation angle measured using the DTI fiber-tractography approach was 21.9 ± 5.2°, with a normal data distribution and a larger interquartile range compared to 3D-US measurements, indicating higher inter-subjects variability. While the pennation angles measured with 3D-US and DTI showed close agreement for most subjects, there were significant differences observed for at least 3 subjects, with the DTI measurements yielding larger values.

Figure 3B demonstrates the comparison of VL fiber lengths between 3D-US and DTI. The average fiber length measured with 3D-US was 77.6 ± 15.4 mm, and the data distribution exhibited left-skewness with scattered data points. In contrast, the average length measured using DTI fiber-tractography was

59.7 ± 15.4 mm, with a right-skewed data distribution and a larger interquartile range compared to the 3D-US measurements. Similar to the pennation angle, considerable differences in fiber lengths between 3D-US and DTI were observed for individual subjects, where DTI measurements resulted in smaller values.

Figure 3C presents the comparison of muscle thickness between 3D-US and DTI based on individual measurements and distributions. The average muscle thickness measured with 3D-US was 24.2 ± 3.5 mm, with a left-skewed data distribution. In contrast, the average muscle thickness measured with DTI was 21.5 ± 4.7 mm, and the data distribution was normal. Similarly to fiber length, DTI measurements of VL muscle thickness resulted in smaller values than 3D-US measurements.

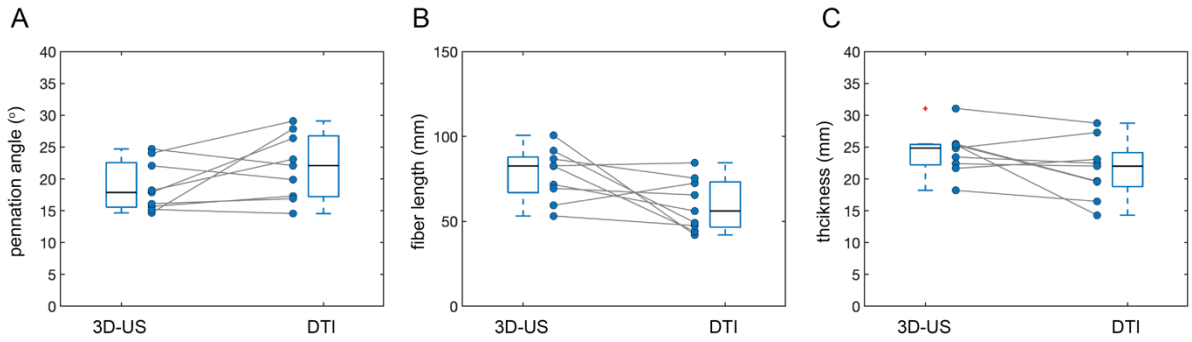

Figure 3*: 3D-US and DTI-based (**A**) pennation angles (°), (**B**) fiber lengths (mm) and (C) muscle thickness (mm) for all subjects. The boxplots indicate the interquartile ranges (the middle 50% of measurements), the median marks indicate the median values, and the upper and lower whiskers represent scores outside the middle 50% of measurements. Whereas the blue data points and grey lines are the measurements for the individual subjects.*

Bland-Altman Analysis

Bland-Altman analysis were carried out for pennation angle, fiber length and muscle thickness. The derived 95% limits of agreement (LoA) and the bias are shown in Figure 4 with black solid line and dashed lines respectively.

The Bland-Altman analysis revealed a non-significant bias in the DTI-derived pennation angles as compared to those from 3D-US of 3.2 ± 5.2° (p = 0.11) (Figure 4A; Table 1). A larger bias in the DTI-derived fiber lengths as compared to those from 3D-US of -18 ± 24 mm (p = 0.052) was found (Figure 4B; Table 1). Figure 4C shows a bias of -2.7± 4.2 mm (p = 0.09) between the DTI and 3D-US estimation of the VL muscle thickness.

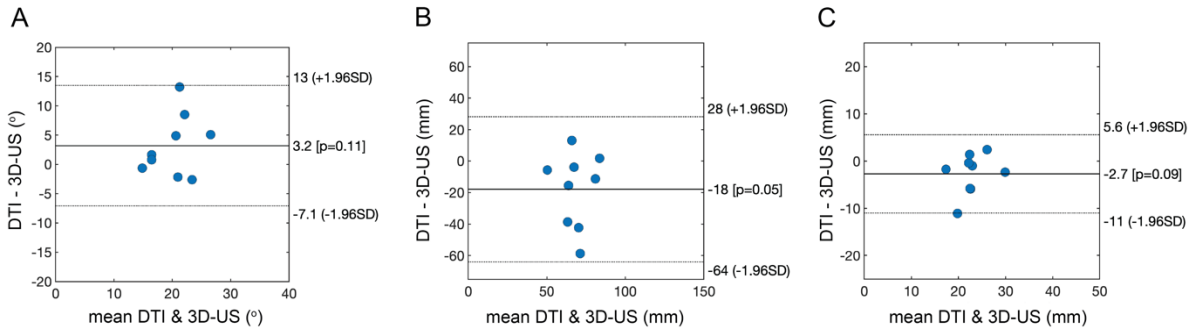

Figure 4*: Bland-Altman analysis. (**A**) 3D-US versus DTI-based pennation angles (°). (**B**) 3D-US versus DTI-based fiber lengths (mm). (C) 3D-US versus DTI-based muscle thickness(mm).The black solid line indicates the bias and the dashed lines indicate the Bias ± Limits of Agreement (LoA), i.e., ±1.96 x standard deviation (SD).*

ICC

The intraclass correlation coefficient with absolute agreement between DTI and 3D-US measurements were calculated for pennation angle and fiber length. The reported values (see Table 1) show poor agreement between the two different measurement modalities.

Table 1 lists the values for the mean ± standard deviation, bias and the percentage of the Limits of Agreement (LoA) following from the Bland-Altman analyses, the p-value following from the paired t-test, as well as the intraclass correlation coefficients with absolute agreement (ICC).

Table 1*: VL muscle pennation angle, fiber length, and muscle thickness measurements by 3D-US and DTI. Values for mean* ± standard deviation*, bias, and p-value of the measurements with DTI and 3D-US acquisitions, the percentage of the Limits of Agreement (LoA) with respect to the mean resulting from the Bland-Altman analysis, and intraclass correlation coefficient (ICC) are listed.*

	Pennation Angle		Fiber Length		Muscle thickness	
	3D-US	DTI	3D-US	DTI	3D-US	DTI
mean ± standard deviation	18.7 ± 3.9°	21.9 ± 5.2°	77.6 ± 15.4 mm	59.6 ± 15.4 mm	24.2 ± 3.5 mm	21.5 ± 4.7 mm
bias (DTI – 3D-US) p-value	3.2 ± 5.2° (p = 0.10)		-17.9 ± 21 mm (p = 0.05)		-2.7 ± 4.2 mm (p = 0.09)	
LoA (%)	8.3° (40%)		46 mm (67%)		8.3 mm (40%)	
ICC (95%-confidence interval)	0.29 -0.23<ICC<0.76		0 (-0.11) -0.44<ICC<0.4		0.41 -0.15<ICC<0.81	

Discussion

The primary aim of this study was to evaluate the non-invasive measurement of the pennation angle in the VL muscle with two 3D imaging modalities, *i.e.*, 3D-US and DTI. The 3D-US technique for measuring pennation angle in the VL muscle has been validated with cadaveric specimens,[4] and therefore we decided to consider 3D-US as the baseline measurement with which to compare the DTI based pennation angle and fiber length measurement methods. The DTI based data for quantifying fiber architecture –based on diffusional properties of water in tissue– is inherently different to the ultrasound data in terms of 3D image resolution and type of data, *i.e.*, vector field instead of intensity based. Therefore, we applied different post-processing steps to arrive at pennation angle and muscle fiber lengths for the VL.

Taken together, the main finding is that the 3D-US and DTI measurements of the VL muscle pennation angle and fiber length show rather poor agreement on an individual subject basis.

Although Bland-Altman analysis revealed that the group-averaged values for the VL pennation angle measured by 3D-US and DTI were not significantly different (Figure 4), differences for several individual subjects were large and amounted even to 13.2° for one subject. The large differences for individual subjects resulted in a poor ICC value. DTI was used by several groups[24,25,26] to quantify pennation angles in the VL muscle. Noehren *et al.* observed pennation angles of 16.4 ± 2.94° and 15.3 ± 2.84° comparing STEAM and TSRE MRI acquisition sequences.[24] Herman *et al.* reported a pennation angle of 18.7° in the stretched leg position,[25] while Valaparla *et al.* measured a pennation angle of 23.78 °.[26] Previous 2D-US studies with stretched leg position reported lower values than those found in this study ranging between 2° and 18°.[27,28]

For most subjects, the DTI-based pennation angle was higher than the one obtained by 3D-US. These differences might be explained from the different postures –seated with stretched legs versus lying supine in the MRI scanner– which could result in different amounts of tension or slack of the VL muscle fibers leading to a different fiber angle. Another explanation would be that for the 3D-US the pennation angle is evaluated in a mid-longitudinal fascicle plane (Figure 1A),[29] whereas for DTI the pennation angle is calculated from the inner-product of the fiber directions and the aponeurosis plane (Figure 2C). In case that the mid-longitudinal fascicle plane is not perfectly aligned with the fibers, the angle calculated with DTI will be consequently higher than the one calculated from 3D-US. From the point of reproducibility, choosing the muscle mid-longitudinal fascicle plane as a plane of reference might be advantageous, as this plane can be chosen based on well-visible anatomical landmarks. However, from a biomechanics perspective, knowledge on the precise 3D architecture of the muscle fibers –including fiber lengths and physiological cross-sectional areas– would be likely preferred.

Previous studies on 2D-US pennation angle measurements confirmed that the orientation of the image plane can cause a variation in the pennation angle estimates when chosen either parallel with the fiber orientation or oriented perpendicular to the aponeurosis.[30] Alternatively, pilot studies are needed to establish the optimal orientation of the 2D imaging plane for a specific muscle. For example, in the study by Bolsterlee *et al.* the optimal orientation of the image plane with 2D-US for the Gastrocnemius muscle was established based on MRI acquisitions, before pennation angle measurements.[31]

The group-averaged value for the VL fiber lengths measured by 3D-US was considerably higher than that measured by DTI. Moreover, differences between individual subjects were large, reflected in a

high LoA (%) value and low ICC. The fiber lengths measured by 3D-US are consistent with those reported in other studies.[19,32] Mpampoulis *et al.* measured fiber lengths of 73 ± 7 mm in the high-power muscles group and 65 ± 8 mm in the low-power muscles group.[19] Bohm *et al*. identified an optimal VL fascicle length of 94 ± 11 mm (the length at which the muscle can produce the most efficient contraction), which would vary slightly during walking (86 ± 14 mm) and running (101 ± 19 mm).[32] However, the fiber length values measured by DTI seem clearly underestimated, although it is worth noting that Noehren *et al.* reported even shorter VL fiber lengths of 30.8 ± 7.5 mm and 27.2 ± 7.9 mm, measured using STEAM and twice-refocused spin echo (TRSE) DTI acquisition sequences, respectively.[24] Whereas intra-subject differences in pennation angles might be explained from differences in posture or slightly different definitions, the low fiber lengths measured by DTI must have a methodological origin. Previous studies have demonstrated that different hip joint angles between 0° and 60° do not significantly affect fiber length and pennation angle in the VL muscle.[33] Hence, we think that the average fiber length by DTI in a number of subjects was underestimated due to incomplete fiber tractography and prematurely terminated fibers at artifacts near muscle boundaries. These problems might be alleviated by a combination of higher imaging resolution, increased SNR, and improved shimming to avoid susceptibility-related artifacts near the leg and muscle boundaries. However, such improvements are not trivially implemented and may only be achieved at the cost of increased scan time and limited 3D spatial coverage, and moreover may require an RF receiver coil optimized for upper leg imaging.

Both 3D-US and DTI have their pros and cons. The post-processing of the DTI images involved registration of the diffusion-weighted images to anatomical Dixon images, manual segmentations of aponeurosis and muscle volume, and fiber tractography to establish the 3D course of a bundle of muscle fibers. Instead, the 3D-US involved in-painting of a 3D volume by sweeping a linear ultrasound probe across the muscle and 3D position tracking with an external device, which involved several registration steps.[4] DTI is difficult to perform with a bend knee position, even if this fits in the physical confinement of the scanner bore. This is because it is difficult to perform magnetic field shimming of the leg at an angle with the main magnetic field direction leading to inhomogeneities and image distortions. 3D-US can, in principle, be performed in any posture.

Conclusions

In this study we compared the measurements of the pennation angle and fiber length of the VL muscle in healthy volunteers using validated 3D-US and DTI fiber-tractography methods. The 3D-US

and DTI measurements of the VL muscle pennation angle and fiber length show poor agreement on an individual subject basis.

References

1. Sánchez Riera C, Lozanoska-Ochser B, Testa S, Fornetti E, Bouché M, Madaro L. Muscle Diversity, Heterogeneity, and Gradients: Learning from Sarcoglycanopathies. *Int J Mol Sci*. 2021;22(5). doi:10.3390/ijms22052502
2. Garrett WEJ, Nikolaou PK, Ribbeck BM, Glisson RR, Seaber A V. The effect of muscle architecture on the biomechanical failure properties of skeletal muscle under passive extension. *Am J Sports Med*. 1988;16(1):7-12. doi:10.1177/036354658801600102
3. Patel TJ, Lieber RL. Force transmission in skeletal muscle: from actomyosin to external tendons. *Exerc Sport Sci Rev*. 1997;25:321-363.
4. Weide G, Van Der Zwaard S, Huijing PA, Jaspers RT, Harlaar J. 3D ultrasound imaging: Fast and cost-effective morphometry of musculoskeletal tissue. *J Vis Exp*. 2017;2017(129). doi:10.3791/55943
5. Colley E, Carroll J, Thomas S, Varcoe RL, Simmons A, Barber T. A methodology for non-invasive 3-D surveillance of arteriovenous fistulae using freehand ultrasound. *IEEE Trans Biomed Eng*. 2018;65(8). doi:10.1109/TBME.2017.2782781
6. Lee D, Li Z, Sohail QZ, Jackson K, Fiume E, Agur A. A three-dimensional approach to pennation angle estimation for human skeletal muscle. *Comput Methods Biomech Biomed Engin*. 2015;18(13). doi:10.1080/10255842.2014.917294
7. NITRC: vIST/e: Tool.
8. Damon BM, Ding Z, Hooijmans MT, et al. A MATLAB toolbox for muscle diffusion-tensor MRI tractography. *J Biomech*. 2021;124. doi:10.1016/j.jbiomech.2021.110540
9. Froeling M. QMRTools: a Mathematica toolbox for quantitative MRI analysis. *J Open Source Softw*. 2019;4(38). doi:10.21105/joss.01204
10. Bolsterlee B, Veeger HE, van der Helm FC, Gandevia SC, Herbert RD. Comparison of measurements of medial gastrocnemius architectural parameters from ultrasound and diffusion tensor images. J Biomech. 2015 Apr 13;48(6):1133-40. doi: 10.1016/j.jbiomech.2015.01.012. Epub 2015 Jan 21. PMID: 25682540.
11. Behan, Fearghal P. & Vermeulen, Robin & Smith, Tessa & Arnaiz, Javier & Whiteley, Rodney & Timmins, Ryan & Opar, David. (2018). Poor agreement between ultrasound and inbuilt diffusion tensor MRI measures of biceps femoris long head fascicle length. Translational Sports Medicine. 2. 10.1002/tsm2.58.
12. Klein S, Staring M, Murphy K, Viergever MA, Pluim JPW. Elastix: A toolbox for intensity-based medical image registration. *IEEE Trans Med Imaging*. 2010;29(1). doi:10.1109/TMI.2009.2035616
13. Secondulfo L, Ogier AC, Monte JR, et al. Supervised segmentation framework for evaluation of diffusion tensor imaging indices in skeletal muscle. *NMR Biomed*. 2021;34(1). doi:10.1002/nbm.4406
14. Hooijmans MT, Monte JRC, Froeling M, et al. Quantitative MRI Reveals Microstructural Changes in the Upper Leg Muscles After Running a Marathon. *J Magn Reson Imaging*. 2020;52(2). doi:10.1002/jmri.27106
15. Suskens JJM, Secondulfo L, Kiliç Ö, et al. Effect of two eccentric hamstring exercises on muscle architectural characteristics assessed with diffusion tensor MRI. *Scand J Med Sci Sports*. 2023;33(4):393-406. doi:10.1111/sms.14283
16. Derzsi Z, Volcic R. MOTOM toolbox: MOtion Tracking via Optotrak and Matlab. *J Neurosci Methods*. 2018;308. doi:10.1016/j.jneumeth.2018.07.007
17. Wolf I, Vetter M, Wegner I, et al. The medical imaging interaction toolkit. *Med Image Anal*. 2005;9(6). doi:10.1016/j.media.2005.04.005
18. Álvaro Huerta Ojeda, Miguel Riquelme Guerra, Walter Coronado Román, María-Mercedes Yeomans, Rodrigo Fuentes-Kloss. (2022) Kinetics of ventilatory and mechanical parameters of novice male rowers on the rowing ergometer. *International Journal of Performance Analysis in Sport* 22:3, pages 422-436.
19. Mpampoulis T, Methenitis S, Papadopoulos C, Papadimas G, Spiliopoulou P, Stasinaki A-N, Bogdanis GC, Karampatsos G, Terzis G. Weak Association between Vastus Lateralis Muscle Fiber Composition and Fascicle Length in Young Untrained Females. *Sports*. 2021; 9(5):56.

https://doi.org/10.3390/sports9050056
20. Bartko JJ. The intraclass correlation coefficient as a measure of reliability. *Psychol Rep*. 1966;19(1). doi:10.2466/pr0.1966.19.1.3
21. Vaz S, Falkmer T, Passmore AE, Parsons R, Andreou P. The Case for Using the Repeatability Coefficient When Calculating Test-Retest Reliability. *PLoS One*. 2013;8(9). doi:10.1371/journal.pone.0073990
22. Froeling M, Oudeman J, Van Den Berg S, et al. Reproducibility of diffusion tensor imaging in human forearm muscles at 3.0 T in a clinical setting. *Magn Reson Med*. 2010;64(4). doi:10.1002/mrm.22477
23. Damon BM, Buck AKW, Ding Z. Diffusion-tensor MRI-based skeletal muscle fiber tracking. *Imaging Med*. 2011;3(6). doi:10.2217/iim.11.60
24. Noehren B, Andersen A, Feiweier T, Damon B, Hardy P. Comparison of twice refocused spin echo versus stimulated echo diffusion tensor imaging for tracking muscle fibers. J Magn Reson Imaging. 2015 Mar;41(3):624-32. doi: 10.1002/jmri.24585. Epub 2014 Feb 19. PMID: 24554376; PMCID: PMC4231024.
25. Kan JH, Heemskerk AM, Ding Z, Gregory A, Mencio G, Spindler K, Damon BM. DTI-based muscle fiber tracking of the quadriceps mechanism in lateral patellar dislocation. J Magn Reson Imaging. 2009 Mar;29(3):663-70. doi: 10.1002/jmri.21687. PMID: 19243049; PMCID: PMC2676427.
26. Valaparla SK, Gao F, Daniele G, Abdul-Ghani M, Clarke GD. Fiber orientation measurements by diffusion tensor imaging improve hydrogen-1 magnetic resonance spectroscopy of intramyocellular lipids in human leg muscles. J Med Imaging (Bellingham). 2015 Apr;2(2):026002. doi: 10.1117/1.JMI.2.2.026002. Epub 2015 Jun 9. PMID: 26158115; PMCID: PMC4478933.
27. Sjoerdsma M, Caresio C, Tchang B, Meeder A, Van De Vosse F, Lopata R. The feasibility of dynamic musculoskeletal function analysis of the vastus lateralis in endurance runners using continuous, hands-free ultrasound. *Appl Sci*. 2021;11(4). doi:10.3390/app11041534
28. Raj IS, Bird SR, Westfold BA, Shield AJ. Effects of eccentrically biased versus conventional weight training in older adults. *Med Sci Sports Exerc*. 2012;44(6). doi:10.1249/MSS.0b013e3182442ecd
29. Ruple BA, Mesquita PHC, Godwin JS, et al. Changes in vastus lateralis fibre cross-sectional area, pennation angle and fascicle length do not predict changes in muscle cross-sectional area. *Exp Physiol*. 2022;107(11):1216-1224. doi:10.1113/EP090666
30. Bolsterlee B, Gandevia SC, Herbert RD. Effect of Transducer Orientation on Errors in Ultrasound Image-Based Measurements of Human Medial Gastrocnemius Muscle Fascicle Length and Pennation. *PLoS One*. 2016;11(6). doi:10.1371/journal.pone.0157273
31. Bolsterlee B, Gandevia SC, Herbert RD. Ultrasound imaging of the human medial gastrocnemius muscle: How to orient the transducer so that muscle fascicles lie in the image plane. *J Biomech*. 2016;49(7). doi:10.1016/j.jbiomech.2016.02.014
32. Bohm, S., Marzilger, R., Mersmann, F. *et al.* Operating length and velocity of human vastus lateralis muscle during walking and running. *Sci Rep* **8**, 5066 (2018). https://doi.org/10.1038/s41598-018-23376-5
33. Garnier YM, Lepers R, Canepa P, Martin A, Paizis C. Effect of the Knee and Hip Angles on Knee Extensor Torque: Neural, Architectural, and Mechanical Considerations. Front Physiol. 2022 Jan 4;12:789867. doi: 10.3389/fphys.2021.789867. PMID: 35058798; PMCID: PMC8764280.

CHAPTER 5

Effect of two eccentric hamstring exercises on muscle architectural characteristics assessed with diffusion tensor MRI

Jozef J. M. Suskens
Laura Secondulfo
Özgur Kiliç
Melissa T. Hooijmans
Gustav Reurink
Martijn Froeling
Aart J. Nederveen
Gustav J. Strijkers
Johannes L. Tol

Scandinavian Journal of Medicine & Science Sports in Sports, 2022

The second part of this thesis focuses on the application of the techniques presented in the previous chapters for the measurement of fiber angles in a relevant application.

To this end, in this chapter we illustrate a study on the comparison between the effects of two different injury prevention programs on basketball players. Changes in fiber fascicle orientations of the full muscle volume and fiber length in the hamstring muscles, as obtained with DTI, were the primary outcome parameters.

In this chapter the fiber angles are referred to as fascicle orientations.

Abstract

The aim of this study was to evaluate the effect of a Nordic hamstring exercise or Diver hamstring exercise intervention on Biceps femoris long head, semitendinosus and semimembranosus muscle's fascicle length and orientations through diffusion tensor imaging (DTI) with magnetic resonance imaging.

In this three-arm, single-center, randomized controlled trial, injury-free male basketball players were randomly assigned to a Nordic, Diver hamstring exercise intervention or control group. The primary outcome was the DTI-derived fascicle length and orientation of muscles over 12 weeks.

Fifty-three participants were included for analysis (mean age 22 ± 7 years). Fascicle length in the semitendinosus over 12 weeks significantly increased in the Nordic-group (mean [*M*]: 20.8 mm, 95% confidence interval [95% CI]: 7.8 to 33.8) compared with the Control-group (*M*: 0.9 mm, 95% CI: −7.1 to 8.9), mean between-groups difference: 19.9 mm, 95% CI: 1.9 to 37.9, $p = 0.026$. Fascicle orientation in the Biceps femoris long head over 12 weeks significantly decreased in the Diver-group (mean: -2.6°, 95% CI: −4.1 to −1.0) compared with the Control-group (mean: −0.2°, 95% CI: −1.4 to 1.0), mean between-groups difference: -2.4°, 95% CI: −4.7 to −0.1, $p = 0.039$.

The Nordic hamstring exercise intervention did significantly increase the fascicle length of the semitendinosus and the Diver hamstring exercise intervention did significantly change the orientation of fascicles of the Biceps femoris long head. As both exercises are complementary to each other, the combination is relevant for preventing hamstring injuries.

Introduction

Exercise-based interventions are effective in lowering hamstring injury rates.[1] There is strong evidence from a meta-analysis that a 12-week Nordic hamstring exercise intervention can reduce hamstring injury rate by on average 51%.[2] Although effective in daily practice, the underlying preventive mechanism is yet not fully unraveled.[3]

A suggested preventive mechanism of the Nordic hamstring exercise intervention are changes in muscle fiber architecture on two-dimensional (2D) ultrasonography.[4] Lengthening of the Biceps femoris long head fascicles of up to 2 centimeters is reported.[5-10] If the increased fascicle length involves an increased number of sarcomeres in series, it might positively affect flexibility and so reduce the risk of sarcomere overstretching.[11-13] A change in pennation angle of the Biceps femoris long head might be the other preventive mechanism, but the evidence is conflicting.[6-10] Other reported (functional) results of the intervention is an increase in eccentric hamstring strength,[14, 15] and increased anatomical cross-sectional area of the semitendinosus.[5]

The semitendinosus is significantly more recruited than the Biceps femoris long head during the knee-orientated Nordic hamstring exercise.[16, 17] The majority of injuries involve, however, the Biceps femoris long head and occur at relative long muscle length, with hip flexed, and knee extended.[18-21] This has led to the discussion whether the Nordic hamstring exercise is the most appropriate preventive exercise.[22-24] Hip-orientated hamstring exercises (e.g., Romanian deadlift, single-leg deadlift and Diver hamstring exercise) are suggested as alternatives, as hip exercises are executed at a longer muscle length with a relatively higher muscle activation pattern for the Biceps femoris long head.[19] The Diver hamstring exercise is a simple hip-orientated hamstring exercise that requires no additional equipment, performed over a range of motion at longer muscle lengths, compared with the Nordic hamstring exercise.[19] Effects of the Diver exercise on 2D ultrasound muscle fiber architecture of the Biceps femoris long head, semitendinosus and semimembranosus are unknown.

Limitations of 2D ultrasound in Nordic hamstring exercise studies are that findings are predominantly limited to Biceps femoris long head,[5-9] based on a single fascicle and these measurements are highly operator dependent.[5, 7-9, 25] There is furthermore no literature, supporting the generalizability of changes in muscle fiber architecture in the Biceps femoris long head to other hamstring muscles. The effect of the Nordic hamstring exercise intervention on the muscle fiber architecture of the semitendinosus and semimembranosus is unknown.

A novel method for evaluating muscle fiber architecture is diffusion tensor imaging (DTI). Diffusion tensor imaging is a non-invasive quantitative magnetic resonance imaging (MRI) technique that measures the motion of water molecules in tissue. Water diffusion in healthy muscle tissue is anisotropic, which means that the majority of water molecules diffuse along the longitudinal axis of the muscle fibers.[26] With custom-built DTI data analysis methods and tractography software, fascicle length and orientation can be reliably determined in lower limb muscles.[27-30]

The aim of this study was to evaluate the effect of the Nordic hamstring exercise and Diver hamstring exercise on muscle fascicle length and orientation in the Biceps femoris long head, semitendinosus and semimembranosus through DTI. Secondary aims were to evaluate the effect of these hamstring exercises on strength, flexibility, and individual hamstring muscle volume.

Materials and Methods

Study design

The study was a three-arm, single-center, randomized controlled trial performed in a university medical center in the Netherlands. The study was registered in the Netherlands Trial Register (NL7248) on July 13th, 2018, approved by the medical research ethics committee of the Academic Medical Center Amsterdam (NL63496.018.17) and was in accordance with the Declaration of Helsinki. Due to the COVID-19 pandemic, some participants were unable to attend a second measurement session because of shut down of the MRI facility by Dutch governmental sanctions. The study protocol was amended and approved by the medical ethics review committee on April 22nd, 2020. The COVID-19 amendment voluntarily extended the intervention period of 12 weeks for the already enrolled participants to a maximum of 24 weeks. The effect of an extended intervention period on the primary outcome measures was expected to be marginal as the intervention effect reaches a certain ceiling with time.[7] Patients or the public were not involved in the design, or conduct of this study. At the start of this study, no comparable studies using DTI were available. Therefore, sample size calculation was based on an ultrasonographically determined 16% (19 mm) increase in fascicle length of the Biceps femoris long head, following eccentric training.[31] With an approximate effect size of 1.2, power of 80% and an alpha of 0.05, a sample size of 24 participants per group were needed.

Participants

Participants were recruited from both recreational active and elite basketball teams, via promotion at sports and hospital facilities as well as social media platforms. Detailed information about the study procedure, participant rights, and contact information for further questioning was sent via email or handed over in paper-form before screening for inclusion. Inclusion criteria were 16 years of age or older, basketball player and capable of doing an active exercise program. Exclusion criteria were a hamstring injury within the past year and contraindication for the MRI device (e.g., claustrophobia and pacemaker). All participants gave written consent before the start of data collection.

Procedure & Randomization

All participants were registered in a data management program by the coordinating researcher (JS) (CastorEDC, CIWIT B.V., Amsterdam, the Netherlands). The participants were randomized by a computer-generated scheme (Microsoft Excel *ASELECT* function) and allocated to a Nordic-group, Diver-group or Control-group by two researchers (GR or JS). The allocation of participants of the same team was made in cluster randomization and allocation of the individual participants were randomized as single entities. All participants took part in two measurement sessions, a baseline measurement in the week preceding the start of the intervention and a follow-up measurement within 7 days after the 12-week intervention period.[7] Participants were included for analysis if they attended both baseline and follow-up measurement sessions. Blinding of participants to their exercise and to the presence of another group was not guaranteed an feasible when they were part of the same club.

Intervention & Compliance

For both the Nordic and Diver-group, a 12-week intervention protocol was prescribed, translated from proven-effective preventive intervention protocols.[32, 33] The number of sessions is described in Table 1. Protocol details were provided via mail, including a step-by-step description and link to a videotaped example.[34] The intervention was unsupervised and participants were advised to execute the exercise at the end of a training yet free to choose appropriate moments. The Control-group allocated participants were asked to continue their usual training regime. In all groups, participants were asked to postpone the start of additional hamstring strengthening exercises to after the follow-up measurement session. In case of participants were already performing hamstring exercises, they were asked to continue their training regime. Compliance with the intervention was evaluated

through online questionnaires. A more detailed description of the online compliance questionnaire is included in Appendix S1.

TABLE 1: *Exercise protocol for Nordic hamstring exercise and Diver hamstring exercise intervention.*

Week no.	Sessions per week (frequency)	Number of sets per session	Repetitions per set[a]
1	1	2	5
2	2	2	6
3	2	3	6
4	2	3	6, 7, 8
5	2	3	8, 9, 10
6–12	2	3	10, 9, 8

Study Preparation and Data Collection

Hamstring Strength and Flexibility

At baseline and 12 -week follow-up, hamstring strength was assessed in a prone position, with the knee to 15° and 90° of knee flexion, as determined by visual estimation. The tester placed a handheld dynamometer (MicroFET2, HOGGAN Scientific) at the heel of the participant and applied force to the heel, gradually increasing in 3–5 s. Participants were instructed to resist the applied force (break test). The highest peak force of three attempts in both knee flexion angles was documented for both positions in Newton. Hamstring flexibility was acquired with the passive leg raise and the active knee extension test in degrees.[35]

Magnetic Resonance Imaging

Magnetic resonance imaging datasets were acquired on a 3 Tesla MRI scanner (Ingenia, Philips, Best). All participants were examined in supine position and feet first using a 16-channel receive coil and 12-channel receive coils located in the scanner table. An elastic band around the feet and sandbags at the lateral side of the lower legs were used to minimize movement and reproduce scanner placement between measurement sessions. The data were acquired in a multi-stack protocol covering the full upper leg region. The scan protocol consisted of four axial proton density weighted Dixon scans for

complete anatomical mapping of the hamstring muscles from proximal ischial origin to the most distal insertion on the tibia. Three axial diffusion-weighted (DWI) and axial noise scans corresponded with the three most proximal Dixon sequences and covered all of the hamstring's muscle tissue. The noise scans were for the purpose of data-quality assessment. The acquisition parameters are provided in Appendix S1.

Primary Outcome Measures

The two primary outcome measures were change in fascicle length (e.g., fiber tract lengths representing fascicle length in millimeters) and fascicle orientation (e.g., angle between DTI parameter eigenvector 1 and a reference line representing the intramuscular tendon in degrees) of the Biceps femoris long head, Semitendinosus and the semimembranosus over 12 weeks, obtained with DTI and fiber tractography.[36]

Secondary Outcome Measures

Secondary outcome measures were change in isometric hamstring strength (15° and 90° knee flexion), hamstring flexibility (passive leg raise and active knee extension) and individual hamstring muscle volume (in cubic centimeters) over 12 weeks.

Data Analysis

Magnetic Resonanceimaging & Processing

Magnetic resonance imaging datasets were processed using QMRITools (www.qmritools.com) for Mathematica (Wolfram Research, Inc., Mathematica, Version 12.1, Champaign).[37] The DWI data were de-noised using a principal component analysis noise algorithm and corrected for motion and Eddy currents using affine registration.[38, 39] The diffusion data were then registered to the anatomical space using sequential rigid and B-spline registration to correct for EPI-distortions. The individual stacks of the Dixon and the diffusion scans were merged with an overlap of five slices without motion correction. The diffusion tensor was calculated using an iterative weighted linear least squares (iWLLS) algorithm. Each dataset was manually segmented in ITK-SNAP on the axial scanner reconstructed Dixon water image, on a slice by slice basis for the Biceps femoris long head, Semitendinosus and the semimembranosus by two examiners, JS and KH (Figure 1A,B).[40] The proximal and distal borders were manually determined by identifying the first and last slice containing a pixel of the segmented muscles by one examiner, JS. The individual longitudinal muscle length was obtained from the sum of number of slices. The volumes of individual muscle segmentations in ITK-SNAP were

stored as secondary outcome measure in cubic centimeters (cm^3). An average signal-to-noise ratio was calculated per muscle segmentation with the noise scan as DTI signal divided by the noise.

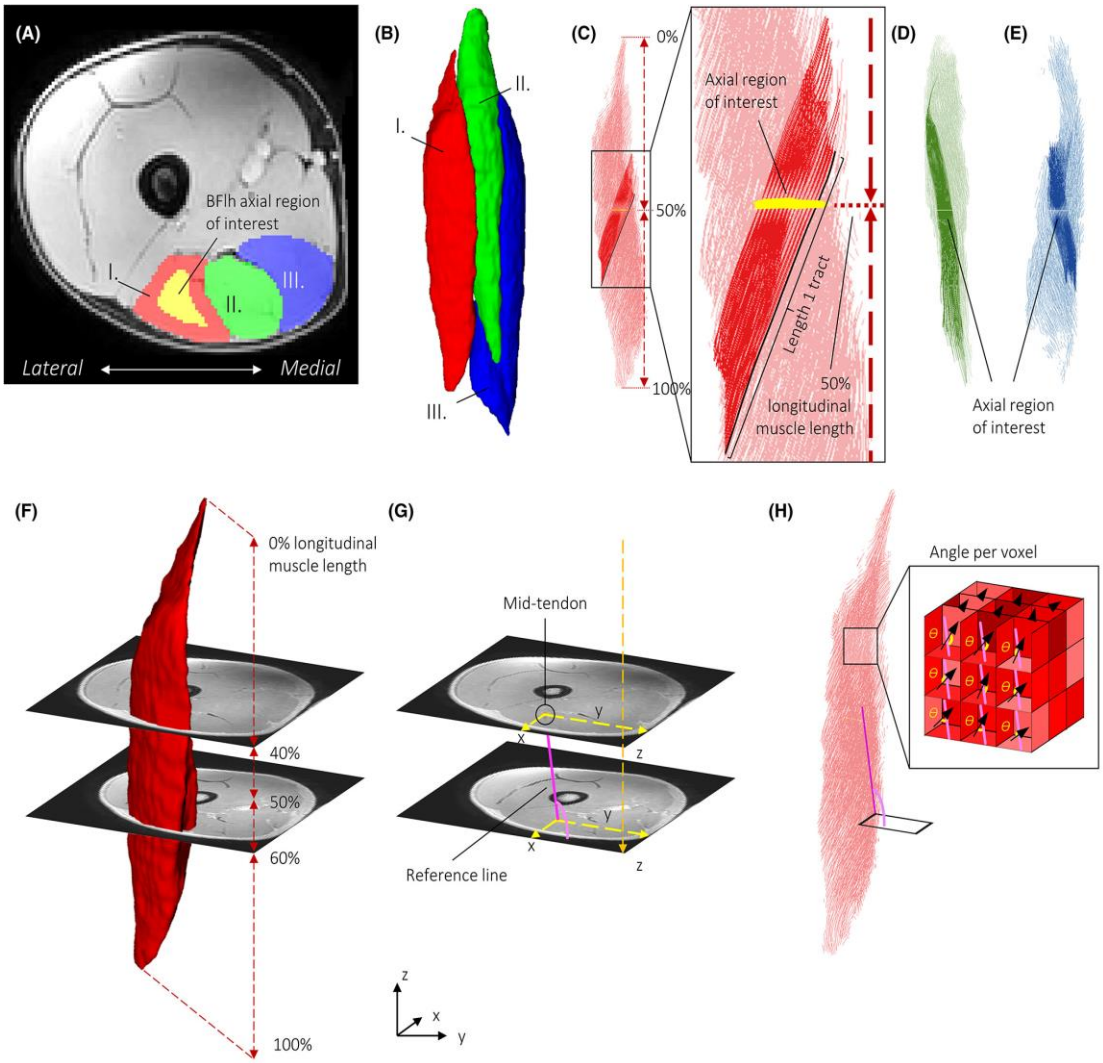

Figure 1: *Overview of methods to measure fascicle length and muscle fascicle orientation from anatomical and diffusion tensor imaging (DTI) scans. (A) Transverse slice of the mDixon scan (water image) at 50% of the longitudinal muscle length of the Biceps femoris long head, showing the Biceps femoris long head (I), Semitendinosus (II) and semimembranosus (III) by manual segmentation. In yellow an example of the axial region of interest for fiber tractography; all tracts running through this window are used for data analysis. (B) Posterior view of the three-dimensional (3D) reconstruction of the manually segmented hamstring muscles. (C) Muscle architecture reconstructions of the Biceps femoris long head. Inset: detailed view of the architecture; yellow window is the axial region of interest at 50% of the individual muscle length; full-red tracts run through axial window and are used for data analysis; solid black diagonal line represents the length of one tract. (D, E) Muscle architecture reconstructions of the Semitendinosus and semimembranosus. Darker tracts are tracts running through axial region of interest at 50% of the individual muscle length. (F) Posterior view of the three-*

dimensional reconstruction of the Biceps femoris long head with transverse slices of the mDixon scan (in-phase image) at 40% and 60% of the longitudinal muscle length. (G) A 3D reference line is placed on the mid-intramuscular tendon at 40% and 60% longitudinal muscle length with respect to a global xyz-orientation. (H) Muscle architecture reconstructions of the Biceps femoris long head. Inset: detailed view within the Biceps femoris long head region of interest, each cube representing a voxel containing a black arrow with the angle Θ between first DTI eigenvector and reference line (pink) in degrees.

Primary Outcome Measure: Fascicle Length

Fiber tractography of the individual segmented hamstring muscles was performed using software (vIST/e; Eindhoven University of Technology, Eindhoven, the Netherlands). Fiber tracts were created through an automatically generated axial region of interest at 50% longitudinal muscle length within each muscle segmentation (Figure 1C–E) and for each muscle, the number of tracts were stored for analysis. The longitudinal center was defined per individual muscle at 50% of the individual longitudinal length. The endpoints of fiber tracts were defined by the borders of segmentation or by stopping criteria of the tractography software (step size of 0.05 per voxel, maximum turning angle per step = 5°, minimal FA = 0.1).[41] These criteria were chosen conservatively to guarantee that the majority of the reconstructed fibers span the full length of intramuscular tissue from proximal to distal. For each participant's measurement session and muscle, the resulting fiber tracts distribution was fitted with a skewed-normal distribution to obtain a mean tract length in millimeters, representing the mean fascicle length of the specific hamstring muscle in millimeters. Fiber tractography and assessment of legitimacy of fiber tracts was carried out by one of the examiners (GS) who was blinded for group randomization. Datasets for which the stitching areas of the stacks caused distinct non-anatomically plausible irregularities in tracts were excluded.

Primary Outcome Measure: Fascicle Orientation

Fascicle orientation maps were determined for the volume of the Biceps Femoris long head, Semitendinosus and semimembranosus individually.[30] The orientation maps consisted of one angle per voxel within the hamstring muscles, with respect to a reference line, placed on the proximal intramuscular tendon of the individual hamstring muscle. To create a reference line, two xyz-coordinates were manually placed in the middle of the intramuscular tendon by one examiner (JS) in the axial in-phase Dixon image, at 40% and 60% of the longitudinal muscle length (Figure 1G). The fascicle orientation between the DTI eigenvector 1 and the reference line were calculated in each voxel (Figure 1H) by one of the examiners (LS) who was blinded for group randomization. Because of skewed distributions in fascicle orientations in all three muscles, median fascicle orientations were

determined in whole muscle volumes for statistical analysis while excluding the stitching areas of the stacks. These stitching areas sometimes contained distinct erroneous fascicle orientations due to the stitching algorithm.

Reliability

We refer to Appendix S1 for the reliability assessment of the manual segmentation, longitudinal muscle length and placement of the reference lines.

Statistical Analysis

Statistical analyses were performed using IBM SPSS Statistics (IBM SPSS Statistics for Windows, Version 27.0. Armonk, NY: IBM Corp). Descriptive statistics were used to describe participant characteristics at baseline, which included: age, height and mass. Adjustments were made for baseline variables that influenced the primary outcome with $p<0.10$. For analysis of the primary outcome measures fascicle length and orientation, a general linear model for repeated measures was used (repeated within-subjects factors: Muscle, non-repeated between-subjects factor: Intervention). In a per-protocol sensitivity analysis of the primary outcome measures, we included the Control-group and compliant participants of the Nordic and Diver-group. For analysis of the secondary outcome measures hamstring strength and flexibility, a univariate general linear model was used (between-subjects factor: Intervention). For analysis of muscle volume, a linear model for repeated measures was used with the same factors as the analysis of the primary outcome measures. Absolute changes from baseline to follow-up were included in all tests to test for the effect of the intervention on the between-group differences over 12 weeks. For all repeated measures tests, when sphericity was violated (Mauchly's test $p<0.05$), the Greenhouse–Geisser correction was used as an adjustment method. The level of significance was set at an alpha of 0.05 for the main and interaction effects. When appropriate, the level of significance was Bonferroni-adjusted in pairwise post-hoc comparisons.

Results

Data Collection

Between September 2018 and March 2020, 100 non-professional competitive basketball players showed interest in participating, from which 72 participants met the inclusion criteria and were allocated to a Nordic-group (n = 24), Diver-group (n = 24), and Control-group (n = 24) (Figure 2). One participant in the Diver-group withdrew before the baseline measurement session. Due to the

COVID-19 lockdown, 20 participants (Nordic-group, *n* = 3; Diver-group, *n* = 6; Control-group, *n* = 11) could not attend the 12-week follow-up measurement session as planned. They were instructed to voluntarily proceed with their exercise protocol, or regular training regime in the Control-group. The median intervention time of these participants was 12.5 weeks (range: 12–17). Two participants withdrew their interest in participation because continuation of the intervention was not desired (Diver-group, *n* = 1; Control-group, *n* = 1). Fifty-three participants (Nordic-group, *n* = 19; Diver-group, *n* = 16; Control-group, *n* = 18) completed a measurement session at baseline and follow-up. Thirty-nine datasets were used for primary outcome measure fascicle length (Nordic-group, *n* = 13; Diver-group, *n* = 13; Control-group, *n* = 13) as 14 datasets were excluded because of distinct non-anatomical irregularities in fascicle tracts in the stitching areas. Example of irregularities is provided in Appendix S1. All 53 datasets were used for the primary outcome fascicle orientation. Detailed results about the reliability tests are presented in Appendix S1, and for detailed results about the scan quality and number of tracts for the fascicle length calculation we refer to Appendix S1.

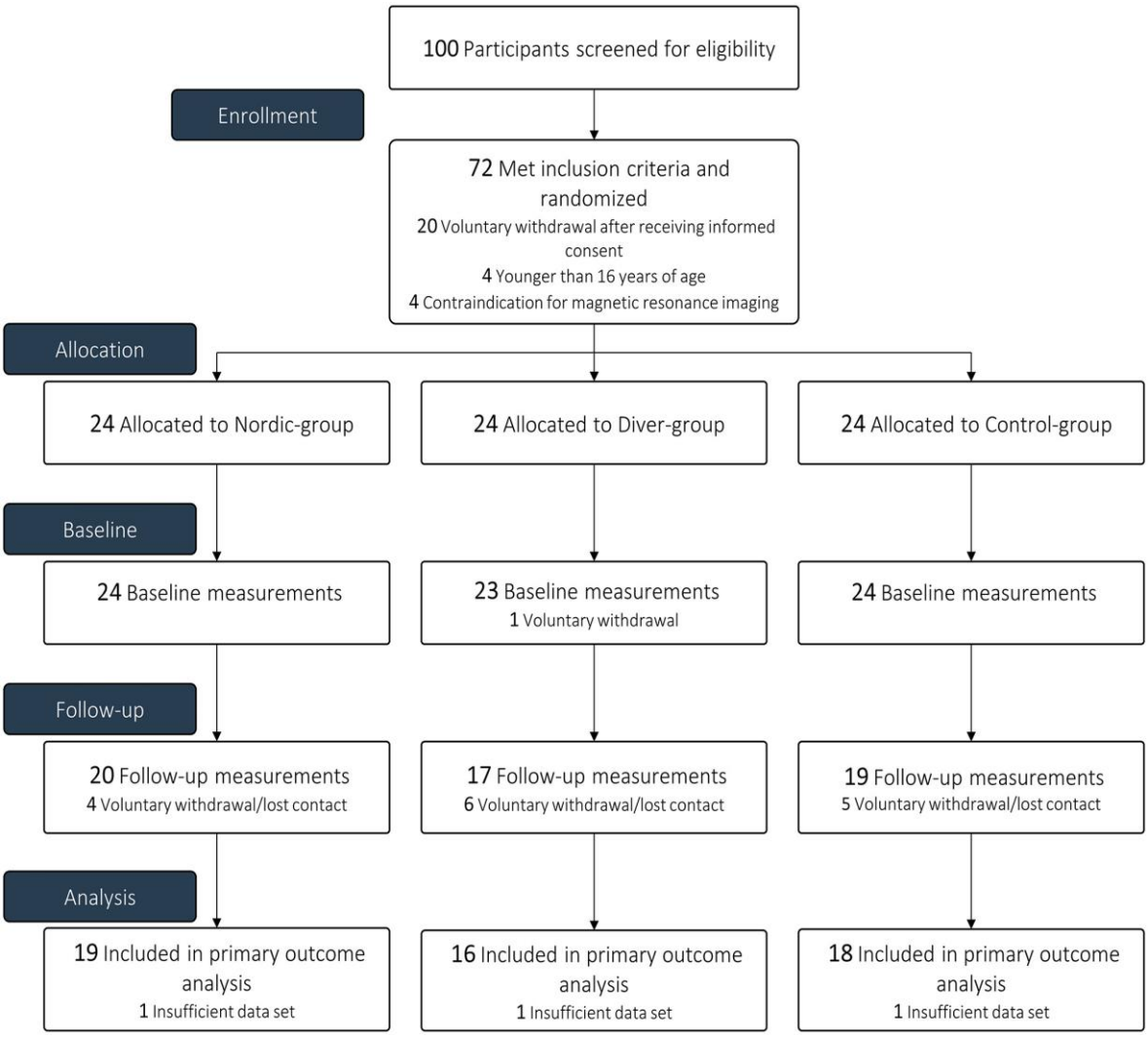

Figure 2: *Flow diagram of participants through the study.*

Baseline Characteristics

Baseline characteristics are illustrated in Table 2. No adjustments of baseline variables were made for the primary outcome analysis, as these variables were not statistically associated with fascicle length and fascicle orientation per individual muscle (p>0.10).

Table 2: *Baseline characteristics.*

Participant characteristics at baseline			
	Nordic-group (n = 19)	Diver-group (n = 16)	Control-group (n = 18)
Age (years)	19.7 ±3.1	25.3 ±8.9	22.1 ±6.2
Height (cm)	190.9 ±8.4	189.8 ±10.1	192.1 ±10.1
Mass (kg)	84.9 ±10.3	86.3 ±12.9	87.3 ±12.6
Primary outcome measures at baseline			
	Nordic-group (n = 13)	Diver-group (n = 13)	Control-group (n = 13)
Fascicle length (mm)			
Biceps femoris	66.4 ±10.4	66.0 ±15.7	74.8 ±22.9
Semitendinosus	137.8 ±31.4	139.5 ±42.9	169.3 ±32.4
Semimembranosus	103.5±16.7	84.5 ±22.2	95.7 ±24.3
	Nordic-group (n = 19)	Diver-group (n = 16)	Control-group (n = 18)
Muscle fascicle orientation (°)			
Biceps femoris	27.1 ±2.2	27.7 ±3.7	27.0 ±4.6
Semitendinosus	17.2 ±2.6	16.7 ±4.3	17.5 ±3.5

	Nordic-group (n = 19)	Diver-group (n = 16)	Control-group (n = 18)
Semimembranosus	21.0 ±3.0	22.2 ±3.7	22.5 ±3.8

- *Note*: Values are means±SD.
- Abbreviations: °, degrees; cm, centimeters; kg, kilograms; mm, millimeters.

Primary Outcome Measures

Fascicle Length of the Biceps Femoris Long Head, Semitendinosus and Semimembranosus

There was a significant interaction effect for type of intervention and muscle on between-group differences over 12 weeks for fascicle length (F(4, 70) = 2.6, p = 0.047). Detailed results are presented in Table 3 and illustrated in Figures 3 and 4. The predefined pairwise post-hoc comparisons revealed that the fascicle length in the Semitendinosus over 12 weeks significantly increased in the Nordic-group (mean [M]: 20.8 mm, 95% confidence interval [95% CI]: 7.8, 33.8) compared with the Control-group (M: 0.9 mm, 95% CI: −7.1, 8.9), mean between-groups difference: 19.9 mm, 95% CI: 1.9, 37.9, p = 0.026. Other post-hoc comparisons were non-significant. Detailed results of all post-hoc comparisons are presented in Appendix S1.

Table 3: *Results for primary and secondary outcome measures between-groups.*

Primary outcome measures absolute Δ over 12 weeks

	Nordic-group (n = 13)	Diver-group (n = 13)	Control-group (n = 13)	p #
Fascicle length (mm)				
Biceps femoris	4.0 ±13.6	4.7 ±12.9	4.6 ±16.1	0.047
Semitendinosus	20.8 ±20.4[a]	5.3 ±19.3	0.9 ±13.3[a]	
Semimembranosus	−1.7 ±20.1	5.3 ±25.7	2.5 ±14.5	

	Nordic-group (n = 19)	Diver-group (n = 16)	Control-group (n = 18)	p #

Primary outcome measures absolute Δ over 12 weeks

	Nordic-group (*n* = 13)	Diver-group (*n* = 13)	Control-group (*n* = 13)	*p* #
Muscle fascicle orientation (°)				
Biceps femoris	−1.6 ±2.9	−2.6 ±2.9[a]	−0.2 ±2.4[a]	0.019
Semitendinosus	−0.7 ±3.8	0.4 ±4.1	−1.1 ±2.8	
Semimembranosus	0.7 ±1.9	1.9 ±4.2	0.3 ±2.7	

Secondary outcome measures absolute Δ over 12 weeks

	Nordic-group (*n* = 19)	Diver-group (*n* = 16)	Control-group (*n* = 18)	*p**
Strength (*N*)				
15° knee flexed	18.6 ±35.7	16.1 ±25.5	7.3 ±42.6	0.605
90° knee flexed	7.3 ±30.0	4.0 ±26.2	−1.4 ±31.0	0.665
Flexibility (°)				
Passive leg raise	−4.7 ±23.8	−1.7 ±7.7	5.9 ±21.1	0.240
Active knee extension	1.5 ±6.5	0.9 ±7.8	1.2 ±7.2	0.965

	Nordic-group (*n* = 19)	Diver-group (*n* = 16)	Control-group (*n* = 18)	*p* #
Muscle volume (cm^3)				
Biceps femoris	−2.9 ±11.3	3.5 ±12.6	−7.2 ±12.0	0.158
Semitendinosus	−4.6 ±10.9	2.1 ±17.1	−4.0 ±8.3	

Secondary outcome measures absolute Δ over 12 weeks

	Nordic-group (*n* = 19)	Diver-group (*n* = 16)	Control-group (*n* = 18)	*p**
Semimembranosus	−3.5 ±7.6	6.8 ±17.6	−5.3 ±13.4	

- *Note*: Values are means±SD.
- Abbreviations: °, degrees; mm, millimeters; *N*, Newton; $p^{\#}$, probability value interaction effect; *p**, probability value univariate analysis for factor Intervention; Δ, change.
- [a] Post-hoc pairwise comparisons $p < 0.05$.

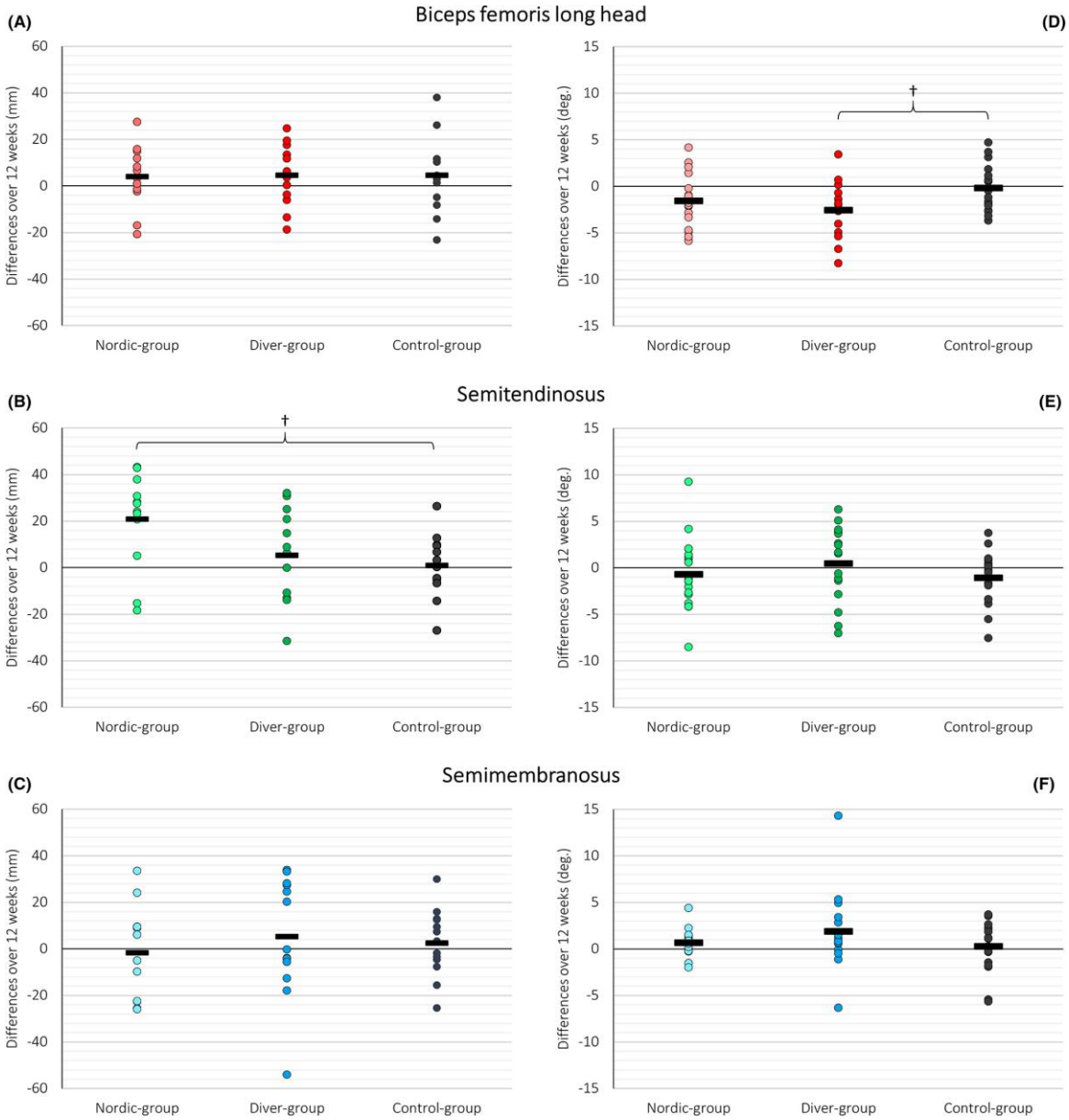

Figure 3: *Changes in fascicle length and fascicle orientation for the Nordic, Diver and control group over 12 weeks. (A–C) Individual dots represent change of muscle's fascicle length in millimeters over 12 weeks per participant, dashes represent group average. (D–F) individual dots represent changes in muscle fascicle orientation in degrees over 12 weeks per participant, dashes represent group average. †, post-hoc pairwise comparisons p<0.05.*

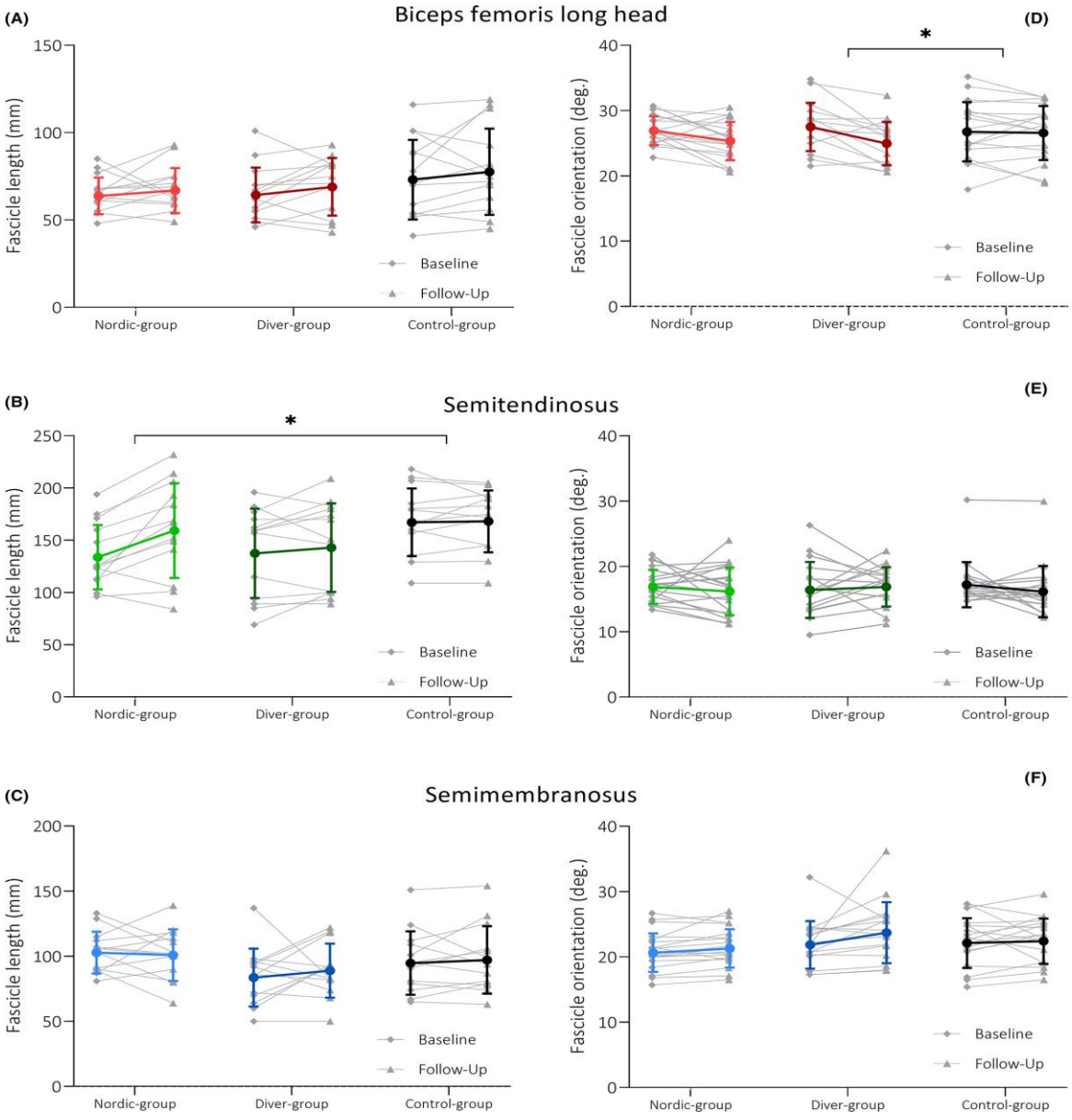

Figure 4: *Fascicle length and fascicle orientation for each participant of the Nordic, Diver and control group over 12 weeks. (A–C) Gray lines represent individual change in muscle's fascicle length in millimeters over 12 weeks per participant. (D–F) Gray lines represent individual change in muscle fascicle orientation in degrees over 12 weeks per participant. Diamonds; baseline values, triangles;*

*follow-up values, circles; group average and standard deviation, *; post-hoc pairwise comparisons p<0.05.*

Fascicle Orientation of the Biceps Femoris Long Head, Semitendinosus and Semimembranosus

There was a significant interaction effect on the type of intervention and muscle on the between-group differences over 12 weeks for fascicle orientation ($F(4, 100) = 3.1$, $p = 0.019$). Detailed results are presented in Table 3 and illustrated in Figures 3 and 4. The predefined pairwise post-hoc comparisons revealed that the angle of fascicle orientation in the biceps Femoris long head over 12 weeks significantly decreased in the Diver-group (mean: -2.6°, 95% CI: −4.1, −1.0) compared to the Control-group (mean: -0.2°, 95% CI: −1.4, 1.0), mean between-groups difference: -2.4°, 95% CI: −4.7, −0.1, $p = 0.039$. Other post-hoc comparisons were non-significant. Detailed results of all post-hoc comparisons are presented in Appendix S1.

Per-protocol Analysis in the Compliant Participants

When considering only the participants considered to be compliant (Nordic-group, $n = 13$; Diver-group, $n = 14$), the between-group analysis showed that there was no significant interaction effect on the type of intervention and muscle on the between-group differences over 12 weeks for fascicle length ($F(4, 58) = 1.7$, $p = 0.147$). There was a significant interaction effect on the type of intervention and muscle on the between-group differences over 12 weeks for fascicle orientation ($F(4,84) = 3.1$, $p = 0.011$). Detailed results of participant's individual intervention compliance and per-protocol analysis are presented in Appendix S1.

Secondary Outcome Measures

There were no significant between-group changes over 12 weeks for the secondary outcome measures. Detailed results are presented in Table 3.

Discussion

In this three-arm randomized controlled trial among amateur basketball players, a 12-week Nordic hamstring exercise intervention, compared with usual training, did significantly increase the fascicle length of the semitendinosus by 14% (2 cm). A 12-week Diver hamstring exercise, compared with

usual training, did significantly decrease the angle of fascicle orientation of the biceps Femoris long head 9% (2.4°). Both outcome parameters were obtained with DTI of the upper legs.

Compared to Literature

Since no studies reported the effect of exercise interventions on hamstring muscle fiber architecture with the use of quantitative DTI, comparisons with existing literature is limited to 2D ultrasound studies. For fascicle length, previous 2D ultrasound studies described an increment of up to 2 cm of the biceps Femoris long head following a Nordic hamstring exercise intervention.[5, 7-9] This observation in the biceps Femoris long head was not confirmed by our results. We did show a significant increment of fascicle length of 2 cm in the semitendinosus, compared to the Control-group. So far, no literature exists on the evaluation of fascicle length of the semitendinosus and Semimembranosus to evaluate the effect of hamstring exercises. The calculated fascicle lengths for biceps Femoris long head and semitendinosus are in the same range as mean fascicle lengths from human cadaveric specimens.[42] The main difference between ultrasound and DTI studies is that with ultrasound, the fascicle lengths are predominantly calculated on only one fascicle of interest in a 2D plane in the central part of the muscle.[5, 7-9] A recent ultrasound study reported adaptation of fascicle length in response to Nordic hamstring exercise training in the distal but not in the central portion of the biceps Femoris long head.[43] In our study, fascicle lengths were calculated on 100–150 fiber tracts per muscle. Diffusion tensor imaging provides a more comprehensive overview of the geometry of the fascicles in 3D, taking into account the curvature of fascicles. Simplification to a 2D plane in conventional ultrasound might underestimate fascicle length calculations.

For ultrasonographically determined fascicle orientation in 2D (e.g., pennation angle), there is conflicting evidence of an effect of the Nordic hamstring exercise intervention.[6-10] Both an increase of and decrease of approximately 1–2° have been reported.[6-10] We did not find any significant effect of the Nordic hamstring exercise intervention on the angle of fascicle orientation in any of the three hamstring muscles. For the Diver hamstring exercise intervention, our finding was a decrease in angle of the biceps Femoris long head fascicle orientation and this has not been studied before.

The reliability of measuring the fascicle length in hamstring muscles with DTI and tractography software was reported once.[44] These measurements were limited to the biceps Femoris long head. They reported good reliability and relative large MDC of 3.5 cm, using a simple and non-modifiable inbuilt manufacturer MRI tractography software.[44] In our analysis, predefined stopping criteria per muscle, manually selected endpoints (e.g., segmentations of the hamstring muscles) and tractography

software specially developed for research purposes were used, resulting in MDCs for respectively fascicle length and orientation of <1 cm and 1°.[28]

The semitendinosus muscle is affected by the Nordic hamstring exercise and the Biceps Femoris long head by the Diver hamstring exercise. The Diver hamstring exercise is part of a proven-effective rehabilitation protocol after an acute hamstring injury, executed at longer muscle lengths.[19] Absolute training volume of the intervention protocol in the Diver-group was matched to a proven-effective Nordic hamstring exercise intervention.[33] Besides eccentric loading, the hamstring muscles are also acting as a stabilizer across the Diver hamstring exercise.[45] Difference in relative muscle load is not specified in literature. Which exercise(s) an athlete should perform might depend on the desired goal and the (un)injured state of the athlete. Since the Biceps Femoris long head is most frequently injured, strength training specifically for this muscle would be a rational decision.[18] The Nordic hamstring exercises intervention has, however, shown its preventive potential in RCTs, increasing eccentric hamstring strength.[2] Training the semitendinosus is possibly behind the success of the Nordic hamstring exercise, protecting the more vulnerable biceps Femoris long head.[46] As both exercises are complementary to each other, the combination might be relevant for preventing hamstring injuries.

This study has several strengths. First, our DTI approach allows for the assessment of full muscle architecture in 3D in the upper leg muscles. Muscle imaging with 2D ultrasound presents a simplified interpretation of the complex geometry of human muscles fascicles. Second, muscle fiber architecture of all three hamstring muscles were evaluated at the same time. Third, the RCT study design minimalized risk of bias.

This study has several limitations. First, compliance to the intervention protocol in both the Nordic-, and Diver-group and participant drop-out did affect the outcome measures which was not taken into account in the sample size calculation. However, compliance rates were in a comparable range as in previous RCTs reporting preventive effects.[47] Our reported compliance was sufficient to detect an effect on muscle fiber architecture. Second, although training volume was matched between intervention groups, exercise intensity and consequently training stimuli is considered different between exercises. Lower levels of hamstring muscle activity is measured for hip-orientated exercises in general compared to the Nordic hamstring exercise.[16, 45, 48] Third, the observed non-anatomical irregularities in fascicle tracts in stitching areas between MRI datasets was the reason for excluding 11 datasets in primary analysis. Together with the exclusion of non-compliant participants, the low number of fascicle length assessments is a risk for false negative outcome of the results (type II error) in the per-protocol analysis. Fourth, compression of the hamstring muscles in a supine position in the

MRI scanner might potentially affect fascicle orientation. Although there might be a general effect of scanner position on absolute fascicle length and orientation, it should not influence the measured difference over time. Fifth, inclusion was restricted to uninjured basketball players, which might limit generalizability to other sports and injured athletes. Furthermore, if participants were already performing hamstring exercises at start of the intervention period, they were no not asked to pause their training temporarily. Sixth, blinding to the allocated exercise intervention for participants was not possible due to the nature of the content of the exercise. Seventh, isometric strength testing is possibly lacking test specificity. An increase in isokinetic eccentric strength would be expected, however the use of a measurement device for such parameter was not feasible within this study.

Future Directions

A combination of Diver hamstring exercises with Nordic hamstring exercises might potentially increase the preventive effect. A three-armed randomized controlled trial (with a combination group: Nordic+Diver hamstring exercise, Nordic hamstring exercise only and a control group) should assess a possible additional value. Analyzing muscle fiber architecture with DTI has the potential for evaluating changes following exercises directed to performance enhancement, prevention and muscle injury recovery in the hamstring and other muscles.

Conclusion

The Nordic hamstring exercise intervention increases the fascicle length of the semitendinosus. The Diver hamstring exercise intervention decreased the angle of fascicle orientation of the Biceps emoris long head. No effect was found for fascicle length and orientation of the Semimembranosus. The combination of exercises might be relevant for preventing hamstring injuries.

Perspective

The effect of exercises on hamstring muscle fiber architecture is predominantly evaluated for the most frequently injured Biceps Femoris long head. A comprehensive overview of the effect of the Nordic and Diver hamstring exercises on the hamstring muscle's three-dimensional fiber architecture through diffusion tensor imaging is described. Our findings suggest that the success behind the Nordic hamstring exercise could be more of a complementary nature; training the semitendinosus protects the more vulnerable Biceps Femoris long head. By showing that both interventions had a different

effect on the muscle's individual fiber architecture, we recognized that exercises have a heterogeneous effect on hamstring muscles. As both exercises are complementary, applying them in combination could become relevant for preventing hamstring injuries.

References

1. Vatovec R, Kozinc Ž, Šarabon N. Exercise interventions to prevent hamstring injuries in athletes: a systematic review and meta-analysis. *Eur J Sport Sci*. 2020; 20(7): 992- 1004.
2. Van Dyk N, Behan FP, Whiteley R. Including the Nordic hamstring exercise in injury prevention programmes halves the rate of hamstring injuries: a systematic review and meta-analysis of 8459 athletes. *Br J Sports Med*. 2019; 53(21): 1362- 1370.
3. BMJ Medicine Talk: *Eccentric Hamstring Exercises–they Work in Practice but Not in Theory?* In Van Dyk N, Opar DA Soundcloud; 2014.
4. Yagiz G, Akaras E, Kubis H-P, Owen JA. Heterogeneous effects of eccentric training and nordic hamstring exercise on the biceps femoris fascicle length based on ultrasound assessment and extrapolation methods: a systematic review of randomised controlled trials with meta-analyses. *PLOS One*. 2021; 16(11):e0259821.
5. Bourne MN, Duhig SJ, Timmins RG, et al. Impact of the Nordic hamstring and hip extension exercises on hamstring architecture and morphology: implications for injury prevention. *Br J Sports Med*. 2017; 51(5): 469- 477.
6. Seymore KD, Domire ZJ, DeVita P, Rider PM, Kulas AS. The effect of Nordic hamstring strength training on muscle architecture, stiffness, and strength. *Eur J Appl Physiol*. 2017; 117(5): 943- 953.
7. Presland JD, Timmins RG, Bourne MN, Williams MD, Opar DA. The effect of nordic hamstring exercise training volume on biceps femoris long head architectural adaptation. *Scand J Med Sci Sports*. 2018; 28(7): 1775- 1783.
8. Lovell R, Knox M, Weston M, Siegler JC, Brennan S, Marshall PWM. Hamstring injury prevention in soccer: before or after training? *Scand J Med Sci Sports*. 2018; 28(2): 658- 666.
9. Alonso-Fernandez D, Docampo-Blanco P, Martinez-Fernandez J. Changes in muscle architecture of biceps femoris induced by eccentric strength training with nordic hamstring exercise. *Scand J Med Sci Sports*. 2018; 28(1): 88- 94.
10. Mendiguchia J, Conceição F, Edouard P, et al. Sprint versus isolated eccentric training: comparative effects on hamstring architecture and performance in soccer players. *PLOS One*. 2020; 15(2):e0228283.
11. Brockett CL, Morgan DL, Proske UWE. Human hamstring muscles adapt to eccentric exercise by changing optimum length. *Med Sci Sports Exerc*. 2001; 33(5): 783- 790.
12. Proske U, Morgan DL. Muscle damage from eccentric exercise: mechanism, mechanical signs, adaptation and clinical applications. *J Physiol*. 2001; 537(2): 333- 345.
13. Wan X, Li S, Best TM, Liu H, Li H, Yu B. Effects of flexibility and strength training on peak hamstring musculotendinous strains during sprinting. *J Sport Health Sci*. 2021; 10(2): 222- 229.
14. Medeiros DM, Marchiori C, Baroni BM. Effect of Nordic hamstring exercise training on knee flexors eccentric strength and fascicle length: a systematic review and meta-analysis. *J Sport Rehab*. 2021; 30(3): 482- 491.
15. Bautista IJ, Vicente-Mampel J, Baraja-Vegas L, Segarra V, Martín F, Van Hooren B. The effects of the Nordic hamstring exercise on sprint performance and eccentric knee flexor strength: a systematic review and meta-analysis of intervention studies among team sport players. *J Sci Med Sport*. 2021; 24(9): 931- 938.
16. Hegyi A, Peter A, Finni T, Cronin NJ. Region-dependent hamstrings activity in Nordic hamstring exercise and stiff-leg deadlift defined with high-density electromyography. *Scand J Med Sci Sports*. 2018; 28(3): 992- 1000.
17. Bourne MN, Williams MD, Opar DA, Al Najjar A, Kerr GK, Shield AJ. Impact of exercise selection on hamstring muscle activation. *Br J Sports Med*. 2017; 51(13): 1021- 1028
18. Koulouris G, Connell DA, Brukner P, Schneider-Kolsky M. Magnetic resonance imaging parameters for assessing risk of recurrent hamstring injuries in elite athletes. *Am J Sports Med*. 2007; 35(9): 1500- 1506.

19. Askling CM, Tengvar M, Thorstensson A. Acute hamstring injuries in Swedish elite football: a prospective randomised controlled clinical trial comparing two rehabilitation protocols. *Br J Sports Med*. 2013; 47(15): 953- 959.
20. Schache AG, Wrigley TV, Baker R, Pandy MG. Biomechanical response to hamstring muscle strain injury. *Gait Posture*. 2009; 29(2): 332- 338.
21. Heiderscheit BC, Hoerth DM, Chumanov ES, Swanson SC, Thelen BJ, Thelen DG. Identifying the time of occurrence of a hamstring strain injury during treadmill running: a case study. *Clin Biomech (Bristol, Avon)*. 2005; 20(10): 1072- 1078.
22. Bourne MN, Timmins RG, Opar DA, et al. An evidence-based framework for strengthening exercises to prevent hamstring injury. *Sports Med*. 2018; 48(2): 251- 267.
23. Oakley AJ, Jennings J, Bishop CJ. Holistic hamstring health: not just the Nordic hamstring exercise. *Br J Sports Med*. 2018; 52(13): 816- 817.
24. Giakoumis M To Nordic or not to Nordic? A different perspective with reason to appreciate Semitendinosus more than ever. 2020
25. Klimstra M, Dowling J, Durkin JL, Macdonald M. The effect of ultrasound probe orientation on muscle architecture measurement. *J Electromyogr Kinesiol*. 2007; 17(4): 504- 514.
26. Heemskerk AM, Damon BM. Diffusion tensor MRI assessment of skeletal muscle architecture. *Curr Med Imaging Rev*. 2007; 3(3): 152- 160.
27. Lee D, Li Z, Sohail QZ, Jackson K, Fiume E, Agur A. A three-dimensional approach to pennation angle estimation for human skeletal muscle. *Comput Methods Biomech Biomed Engin*. 2015; 18(13): 1474- 1484.
28. Oudeman J, Mazzoli V, Marra MA, et al. A novel diffusion-tensor MRI approach for skeletal muscle fascicle length measurements. *Physiol Reports*. 2016; 4(24):e13012.
29. Bolsterlee B, D'Souza A, Herbert RD. Reliability and robustness of muscle architecture measurements obtained using diffusion tensor imaging with anatomically constrained tractography. *J Biomech*. 2019; 86: 71- 78.
30. Secondulfo L, Hooijmans MT, Suskens JJ, et al. A diffusion tensor-based method facilitating volumetric assessment of fiber orientations in skeletal muscle. *PLOS One*. 2022; 17(1):e0261777.
31. Timmins RG, Ruddy JD, Presland J, et al. Architectural changes of the biceps Femoris long head after concentric or eccentric training. *Med Sci Sports Exerc*. 2016; 48(3): 499- 508.
32. Petersen J, Thorborg K, Nielsen MB, Budtz-Jorgensen E, Holmich P. Preventive effect of eccentric training on acute hamstring injuries in men's soccer: a cluster-randomized controlled trial. *Am J Sports Med*. 2011; 39(11): 2296- 2303.
33. Van Der Horst N, Smits D-W, Petersen J, Goedhart EA, Backx FJG. The preventive effect of the Nordic hamstring exercise on hamstring injuries in amateur soccer players. *Am J Sports Med*. 2015; 43(6): 1316- 1323.
34. Sportsinjuryclinic. Hamstring Exercises–Norwegian Curl Nordic Curl Glute Ham Raise. YouTube. Published 2011. Accessed
35. Hansberger BL, Loutsch R, Hancock C, Bonser R, Zeigel A, Baker RT. Evaluating the relationship between clinical assessments of apparent hamstring tightness: a correlational analysis. *Int J Sports Phys Ther*. 2019; 14(2): 253- 263.
36. Oudeman J, Nederveen AJ, Strijkers GJ, Maas M, Luijten PR, Froeling M. Techniques and applications of skeletal muscle diffusion tensor imaging: a review. *J Magn Reson Imaging*. 2016; 43(4): 773- 788.
37. Froeling M. QMRTools: a Mathematica toolbox for quantitative MRI analysis. *J Open Source Software*. 2019; 4(38): 1204.
38. Klein S, Staring M, Murphy K, Viergever MA, Pluim J. Elastix: a toolbox for intensity-based medical image registration. *IEEE Trans Med Imaging*. 2010; 29(1): 196- 205.
39. Veraart J, Novikov DS, Christiaens D, Ades-Aron B, Sijbers J, Fieremans E. Denoising of diffusion MRI using random matrix theory. *NeuroImage*. 2016; 142: 394- 406.

40. Yushkevich PA, Piven J, Hazlett HC, et al. User-guided 3D active contour segmentation of anatomical structures: significantly improved efficiency and reliability. *NeuroImage*. 2006; 31(3): 1116- 1128.
41. Forsting J, Rehmann R, Froeling M, Vorgerd M, Tegenthoff M, Schlaffke L. Diffusion tensor imaging of the human thigh: consideration of DTI-based fiber tracking stop criteria. *MAGMA*. 2020; 33(3): 343- 355.
42. Kellis E, Galanis N, Kapetanos G, Natsis K. Architectural differences between the hamstring muscles. *J Electromyogr Kinesiol*. 2012; 22(4): 520- 526.
43. Pincheira PA, Boswell MA, Franchi MV, Delp SL, Lichtwark GA. Biceps femoris long head sarcomere and fascicle length adaptations after 3 weeks of eccentric exercise training. *J Sport Health Sci*. 2022; 11(1): 43- 49.
44. Behan FP, Vermeulen R, Smith T, et al. Poor agreement between ultrasound and inbuilt diffusion tensor MRI measures of biceps femoris long head fascicle length. *Translational Sports Med*. 2019; 2(2): 58- 63.
45. Severini G, Holland D, Drumgoole A, Delahunt E, Ditroilo M. Kinematic and electromyographic analysis of the Askling L-protocol for hamstring training. *Scand J Med Sci Sports*. 2018; 28(12): 2536- 2546.
46. Schuermans J, Van Tiggelen D, Danneels L, Witvrouw E. Biceps femoris and semitendinosus–teammates or competitors? New insights into hamstring injury mechanisms in male football players: a muscle functional MRI study. *Br J Sports Med*. 2014; 48(22): 1599- 1606.
47. Ripley NJ, Cuthbert M, Ross S, Comfort P, McMahon JJ. The effect of exercise compliance on risk reduction for hamstring strain injury: a systematic review and meta-analyses. *Int J Environ Res Public Health*. 2021; 18(21):11260.
48. Hegyi A, Csala D, Peter A, Finni T, Cronin NJ. High-density electromyography activity in various hamstring exercises. *Scand J Med Sci Sports*. 2019; 29(1): 34- 43.

APPENDIX

SUPPLEMENTARY MATERIAL

Content Supplementary Material

1. Compliance
2. Magnetic resonance imaging acquisition parameters
3. Reliability tests
4. Example of irregularities in fascicle tracts
5. Scan quality and number of tracts per muscle
6. Pairwise *post hoc* analysis
7. Per-protocol sensitivity analysis

Supplementary Material 1. Compliance

Compliance with the intervention was evaluated through online questionnaires bi-weekly and one overall questionnaire at the end of the intervention period. Participants in the Nordic-, and Diver-group were asked in their bi-weekly questionnaire how often they had performed the Nordic hamstring exercise in the two preceding weeks (number of completed sessions as answer). In the overall questionnaire, participants were asked if they had followed the provided exercise protocol (yes/no as a possible answer, and in case of no, how many weeks they had followed the exercise according to the exercise protocol). A detailed description of questions is presented in Supplementary Table 1. Compliance was dichotomized into compliant (at least once per week) and non-compliant (less than once per week) by a decision tree, as illustrated in Supplementary Figure 1.

Supplementary Table 1. *Online questionnaires (biweekly and at the end of intervention period) to assess compliance.*

When	Question
Biweekly	
Question 1	In the two preceding weeks, how often did you execute the exercises according to the provided exercise protocol? This is regarding the number of sessions, not about the specific number of sets per training: *Number (0-4)*
Evaluation at the end of intervention period	
Question 1	Each week, I executed the prescribed exercises at least one time per week: *Yes/No*
Question 2	If not, specify how many weeks you did execute the prescribed exercises: *Number (0-12)*

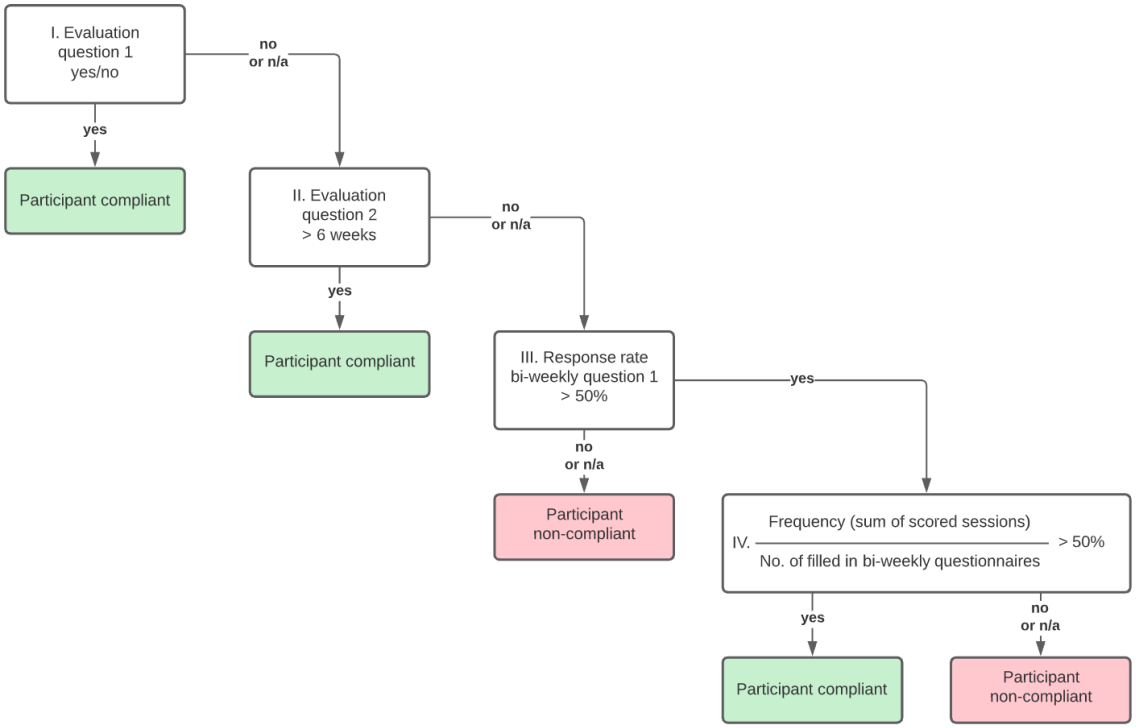

Supplementary Figure 1. *Decision tree to categorize compliance.*

Supplementary Material 2. Magnetic resonance imaging acquisition parameters

Supplementary Table 2. *Magnetic resonance imaging parameters.*

Parameter	PD weighted Dixon	Diffusion tensor imaging	Noise
Acquisition	GRE	SE-EPI	SE-EPI*
Field of view (mm^3)	276 x 480 x 186	480 x 276 x 186	480 x 276 x 186
Voxel size (mm^3)	1.5 x1.5 x 3.0	3.0 x 3.0 x 6.0	3.0 x 3.0 x 6.0
Time of first echo/Echo time	1.33/1.1	-/53	-/53
Number of echoes	6	-	-
Repetition time (ms)	8.0	4630	4630
Sensitivity encoding factor	-	1.5	1.5
Number of signal averages	-	3	-
Fat suppression	-	SSGR & SPAIR	-
Gradient directions	-	48	-
B values (mm^2/s)	-	0(1)/450(48)	-
Acquisition time (min)	01:28	08:34	00:12

PD; proton-density, GE; Gradient Echo, SE-EPI; Spin-Echo Echo-Planar Imaging, SE-EPI; Spin-Echo Echo-Planar Imaging without diffusion weighting, SSGR; Slice-Selection Gradient Reversal, SPAIR; Spectrally Adiabatic Inversion Recovery.*

Supplementary Material 3. Reliability tests

Methods

The reliability of DTI derived fascicle lengths of lower limb muscles showed moderate to good repeatability, with a minimal detectable change (MDC) with the same tractography software ranging between 0.4 and 0.9 cm.[8] The reliability of 1) manual segmentation on the primary outcome measures, 2) the assessments of the longitudinal muscle length and 3) placement of the reference lines on fascicle orientation were calculated.

For inter-observer reliability, the manual segmentations were performed by a second examiner (JS), while blinded for the first assessment of the first examiner (KH). For intra-observer reliability, the manual segmentations were repeated by one examiner (JS), with a 1-week interval between examinations. For inter-observer reliability of the longitudinal muscle length, the proximal and distal borders were determined by a second examiner (OK), while blinded for the first assessment of the first examiner (JS). For inter-observer reliability of the manual placement of the reference line in the fascicle orientation, manual placement of the reference lines on the intramuscular tendon were placed by a second examiner (OK), while blinded for the first assessment of the first examiner (JS). For intra-observer reliability, the placement of the reference lines was repeated by one examiner (JS) with a 6 weeks interval between examinations.

ICCs were calculated with a two-way mixed model and absolute agreement. An ICC less than 0.50 was considered as poor reliability, 0.50 to 0.75 as moderate reliability, 0.75 to 0.90 as good reliability, and greater than 0.90 as excellent reliability. Five random datasets were included for the intra- and inter-observer reliability of manual segmentation on primary outcome measures fascicle length and fascicle orientation. All baseline measurements were included for the inter-observer reliability in the determination of the proximal and distal muscle border. All baseline measurements were included for the intra- and inter-observer reliability and calculation of the MDC for the placement of the reference line. With the intra-observer ICC and standard error of the mean (SEM as: standard deviation (SD) $\times \sqrt{(1 - \mathrm{ICC}_{\mathrm{intra}})}$) the MDC was calculated as: $1.96 \times \sqrt{(2)} \times \mathrm{SEM}$, for the biceps femoris long head, semitendinosus and Semimembranosus.

Results

Excellent reliability was found for the manual segmentations on the intra-observer reliability for fascicle length calculation and intra- and inter-observer reliability of fascicle length calculations. Good reliability was found for the manual segmentations on the inter-observer reliability for fascicle length calculation. Detailed results are described in Supplementary Table 3. Excellent reliability was found for both the intra and inter-observer reliability of determining the proximal and distal borders of the individual hamstring muscles. Detailed results are described in Supplementary Table 4. Excellent reliability was found for both the intra and inter-observer reliability of calculating the muscle fascicle orientation. Detailed results of inter, intra intraclass correlation coefficient (ICC) and minimal detectable change per hamstring muscle are described in Supplementary Table 5.

Supplementary Table 3. *Results of intra- and inter-observer reliability of manual segmentation on primary outcome measures.*

Muscle	intra-observer		Inter-observer	
	ICC	95% confidence interval	ICC	95% confidence interval
Fascicle length	0.94	(0.83 to 0.98)	0.90	(0.63 to 0.97)
Fascicle orientation	1.00	(1.00 to 1.00)	1.00	(1.00 to 1.00)

ICC; Intraclass correlation coefficient.

Supplementary Table 4. *Results of inter-observer reliability in determination of the proximal and distal muscle borders per individual hamstring muscle.*

Muscle	Inter-observer Proximal muscle border		Inter-observer Distal muscle border	
	ICC	95% confidence interval	ICC	95% confidence interval
Biceps femoris	1.00	(1.00 to 1.00)	0.99	(0.99 to 0.99)
Semitendinosus	1.00	n.a.	0.99	(0.99 to 0.99)
Semimembranosus	1.00	n.a.	1.00	(1.00 to 1.00)

ICC; Intraclass correlation coefficient, n.a.; not applicable.

Supplementary Table 5. *Results of intra and inter-observer reliability and minimal detectable change in muscle fascicle orientation per individual hamstring muscle.*

Muscle	Intra-observer		Inter-observer		Minimal detectable Change (degrees)
	ICC	95% confidence interval	ICC	95% confidence interval	
Biceps femoris	1.00	(0.99 to 1.00)	0.99	(0.98 to 1.00)	0.69
Semitendinosus	0.99	(0.98 to 0.99)	0.99	(0.98 to 0.99)	1.00
Semimembranosus	0.99	(0.97 to 0.99)	0.98	(0.96 to 0.99)	1.15

ICC; Intraclass correlation coefficient.

Supplementary Material 4. Example of irregularities in fascicle tracts

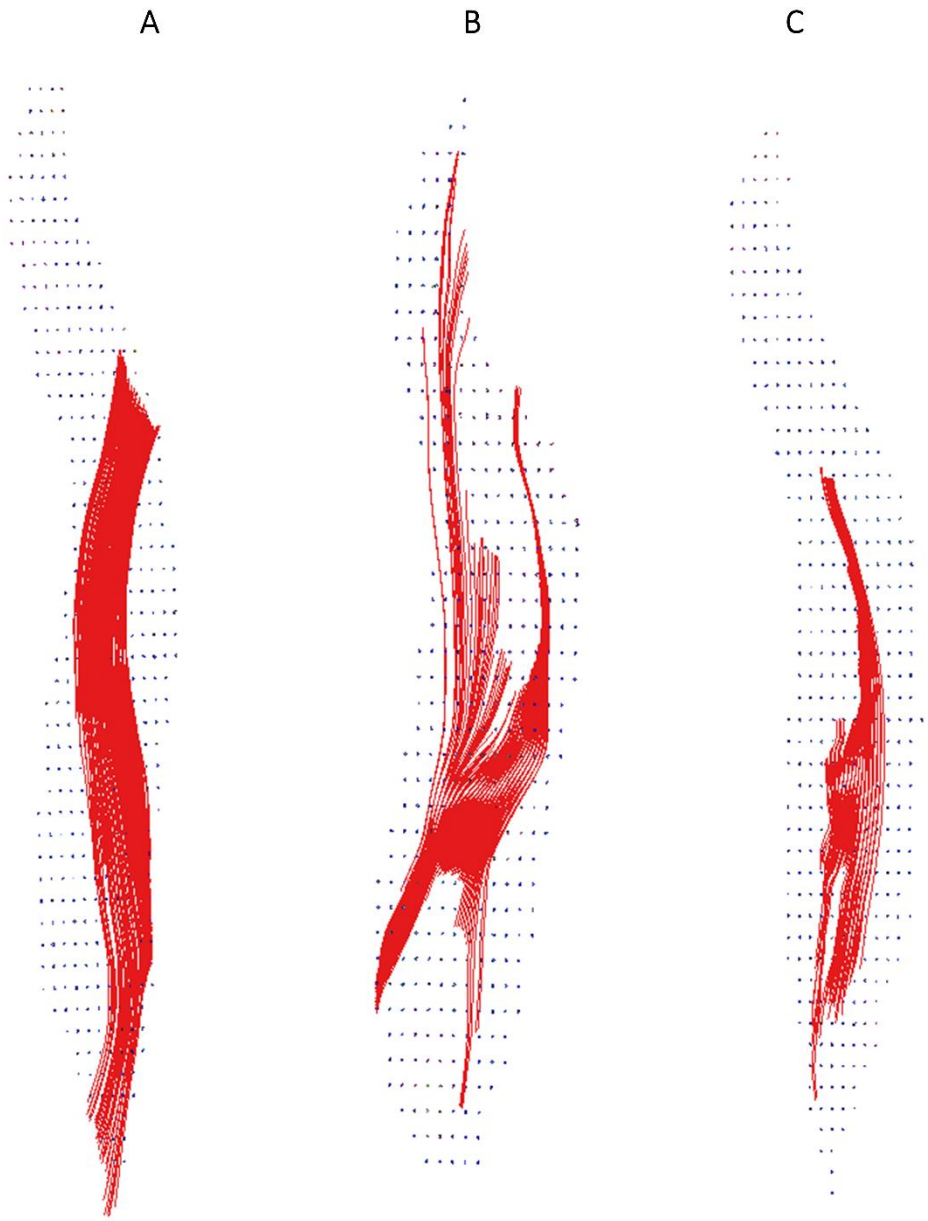

Supplementary Figure 2. *Fiber tracts in the semitendinosus muscle of the left leg. (**A**) correct fiber tracking, sagittal view. (**B**) Distorted fiber tracking, posterior view. (**C**) Distorted tracking, sagittal view.*

Supplementary Material 5. Scan quality and number of tracts per muscle

The mean signal-to-noise ratio combined for baseline and follow-up, was (mean ± standard deviation) 29 ± 6, 34 ± 6, 32 ± 6 for the biceps femoris long head, semitendinosus and Semimembranosus respectively.

The mean number of tracts for fascicle length calculation, combined for baseline and follow-up, was 144 ± 94, 149 ± 77, 106 ± 81 for the biceps femoris long head, semitendinosus and Semimembranosus respectively. A detailed description of number of tracts per group and hamstring in Supplementary Table 5.

Supplementary Table 6. *Number of tracts per group and hamstring muscle at baseline and follow-up.*

Primary outcome measures		Nordic-group		Diver-group		Control-group		Group average
		Baseline	Follow-up	Follow-up	Follow-up	Baseline	Follow-up	
Number of tracts in fiber tractography	Biceps femoris	145 ± 107	155 ± 86	138 ± 93	124 ± 103	151 ± 98	150 ± 67	**144 ± 94**
	Semitendinosus	178 ± 78	184 ± 99	130 ± 54	162 ± 64	116 ± 65	126 ± 65	**149 ± 77**
	Semimembranosus	103 ± 64	69 ± 48	115 ± 102	96 ± 77	113 ± 79	135 ± 89	**106 ± 81**

Values are means ± standard deviations.

Supplementary Material 6. Pairwise (*post hoc)* comparisons

Supplementary Table 7. *Results of the pairwise post hoc comparison for primary outcome measure fascicle length.*

Muscle	Intervention A	Intervention B	Mean difference A-B (mm)	95 % confidence interval (mm)	*p*
Biceps femoris long head	Nordic-group	Diver-group	-0.7	(-15.0 to 13.7)	1.000
	Nordic-group	Control-group	-0.6	(-15.0 to 13.7)	1.000
	Diver-group	Control-group	0.0	(-14.0 to 14.1)	1.000
Semitendinosus	Nordic-group	Diver-group	15.5	(-2.5 to 33.4)	0.112
	Nordic-group	Control-group	19.9	(1.9 to 37.9)	0.026
	Diver-group	Control-group	4.4	(-13.2 to 22.0)	1.000
Semimembranosus	Nordic-group	Diver-group	-6.9	(-27.7 to 13.8)	1.000
	Nordic-group	Control-group	-4.2	(-24.9 to 16.6)	1.000
	Diver-group	Control-group	2.8	(-17.5 to 23.1)	1.000

mm; millimeter, p; probability value pairwise comparisons with Bonferroni correction

Supplementary Table 8. *Results of the pairwise post hoc comparison for primary outcome measure fascicle orientation.*

Muscle	Intervention A	Intervention B	Mean difference A-B (°)	95 % confidence interval (°)	*p*
Biceps femoris long head	Nordic-group	Diver-group	1.0	(-1.3 to 3.2)	0.872
	Nordic-group	Control-group	-1.4	(-3.6 to 0.8)	0.354
	Diver-group	Control-group	-2.4	(-4.7 to -0.1)	0.039
Semitendinosus	Nordic-group	Diver-group	-1.2	(-4.2 to 1.9)	1.000
	Nordic-group	Control-group	0.4	(-2.5 to 3.3)	1.000
	Diver-group	Control-group	1.5	(-1.5 to 4.6)	0.658
Semimembranosus	Nordic-group	Diver-group	-1.2	(-3.7 to 1.2)	0.682
	Nordic-group	Control-group	0.4	(-2.0 to 2.8)	1.000
	Diver-group	Control-group	1.6	(-0.9 to 4.1)	0.352

°; degrees, p; probability value pairwise comparisons with Bonferroni correction

Additional within-group comparisons (paired samples t-tests, without *Bonferroni* correction) are presented below in Supplementary Table 9 and 10.

Supplementary Table 9. *Results of the within-group pairwise comparison for primary outcome measure fascicle length.*

Muscle	Mean difference ± standard deviation: Follow-up – Baseline (mm)	*p*
Biceps femoris long head		
Nordic-group	3.83 ± 13.63	0.351
Diver-group	4.69 ± 13.02	0.218
Control-group	4.54 ± 15.95	0.325
Semitendinosus		
Nordic-group	20.83 ± 20.22	0.004
Diver-group	5.38 ± 19.29	0.334
Control-group	0.85 ± 13.29	0.822
Semimembranosus		
Nordic-group	-1.67 ± 18.84	0.776
Diver-group	5.31 ± 25.71	0.471
Control-group	2.38 ± 14.30	0.559

mm; millimeter, p; probability value pairwise comparisons

Supplementary Table 10. *Results of the within-group pairwise comparison for primary outcome measure fascicle orientation.*

Muscle	Mean difference ± standard deviation: Follow-up – Baseline (°)	*p*
Biceps femoris long head		
Nordic-group	-1.60 ± 2.74	0.020
Diver-group	-2.56 ± 2.89	0.003
Control-group	-0.18 ± 2.44	0.754
Semitendinosus		
Nordic-group	-0.71 ± 3.80	0.429
Diver-group	0.46 ± 4.09	0.662
Control-group	-1.08 ± 2.84	0.125
Semimembranosus		
Nordic-group	065 ± 1.36	0.053
Diver-group	1.87 ± 4.25	0.099
Control-group	0.28 ± 2.69	0.661

°; degrees, p; probability value pairwise comparisons

Supplementary Material 7. Per-protocol sensitivity analysis

Supplementary Table 11. *Results compliance questionnaires per participant.*

Participant	Statement I.	Statement II.	Statement III.	Statement IV.	(Non-)compliant
Nordic_A	N/a		Yes: 4/6	11/16	Compliant
Nordic_B	Yes				Compliant
Nordic_C	Yes				Compliant
Nordic_D	Yes				Compliant
Nordic_E	No	No: 0	No: 1/6		Non-compliant
Nordic_F	N/a	N/a	No: 0/6		Non-compliant
Nordic_G	Yes				Compliant
Nordic_H	N/a	N/a	Yes: 5/6	Yes: 20/20	Compliant
Nordic_I	Yes				Compliant
Nordic_J	Yes				Compliant
Nordic_K	N/a	No: n/a	No: 1/6		Non-compliant
Nordic_L	N/a	No: n/a	No: 2/6		Non-compliant
Nordic_M	No	No: 1	Yes: 5/6	Yes: 13/20	Compliant
Nordic_N	N/a	N/a	No: 1/6		Non-compliant
Nordic_O	N/a	N/a	Yes: 3/6	No: 4/12	Non-compliant
Nordic_P	N/a	N/a	Yes: 6/6	17/24	Compliant
Nordic_Q	Yes				Compliant
Nordic_R	N/a	N/a	Yes: 6/6	20/24	Compliant
Nordic_S	Yes				Compliant
Diver_A	Yes				Compliant
Diver_B	N/a	N/a	No: 0/6		Non-compliant
Diver_C	Yes				Compliant
Diver_D	Yes				Compliant
Diver_E	Yes				Compliant
Diver_F	Yes				Compliant
Diver_G	Yes				Compliant
Diver_H	Yes				Compliant
Diver_I	Yes				Compliant
Diver_J	Yes				Compliant
Diver_K	Yes				Compliant
Diver_L	Yes				Compliant
Diver_M	N/a	No: n/a	No: 1/6		Non-compliant
Diver_N	Yes				Compliant
Diver_O	Yes				Compliant
Diver_P	N/a	N/a	Yes: 6/6	19/24	Compliant

Supplementary Table 12. *Results per-protocol sensitivity analysis.*

Primary outcome measures		Nordic-group (n = 13)		Diver-group (n = 14)		Control-group (n = 18)		
		Follow-up	Absolute Δ over 12 weeks	Follow-up	Absolute Δ over 12 weeks	Follow-up	Absolute Δ over 12 weeks	*p*
Fascicle length (mm)	Biceps femoris	72.7 ± 9.7	2.5 ± 17.0	68.8 ± 15.8	4.5 ± 13.5	79.4 ± 24.8	4.6 ± 16.1	*0.147*
	Semitendinosus	168.1 ± 52.2	24.1 ± 22.8	144.4 ± 44.4	8.4 ± 16.5	170.2 ± 29.6	0.9 ± 13.3	
	Semimembranosus	109.7 ± 18.0	2.5 ± 22.8	89.7 ± 21.7	6.2 ± 26.6	98.1 ± 25.9	2.5 ± 14.5	
Muscle fascicle orientation (°)	Biceps femoris	25.5 ± 3.4	-1.5 ± 3.2	25.1 ± 3.3	-3.0 ± 2.8	26.8 ± 4.2	-0.2 ± 2.4	*0.011*
	Semitendinosus	16.2 ± 4.1	-0.3 ± 3.6	17.7 ± 2.7	0.5 ± 4.3	16.4 ± 4.0	-1.1 ± 2.8	
	Semimembranosus	21.6 ± 3.5	0.8 ± 1.4	23.6 ± 3.3	1.1 ± 2.9	22.7 ± 3.5	0.3 ± 2.7	

Values are means ± standard deviations, Δ; change, p; probability value interaction effect, mm; millimeter, °; degrees.

References

1. Froeling M. QMRTools: a Mathematica toolbox for quantitative MRI analysis. *Journal of Open Source Software.* 2019;4(38):1204.
2. Klein S, Staring M, Murphy K, Viergever MA, Pluim J. elastix: A Toolbox for Intensity-Based Medical Image Registration. *IEEE Transactions on Medical Imaging.* 2010;29(1):196-205.
3. Veraart J, Novikov DS, Christiaens D, Ades-Aron B, Sijbers J, Fieremans E. Denoising of diffusion MRI using random matrix theory. *NeuroImage.* 2016;142:394-406.
4. Yushkevich PA, Piven J, Hazlett HC, et al. User-guided 3D active contour segmentation of anatomical structures: Significantly improved efficiency and reliability. *NeuroImage.* 2006;31(3):1116-1128.
5. Forsting J, Rehmann R, Rohm M, Froeling M, Schlaffke L. Evaluation of interrater reliability of different muscle segmentation techniques in diffusion tensor imaging. *NMR in Biomedicine.* 2021;34(2).
6. Forsting J, Rehmann R, Froeling M, Vorgerd M, Tegenthoff M, Schlaffke L. Diffusion tensor imaging of the human thigh: consideration of DTI-based fiber tracking stop criteria. *Magnetic Resonance Materials in Physics, Biology and Medicine.* 2020;33(3):343-355.
7. Secondulfo L, Hooijmans MT, Suskens JJ, et al. A diffusion tensor-based method facilitating volumetric assessment of fiber orientations in skeletal muscle. *PLOS ONE.* 2022;17(1):e0261777.
8. Oudeman J, Mazzoli V, Marra MA, et al. A novel diffusion-tensor MRI approach for skeletal muscle fascicle length measurements. *Physiological Reports.* 2016;4(24):e13012.

CHAPTER 6

Discussion

Summary

This thesis aimed to develop various approaches for measuring muscle architectural parameters using Diffusion Tensor MR Images (DTI) and apply them to study changes in muscle architecture after an injury prevention program.

To address the time-consuming nature of manual segmentation, the thesis evaluated semi-automatic segmentation methods for analyzing large cohorts efficiently. In Chapter 2, a validation of a semi-automatic segmentation framework for estimating DTI indices in upper leg muscles was presented. The method facilitated segmentations three times faster than manual techniques cross-sectionally and nearly fully automatic segmentation longitudinally, with good accuracy for most muscles except the Sartorius and the Vastus Intermedius muscles.

Chapter 3 describes a feasibility study using a volumetric DTI-based approach to measure changes in fiber orientation (or 'fiber angles') in calf muscles and sub-compartments of the Soleus and Tibialis Anterior muscles during plantarflexion and dorsiflexion. The study revealed that fiber orientations change in line with the expected agonist and antagonist functions of these muscles and their sub-compartments. The fiber orientation alterations in the Soleus muscle and the Tibialis Anterior were in opposite directions, reflecting their biomechanical behavior during muscle shortening and lengthening.

In this thesis we compared DTI fibertractography, which enables visualization of muscle fibers and measurement of muscle properties, with 3D ultrasonography (3D-US). To that end, in Chapter 4 a comparison was made between DTI-based fiber tractography measurements and 3D ultrasound-based measurements of the pennation angle in the Vastus Lateralis muscle. Pennation angles and fiber length estimations between the two methods were evaluated in the same muscle location.

In chapter 5 we investigated the effect of different exercise intervention programs on preventing hamstring injuries in basketball players. DTI was utilized as a quantitative method to analyze exercise-induced changes in fiber orientation and fiber length estimation using fiber tractography and fiber orientation maps. Notable findings included an increase in fascicle length of the semitendinosus muscle following Nordics exercise and a decrease in muscle fascicle orientation in the Biceps Femoris long head following the Divers intervention.

By combining these different chapters, the thesis provided valuable insights into the development of measurement approaches for muscle architectural parameters, the comparison of techniques, and the analysis of exercise interventions in an injury prevention program.

Discussion

Semi-automatic segmentation methods.

In musculoskeletal MRI studies on injuries, one is commonly confronted with large variability of the injury location, extent and severity, as well as with normal biological variation between humans. Consequently, such MRI studies require the use of large patient cohorts which directly results in large datasets. To keep the acquisition and analyses of these large muscle datasets manageable, efficient MR imaging protocols, post-processing, and analysis pipelines need to be designed in a way which preferably require minimal user input.

With respect to the post-processing pipeline, manual segmentation, i.e., the delineation of muscle borders, remains a highly time-consuming process. Therefore, at the beginning of this thesis in Chapter 2 we focused on the evaluation of the performance of a semi-automated segmentation method, optimized for the upper leg muscles. Segmentation is a challenging process due to the low contrast between different muscles and because intramuscular tendons and connective tissues are often thin and therefore difficult to discern at limited spatial resolution, especially in elite athletes due to the low level of subcutaneous fat tissue. Additionally, there are large differences in muscle shapes between individuals. The semi-automated segmentation tool presented in Chapter 2 resulted in reducing the time for the individual manual segmentation of all upper leg muscles by 30% in healthy subjects, while maintaining high accuracy compared to the full manual segmentation approach. The application of this tool is quite promising for the segmentation of the lower extremities muscles; however, its application in the upper extremities or other body parts could be more challenging due to differences in the shape of the muscles compared to leg muscles.

An important aspect to be considered when assessing the feasibility of segmentation tools is the size of the segmented muscles, because the smaller the muscle, the higher imaging resolution might be needed. In the case of injured, diseased and fat infiltrated muscles the segmentation becomes more difficult since muscle volume and borders become irregular and there is poor visibility of tendons and aponeurosis. The efficacy of the segmentation tool of Chapter 2, however, was successfully applied in a longitudinal study of patients with muscular dystrophies.[1] Future work should explore the potential of these semi-automated approaches in muscle injury.

So far, different types of segmentation tools have been successfully developed, including: atlas based automated segmentations, semi-automated segmentations, and deep learning based (fully) automated segmentation techniques, which target individual muscles of the whole body in healthy subjects.[2] Even if it remains challenging to obtain comparable results in diseased and fat infiltrated

individual muscles, valuable semi and fully automated techniques are now available for the segmentation of muscle groups in the entire body.[3] Currently researchers are working on deep learning-based methods for automated segmentation tools of individual muscles of the entire body, including those in diseased patients. However large and heterogeneous databases should be available for training such algorithms which could present a limitation when applied to rare neuromuscular diseases.[4]

Muscle architecture parameters.

Muscle architecture parameters are an important predictor of muscle strength.[5] The muscle's architectural properties, such as volume and anatomical and physiological cross-sectional areas contribute to understanding the muscle's capacity to produce force[6,7] and are thus an indicator of muscle quality in healthy and diseased patients. Moreover, pennation angle, fiber length, muscle volume and fiber curvature are relevant to determine a muscle's strength. In Chapter 3 of this thesis we focused on a volumetric approach to measure changes in fiber orientation.

Pennation Angle:

The concept of pennation angle was introduced in biomechanics in the context of understanding muscle force generation. Muscles with the same mass can generate very different forces. The most appropriate value to normalize muscle force is the physiological cross-sectional area (PCSA).

$$PCSA(cm^2) = \frac{Muscle\ mass(g) \cdot \cos\theta}{\rho\left(\frac{\mathrm{g}}{cm^2}\right) \cdot \mathrm{fiber\ length(cm)}}$$

Where muscle pennation angle θ is measured on the muscle surface relative to the axis of force generation and ρ is the muscle density. The packing strategy allows short fibers to be packed in a limited volume. Pennation angle changes during force generation, but little is known about its functional significance. For improved understanding of the functional significance of pennation angle new methods and studies are needed.

Pennation angle can be measured with 2D and 3D ultrasonography and with DTI. The precision and accuracy of the measurements with ultrasonography is 3.0 ± 7.3° degrees, with Intra-observer (ICC 0.92-0.97), interobserver (ICC 0.78-0.92) reproducibility[8] and is operator dependent. The measurement of the pennation angle on the muscle surface can be obtained in specific locations, however changes could occur in the entire muscle volume. Selecting the location which is most subject to changes in muscle architecture could be time-consuming and require pilots for each specific application. Therefore, the use of volumetric maps of fiber orientation makes it possible to select the

location where the most significant changes happen in a retrospective fashion, following the acquisition and the calculation of the maps.

The fiber orientation maps introduced in chapter 3 are a volumetric approach which offers several advantages to measure changes in fiber orientation. Changes in fiber architecture can be measured within the full muscle volume rather than only in a specific location, thus reflecting the total variations. If preferable, it is possible to focus on smaller ROIs at specific locations within the muscle. Moreover, the measurement is semi-automatic, easily applicable for large datasets and thus suitable for longitudinal studies. The aim of these studies could be the prediction of changes in muscle architecture parameters following intervention therapies. This method still includes one manual step, which is the definition of the reference line. The feasibility study proved robust to this step, but complete automation would further improve the repeatability and facilitate the application in longitudinal studies.

In order to apply this method in clinical practice, additional improvements would be desired. For example, a revision of the post-processing steps with an improvement of the registration of diffusion images to Dixon images and the erosion of small ROIs in order to exclude tendon tissue or aponeurosis. Finally, the exclusion of highly fat infiltrated voxels could reduce the standard deviation of the measurements. Finally, the measurement of the resultant fiber orientation change can be obtained in sub-volumes of the entire muscles in a retrospective fashion in order to detect the most significant changes. In the study presented in chapter 5, we presented good precision of this method to evaluate changes due to interventions for injury prevention.

Fiber length: An increase in fiber length (increased number of sarcomeres in series or increase in sarcomeres length) corresponds to changes in mechanical properties, such as an increased muscle elasticity in the case sarcomere length increases,[9] muscle contraction velocity and consequently muscle power capacity (velocity x force).[10] Poor elasticity is described as a risk factor for hamstring injuries,[11] however no conclusive statements can be made on the influence of eccentric exercises on flexibility and its role in the prevention of muscle injuries.[11] Fiber length can be measured by mean of 2D and 3D ultrasonography and DTI fibertractography.

Muscle volume: Muscle volume can be measured with different imaging modalities, of which 3D MRI represents the most accurate option and gold standard.[12] Moreover, Dixon imaging [13] offers the possibility to distinguish muscle tissue from fat tissue within the muscle volume and thus to quantify the true lean muscle volume.[3] In fitness the lean muscle volume is an indicator of muscle strength and muscle power,[14,15] which is the capability to exert maximal strength in the shortest time possible, and

therefore indicates the disposition to accelerating and jumping.[15,16] On the other hand, in diseased muscles, it correlates with the (in)capability to produce movement.[15]

Fiber curvature: The importance of fiber curvature as architectural parameter is investigated less than the other ones, probably because it is difficult to measure. Fiber curvature and fiber length are related to active and passive states of force production,[17] and fiber curvature is specifically related to strain patterns during muscle contraction.[18] Therefore, a technique to accurately assess fiber curvature is highly desired. It seems very difficult to assess fiber fascicle curvature from 2D ultrasound. 3D diffusion tensor MRI, fibertractography and 3D-US, however, facilitate reconstructions of whole-muscle fiber architecture in 3D, including fiber curvature , and thus offers new opportunities to investigate the role of curvature in biomechanics.[18]

The study of the muscle architecture parameters leads to the conception and development of biomechanical models for the understanding of the activation and specific functional role of muscles during the execution of body movements like walking, running, and specific physical exercises.[19,20,21] However, the fiber orientation maps cannot be used for the purpose of creating biomechanical models and to calculate the physiological cross-sectional area, but they are useful to detect changes in muscle architecture. Anyhow, all these studies are instrumental to foster programs of muscle strengthening, injury prevention, and muscle rehabilitation.[22,23] Several studies showed that the effect of exercise can be linked to exercise-induced changes in muscle architecture parameters, including increased muscle volume, longer muscle fibers, smaller pennation angle, leading to increased muscle strength.[24,25,26]

Pennation angle: comparison of different techniques.

Muscle fiber length and pennation angle are traditionally measured with 2D ultrasound in few muscle location.[27] When the muscle's architecture and fiber orientations change because of training or injury, a 3D approach to measuring muscle fiber architecture in the full volume is preferable because would take into consideration fibers curvature. Both 3D ultrasonography (3D-US) and MRI are viable techniques to measure muscle fiber architecture.[28,29] In Chapter **4** of this thesis a fibertractography method for the measurement of pennation angle with Diffusion Tensor MRI has been introduced and compared with 3D ultrasonography. DTI fiber tractography in musculoskeletal MRI has been object of study in sport and in clinical studies.[30]

In the comparison between MRI fiber-tractography and 3D-US, we could test the advantages and disadvantages of these technologies. First of all, in MRI it is possible to image the full leg volume and thus all leg muscles in a single scan, which is an advantage when one is interested in multiple muscles

at the same time. In 3D-US, it is more difficult to image multiple and not superficial muscles at the same time. Moreover, in MRI the attachment points of the muscles can be visualized more easily which facilitates defining the locations for the pennation angle and the fiber length measurements. On the other hand, in MRI the body position is constrained by the limited scanning space, whereas in ultrasonography imaging there are no such space restrictions. This enables acquisitions of images in the optimal position of the leg in which the muscle fibers are in tension.

In post-processing, MRI fibertractography in the muscles is time-consuming due to the selection of the optimal tracking parameters.[31,28] These tracking parameters can result in for example an underestimation of the fiber length or an under or overestimation in fiber curvature.[32] Moreover, the registration of the DTI images to the anatomical reference can cause image deformation and consequently affect the pennation angle measurements. Also the fiber length measurements can be affected by mis-registration as tracking is generally initiated based on anatomical references delineated on the anatomical images. In recent years, several fibertractography tools were developed, such as those by Damon[33] *et al.* and Froeling *et al.*,[34] which simplify the entire post-processing pipeline and facilitate the measurement of fiber length, fascicle curvature and pennation angle.[33,34]

For both imaging modalities stitching of the images is required for all full 3D assessment of the muscle volume. In the post-processing of the 3D-US technique, 2D images were stitched together by an operator to create a 3D image of the muscle of interest based on a position tracking device.

For DTI, the images are acquired in three separate stacks to cover the full upper leg muscles. These stacks are stitched together in post-processing and could result in a stitching artefact creating some strange running fibers which could affect pennation angle, fiber length and fiber curvature estimates.

In 3D-US technique, 2D images are stitched together to create a 3D image of the muscle of interest. Within this 3D volume a 2D plane is generally selected to measure pennation angle and fiber lengths. Within this plane selected by the operator, fibers run from the deep aponeurosis to the superficial aponeurosis. Being an operator-dependent technique and to make sure that the imaging plane aligns with the plane in which the fibers lay, the measurement is repeated more times and the mean value is considered (see Chapter 4).

Both techniques allow to visualize the muscle fibers in 3D from the deep aponeurosis towards an intramuscular tendon or the superficial aponeurosis. In some cases, the fiber length is too short to run from the deep aponeurosis to the superficial aponeurosis.

Study of changes in muscle fibers due to physical intervention.

In Chapter 5 we used DTI as a quantitative method to analyze the effect of different intervention programs to prevent hamstring injuries in basketball players by inducing changes in muscle fiber architecture. In this study there were three main challenges: in addition to the technical challenges, it was important to establish the equivalence of the workload of the two intervention programs, and finally the compliance of the subjects to this program.

Concerning the equivalence of the workload it is important to distinguish between absolute and relative workload volume. The rehabilitation exercise called diver subjects the hamstrings to a lighter load[35] than the prevention exercise to which it is compared, called Nordics. However, the workload comparison was established in more recent studies and were unknown at the time of the study set-up. Our study reported both a significant decrease in fiber orientation in the Biceps Femoris Long Head (BFLH) after an intervention program of 12 weeks of diver exercise, which indicates the adaptation of muscle architecture, and increases of fiber length following Nordic exercise in the semitendinosus. These changes were significant with compliance of 68% and 88% for the diver group and the Nordic group respectively.

The impact of exercise selection in intervention programs has been subject of research in previous MRI studies[35] using T2 acquisitions immediately after the exercise. In sports medicine, a T2 map may be useful to isolate the activated muscles after specific exercises, as T2 values increase.

The degree of muscle activation and strength were assessed, as these may be related to the degree of increase in T2 values. In the above-mentioned study, measurement of T2 changes revealed that the Nordic exercise activates mainly the Semitendinosus muscle rather than the semimembranosus and the Biceps Femoris Long Head muscles. On the other hand, the hip extension exercise induced minimal activation in the Biceps Femoris Short Head. Whereas, fMRI revealed a more intense activation of the Biceps Femoris Long Head during the 45 degrees hip extension exercise rather than during the Nordics. To summarize, these results showed that the activation of the Semitendinosus muscle is induced by the Nordic exercise and by the hip extension exercise (or diver), whereas the activation of the Biceps Femoris Short Head is induced by 45 degrees hip extension exercise.

In the long period, the muscle activation may correspond to a consequent change in muscle structure, whose entity depends on the workload included in the program and the compliance to it. Direct correlations between muscle activation during or immediately after exercise and subsequent changes in muscle architecture were not measured.

The expected impact of eccentric training on muscle architecture parameters is an increase of fiber length, muscle thickness and physiological cross-sectional area.[26,36,37] However, the impact of eccentric training on the pennation angle can vary in different muscles,[37,38] because different packing strategies of the fibers apply in different muscles. Previous ultrasound studies in the Biceps Femoris showed

decreased pennation angle[26,37] following eccentric exercise. In the Biceps Femoris muscle, we measured a decrease in pennation angle as measured between the line of force generation and the fibers. Direct comparison of the entity of the changes with previous studies is not possible because the training programs vary in duration and workload. Certain studies did not show a significant change in pennation angle after eccentric training,[36] specifically in the case of short muscle length hip flexion (0° hip flexion).

Future studies could focus on the understanding of the weight sharing mechanism and changes of different architecture parameters between muscles within the same muscle group during an exercise.

Return to play

In Chapter 5 of this thesis we focused on injury prevention, in the future it would be interesting to investigate whether the architectural parameters or changes therein can be linked to predict return to play (RTP) time after injury.

The complications which arise during the healing process are hamstring weakness and fatigue, imbalances in Hamstring eccentric and Quadriceps concentric strength, decreased quadriceps flexibility, reduced hip flexor flexibility, and strength and coordination deficits of the pelvic and trunk musculature. Little is known about the way in which all these factors interact, but future research may improve prevention and decrease risk for re-injury[40]. The RTP time after hamstring injury depends on the severity and extent of the injury. Injuries involving the proximal free tendon generally require longer recovery period than injuries involving the intramuscular tendon and the adjacent muscle fibers[40]. Previous studies showed that hamstring injuries occurring during sprinting activities took on average 23 days to return to sport at a level of performance before the injury with minimal risk of recurrence of the injury[40].

Previous musculoskeletal MRI studies investigated the RTP after muscle injury by applying various protocols. The most traditional protocol included T1 weighted sequences for assessing anatomy, blood products, and fatty muscle atrophy or the presence of a lipoma, as well as Short Tau Inversion-Recovery (STIR) or a proton density T2 weighted, which are fat suppressed fluid sensitive sequences, utilized for depicting muscle edema and hemorrhage. Acute intramuscular hematoma appears as isointense to muscles on T1 weighted sequence and hypo intense on T2 weighted imaging. A subacute hematoma with extracellular hemoglobin has progressively increasing T1 and T2 signal. Chronic hematomas appear low signal on T1 and T2 weighted sequences due to hemosiderin deposits.[39] Additionally, T2 mapping, proton MR spectroscopy, and fat-water separation techniques can be devised for evaluation of muscle injuries and are available on clinical scanners.[39]

In the context of muscle injury, the study of muscle architecture parameters would be of interest, in order to assess the recovery of muscle properties, like muscle strength, elasticity and contraction velocity.
Further research could be on the effect of muscle injury on pennation angle and fiber length, and the correlation of their possible consequential changes with physical tests during rehabilitation. In order to define the RTP time, it could be helpful to define thresholds of the expected percentual changes in muscle architecture parameters.
Mapping muscle architecture parameters at the hemorrhage or edema location is not possible with the DTI techniques that we have presented in these theses, due to the fact that in these circumstances fluids do not have a preferential direction corresponding to the direction of the fibers like it would be in healthy tissue, but they are spread in random directions.
Usually, the injury weakens large part of the muscle therefore DTI based measurement of fiber length and pennation angle immediately after the injury does not have to be necessarily localized at the level of the injury, for example a general approach can be used by including measurements in different anatomical locations along the muscle volume and could be repeated during the healing process.
DTI changes of mean diffusivity and fractional anisotropy can detect changes due to healing following muscle tear.[41] However, radiologist's visual evaluation would still constitute the best prediction for return to play after acute muscle injury.

Conclusions

This thesis presented different approaches for the evaluation of muscle architecture parameters in the leg muscles from Diffusion tensor MR images. Studies of validation and feasibility as well as comparisons with different imaging modalities to ascribe changes in skeletal muscle of healthy subjects were performed in this thesis, with the purpose of facilitating the applicability of the methods that we presented in clinical studies. More specifically, this thesis showed that DTI fiber tractography and fiber orientation maps are tools for robust estimations of muscle architecture outcomes and can be used as outcome measure in sport applications. In addition, physical intervention programs for the prevention of injuries may be optimized according to these quantitative MRI outcome measures. The use of muscle-specific volumetric measurements in multiple muscles may contribute to a better understanding of the intervention related changes in athletes.
In addition, the work presented in this thesis showed how the analysis of DTI data for the study of architecture parameters could be applied to large scale cohorts with semi-automatic segmentation

methods and volumetric fiber orientation maps. In the future, MRI muscle architecture outcomes, multi-parametric MRI such as DTI indices, fat fraction, fat infiltration and MRI technical progress such as accelerated or higher resolution DTI acquisitions should be combined in an effort to advance the understanding of injury prevention and RTP time and link the muscle architecture to muscle function and to the physiological and mechanical mechanisms of muscles groups.

References

1. Ogier AC, Heskamp L, Michel CP, et al. A novel segmentation framework dedicated to the follow-up of fat infiltration in individual muscles of patients with neuromuscular disorders. *Magn Reson Med*. 2020;83(5). doi:10.1002/mrm.28030
2. Ogier AC, Hostin MA, Bellemare ME, Bendahan D. Overview of MR Image Segmentation Strategies in Neuromuscular Disorders. *Front Neurol*. 2021;12. doi:10.3389/fneur.2021.625308
3. Karlsson A, Rosander J, Romu T, et al. Automatic and quantitative assessment of regional muscle volume by multi-atlas segmentation using whole-body water-fat MRI. *J Magn Reson Imaging*. 2015;41(6). doi:10.1002/jmri.24726
4. Rohm M, Markmann M, Forsting J, Rehmann R, Froeling M, Schlaffke L. 3d automated segmentation of lower leg muscles using machine learning on a heterogeneous dataset. *Diagnostics*. 2021;11(10). doi:10.3390/diagnostics11101747
5 Lieber RL, Fridén J. Functional and clinical significance of skeletal muscle architecture. Muscle Nerve. 2000 Nov;23(11):1647-66. doi: 10.1002/1097-4598(200011)23:11<1647::aid-mus1>3.0.co;2-m. PMID: 11054744
6. Müller M, Dohrn MF, Romanzetti S, et al. Semi-automated volumetry of MRI serves as a biomarker in neuromuscular patients. *Muscle and Nerve*. 2020;61(5). doi:10.1002/mus.26827
7. Bamman MM, Newcomer BR, Larson-Meyer DE, Weinsier RL, Hunter GR. Evaluation of the strength-size relationship in vivo using various muscle size indices. *Med Sci Sports Exerc*. 2000;32(7). doi:10.1097/00005768-200007000-00019
8. Chiaramonte R, Bonfiglio M, Castorina EG, Antoci SAM. The primacy of ultrasound in the assessment of muscle architecture: Precision, accuracy, reliability of ultrasonography. Physiatrist, radiologist, general internist, and family practitioner's experiences. *Rev Assoc Med Bras*. 2019;65(2). doi:10.1590/1806-9282.65.2.165
9. Noonan AM, Mazara N, Zwambag DP, Weersink E, Power GA, Brown SHM. Age-related changes in human single muscle fibre passive elastic properties are sarcomere length dependent. *Exp Gerontol*. 2020;137. doi:10.1016/j.exger.2020.110968
10. Tomalka A, Weidner S, Hahn D, Seiberl W, Siebert T. Power Amplification Increases With Contraction Velocity During Stretch-Shortening Cycles of Skinned Muscle Fibers. *Front Physiol*. 2021;12. doi:10.3389/fphys.2021.644981
11. Avrillon S, Lacourpaille L, Hug F, et al. Hamstring muscle elasticity differs in specialized high-performance athletes. *Scand J Med Sci Sport*. 2020;30(1). doi:10.1111/sms.13564
12. Arbeille P, Kerbeci P, Capri A, Dannaud C, Trappe SW, Trappe TA. Quantification of Muscle Volume by Echography: Comparison with MRI Data on Subjects in Long-Term Bed Rest. *Ultrasound Med Biol*. 2009;35(7). doi:10.1016/j.ultrasmedbio.2009.01.004
13. Borga M, West J, Bell JD, et al. Advanced body composition assessment: From body mass index to body composition profiling. *J Investig Med*. 2018;66(5). doi:10.1136/jim-2018-000722
14. Raj IS, Bird SR, Westfold BA, Shield AJ. Effects of eccentrically biased versus conventional weight training in older adults. *Med Sci Sports Exerc*. 2012;44(6). doi:10.1249/MSS.0b013e3182442ecd
15. Davison MJ, Maly MR, Keir PJ, et al. Lean muscle volume of the thigh has a stronger relationship with muscle power than muscle strength in women with knee osteoarthritis. *Clin Biomech*. 2017;41. doi:10.1016/j.clinbiomech.2016.11.005
16. Sanchis-Moysi J, Idoate F, Olmedillas H, et al. The upper extremity of the professional tennis player: muscle volumes, fiber-type distribution and muscle strength. *Scand J Med Sci Sport*. 2010;20(3). doi:10.1111/j.1600-0838.2009.00969.x

17. Bolsterlee B, D'Souza A, Gandevia SC, Herbert RD. How does passive lengthening change the architecture of the human medial gastrocnemius muscle? *J Appl Physiol*. 2017;122(4). doi:10.1152/japplphysiol.00976.2016
18. Franchi M V., Raiteri BJ, Longo S, Sinha S, Narici M V., Csapo R. Muscle Architecture Assessment: Strengths, Shortcomings and New Frontiers of in Vivo Imaging Techniques. *Ultrasound Med Biol*. 2018;44(12). doi:10.1016/j.ultrasmedbio.2018.07.010
19. Galbusera, F., Cina, A., Panico, M. *et al.* Image-based biomechanical models of the musculoskeletal system. *Eur Radiol Exp* **4**, 49 (2020). https://doi.org/10.1186/s41747-020-001723
20. Lavaill M, Martelli S, Gilliland L, Gupta A, Kerr G, Pivonka P. The effects of anatomical errors on shoulder kinematics computed using multi-body models. Biomech Model Mechanobiol. 2022 Oct;21(5):1561-1572. doi: 10.1007/s10237-022-01606-0. Epub 2022 Jul 22. PMID: 35867281; PMCID: PMC9626434.
21. Charles JP, Suntaxi F, Anderst WJ. In vivo human lower limb muscle architecture dataset obtained using diffusion tensor imaging. PLoS One. 2019 Oct 15;14(10):e0223531. doi: 10.1371/journal.pone.0223531. PMID: 31613899; PMCID: PMC6793854.
22. Bourne MN, Timmins RG, Opar DA, et al. An Evidence-Based Framework for Strengthening Exercises to Prevent Hamstring Injury. *Sport Med*. 2018;48(2). doi:10.1007/s40279-017-0796-x
23. Schache AG, Dorn TW, Blanch PD, Brown NAT, Pandy MG. Mechanics of the human hamstring muscles during sprinting. *Med Sci Sports Exerc*. 2012;44(4). doi:10.1249/MSS.0b013e318236a3d2
24. Emirzeoğlu M, Fırat T, Ülger Ö. The effects of eccentric training on hamstring muscle architecture: A systematic review. *Language (Baltim)*. 2021;97(2). doi:10.26582/K.53.1.17
25. Schache A. Eccentric hamstring muscle training can prevent hamstring injuries in soccer players. *J Physiother*. 2012;58(1). doi:10.1016/S1836-9553(12)70074-7
26. Gérard R, Gojon L, Decleve P, Van Cant J. The effects of eccentric training on biceps femoris architecture and strength: A systematic review with meta-analysis. *J Athl Train*. 2020;55(5). doi:10.4085/1062-6050-194-19
27. Cronin K, Foley S, Cournane S, De Vito G, Delahunt E. Hamstring muscle architecture assessed sonographically using wide field of view: A reliability study. Loenneke JP, ed. *PLoS One*. 2022;17(11):e0277400. doi:10.1371/journal.pone.0277400
28. Damon BM, Buck AKW, Ding Z. Diffusion-tensor MRI-based skeletal muscle fiber tracking. *Imaging Med*. 2011;3(6):675-687. doi:10.2217/iim.11.60
29. Weide G, Van Der Zwaard S, Huijing PA, Jaspers RT, Harlaar J. 3D ultrasound imaging: Fast and cost-effective morphometry of musculoskeletal tissue. *J Vis Exp*. 2017;2017(129). doi:10.3791/55943
30. Veeger TTJ, van Zwet EW, al Mohamad D, et al. Muscle architecture is associated with muscle fat replacement in Duchenne and Becker muscular dystrophies. *Muscle and Nerve*. 2021;64(5). doi:10.1002/mus.27399
31. Heemskerk AM, Sinha TK, Wilson KJ, Ding Z, Damon BM. Quantitative assessment of DTI-based muscle fiber tracking and optimal tracking parameters. *Magn Reson Med*. 2009;61(2). doi:10.1002/mrm.21819
32. Forsting J, Rehmann R, Froeling M, Vorgerd M, Tegenthoff M, Schlaffke L. Diffusion tensor imaging of the human thigh: consideration of DTI-based fiber tracking stop criteria. *Magn Reson Mater Physics, Biol Med*. 2020;33(3). doi:10.1007/s10334-019-00791-x
33. Damon BM, Ding Z, Hooijmans MT, et al. A MATLAB toolbox for muscle diffusion-tensor MRI tractography. *J Biomech*. 2021;124. doi:10.1016/j.jbiomech.2021.110540
34. Froeling M. QMRTools: a Mathematica toolbox for quantitative MRI analysis. *J Open Source Softw*. 2019;4(38). doi:10.21105/joss.01204
35. Bourne MN, Williams MD, Opar DA, Al Najjar A, Kerr GK, Shield AJ. Impact of exercise selection on hamstring muscle activation. *Br J Sports Med*. 2017;51(13). doi:10.1136/bjsports-2015-095739

36. Askling CM, Tengvar M, Saartok T, Thorstensson A. Acute first-time hamstring strains during high-speed running: A longitudinal study including clinical and magnetic resonance imaging findings. *Am J Sports Med*. 2007;35(2). doi:10.1177/0363546506294679
37. Guex K, Degache F, Morisod C, Sailly M, Millet GP. Hamstring architectural and functional adaptations following long vs. short muscle length eccentric training. *Front Physiol*. 2016;7(AUG):1-9. doi:10.3389/fphys.2016.00340
38. Marušič J, Vatovec R, Marković G, Šarabon N. Effects of eccentric training at long-muscle length on architectural and functional characteristics of the hamstrings. *Scand J Med Sci Sport*. 2020;30(11). doi:10.1111/sms.13770
39. Kim SY, Ko JB, Farthing JP, Butcher SJ. Investigation of supraspinatus muscle architecture following concentric and eccentric training. *J Sci Med Sport*. 2015;18(4). doi:10.1016/j.jsams.2014.05.007
40. Erickson LN, Sherry MA. Rehabilitation and return to sport after hamstring strain injury. *J Sport Heal Sci*. 2017;6(3). doi:10.1016/j.jshs.2017.04.001
41. Kumaravel M, Bawa P, Murai N. Magnetic resonance imaging of muscle injury in elite American football players: Predictors for return to play and performance. *Eur J Radiol*. 2018;108. doi:10.1016/j.ejrad.2018.09.028

CHAPTER 7

Summary

Summary

The objective of this thesis was to develop various approaches for measuring muscle architectural parameters using Diffusion Tensor MR Images (DTI) in order to examine changes in muscle architecture after an injury prevention program.

Due to the time-consuming nature of manual segmentation, we initially evaluated semi-automatic segmentation methods to analyze studies involving large cohorts within a shorter timeframe. In Chapter 2, our focus was on validating a semi-automatic segmentation framework for estimating DTI indices in the upper leg muscles. We demonstrated that this method allowed for three times faster segmentation of the upper leg muscles compared to manual segmentation in cross-sectional analysis. Moreover, the process of longitudinal segmentation can be mostly automated, with only minimal manual adjustments necessary. This is not a concern, as clinical settings typically prioritize visual quality control. The accuracy of DTI indices estimations resulting from the semi-automated segmentations was generally very good across all DTI indices and most of the upper leg muscles, except for the Sartorius muscle.

In Chapter 3, we presented a feasibility study on a volumetric DTI-based approach to measure changes in fiber orientation in calf muscles and sub-compartments of the Soleus and Tibialis Anterior muscles during plantarflexion and dorsiflexion. We observed that the average fiber orientations relative to the line between the knee and ankle changed according to the expected agonist and antagonist functions of the Soleus and Tibialis Anterior muscles, as well as the sub-compartments of the Soleus muscle, in different ankle positions. Specifically, the fiber orientation changes in the Soleus muscle and Tibialis Anterior were in opposite directions, reflecting the biomechanical behavior of these complementary muscles. In the plantarflexion phase, the Soleus muscle undergoes contraction and shortens, whereas the Tibialis Anterior muscle elongates. Conversely, in dorsiflexion, the Soleus muscle lengthens, while the Tibialis Anterior muscle shortens.

In comparison to 3D ultrasonography, DTI fiber tractography was explored as a method to visualize muscle fibers and measure muscle properties, such as pennation angle and fiber length, at specific locations. In Chapter 4, we compared DTI-based fiber tractography measurements of the pennation angle with measurements obtained from 3D ultrasound (3D-US) in the Vastus Lateralis muscle. We evaluated pennation angles and fiber length estimations between the two methods at the same location within the muscle.

The underlying mechanisms of preventive physical interventions for hamstring injuries are still not fully understood. In Chapter 5, we employed DTI as a quantitative method to analyze the effects of different exercise intervention programs aimed at preventing hamstring injuries in basketball players. The techniques presented in this thesis were employed to estimate the lengths and orientations of

muscle fibers, which were further utilized to quantify alterations resulting from exercise. We observed an increase in fascicle length of the semitendinosus muscle following Nordics exercise and a decrease in muscle fascicle orientation in the biceps femoris long head following the so-called divers intervention.

Samenvatting

Het doel van deze scriptie was het ontwikkelen van verschillende methoden om spierarchitectonische parameters te meten met behulp van *Diffusion Tensor MR Imaging* (DTI), die kunnen worden toegepast om veranderingen in spierarchitectuur na een blessurepreventieprogramma te bestuderen. Handmatige segmentatie is tijdrovend, daarom werden in eerste instantie semiautomatische segmentatiemethoden geëvalueerd om onderzoeken met grote groepen deelnemers in kortere tijd te kunnen analyseren. In Hoofdstuk 2 lag de focus op de validatie van een semiautomatische segmentatiemethode voor de schatting van DTI-parameters in de spieren van het bovenbeen. We hebben aangetoond dat deze methode drie keer sneller was in het segmenteren van de spieren van het bovenbeen dan handmatig segmenteren, en dat de segmentatie bij herhaalde metingen vrijwel volledig automatisch kon worden uitgevoerd. Enkele handmatige aanpassingen waren nodig, maar dat is geen probleem, aangezien visuele kwaliteitscontrole doorgaans toch moet worden uitgevoerd in de klinische praktijk. De nauwkeurigheid van de schattingen van de DTI-parameters die voortkwamen uit de semi-geautomatiseerde segmentaties was zeer goed voor alle DTI-parameters en in de meeste spieren van het bovenbeen, met uitzondering van de Sartorius-spier.
In Hoofdstuk 3 presenteerden we een haalbaarheidsstudie naar een volumetrische DTI-gebaseerde benadering voor het meten van veranderingen in vezeloriëntatie in kuitspieren en subcompartimenten van de Soleus en Tibialis Anterior spieren tijdens plantairflexie en dorsiflexie. We toonden aan dat de gemiddelde vezeloriëntaties ten opzichte van de lijn tussen de knie en enkel veranderden in overeenstemming met de verwachte agonistische en antagonistische functies van de Soleus en Tibialis Anterior spieren, evenals de subcompartimenten van de Soleus spier, in verschillende enkelposities. Specifiek waren de veranderingen in vezeloriëntatie in de Soleus-spier en Tibialis Anterior in tegengestelde richtingen, wat het biomechanisch gedrag van deze complementaire spieren weerspiegelt. De Soleus-spier verkort tijdens plantairflexie en verlengt tijdens dorsiflexie, terwijl de Tibialis Anterior verlengt tijdens plantairflexie en verkort tijdens dorsiflexie. De vezelhoek neemt toe tijdens spierverkorting en neemt af tijdens spierverlenging.

In Hoofdstuk 4 hebben we DTI-gebaseerde metingen van de pennatiehoek in de spier Vastus Lateralis vergeleken met metingen verkregen uit 3D-echografie (3D-US). We hebben pennatiehoeken en schattingen van de vezellengte tussen de twee methoden geëvalueerd op dezelfde locatie binnen de spier.
Het volledige begrip van de onderliggende mechanismen van preventieve fysieke interventies voor hamstringblessures ontbreekt momenteel nog. In Hoofdstuk 5 hebben we DTI als een kwantitatieve methode gebruikt om de effecten van verschillende trainingsprogramma's voor blessurepreventie van de hamstrings bij basketbalspelers te analyseren. DTI-gebaseerde vezeltractografie werd gebruikt om de vezellengte te schatten, en de in dit proefschrift geïntroduceerde vezeloriëntatiekaarten werden gebruikt om door oefeningen veroorzaakte veranderingen in vezeloriëntatie te beoordelen. We hebben een toename in vezellengte van de Semitendinosus-spier waargenomen na de Nordic-oefening en een afname in spiervezelhoek in de lange kop van de Biceps Femoris na de zogenaamde duikersinterventie.

Riassunto

L'obiettivo di questa tesi è stato sviluppare diversi approcci per misurare i parametri architettonici del muscolo utilizzando le immagini di risonanza magnetica a tensore di diffusione (DTI) al fine di esaminare i cambiamenti nell'architettura muscolare dopo un programma di prevenzione degli infortuni. Poiché la segmentazione manuale è un processo molto laborioso, abbiamo valutato inizialmente metodi di segmentazione semi-automatica per analizzare in un periodo di tempo più breve studi che coinvolgono grandi gruppi. Nel Capitolo 2, il nostro focus è stato sulla validazione di un framework di segmentazione semi-automatica per stimare gli indici DTI nei muscoli della coscia. Abbiamo dimostrato che questo metodo ha permesso una segmentazione tre volte più rapida dei muscoli della coscia rispetto alla segmentazione manuale nell'analisi trasversale. Inoltre, il processo di segmentazione longitudinale può essere in gran parte automatizzato, con solo minimi aggiustamenti manuali necessari. Questo non è un problema, poiché nei contesti clinici di solito viene data priorità al controllo visivo della qualità. L'accuratezza delle stime degli indici DTI ottenute dalle segmentazioni semi-automatiche è stata generalmente molto buona per tutti gli indici DTI e per la maggior parte dei muscoli della coscia, ad eccezione del muscolo Sartorio. Nel Capitolo 3, abbiamo presentato uno studio di fattibilità su un approccio volumetrico basato su DTI per misurare i cambiamenti nell'orientamento delle fibre nei muscoli del polpaccio e nei sotto-comparti dei muscoli Soleo e Tibiale Anteriore durante la flessione plantare e la dorsiflessione. Abbiamo osservato che le orientazioni medie delle fibre relative alla linea tra il ginocchio e la caviglia cambiano secondo le funzioni agonista

e antagonista attese dei muscoli Soleo e Tibiale Anteriore, così come dei sotto-comparti del muscolo Soleo, nelle diverse posizioni della caviglia. In particolare, i cambiamenti nell'orientamento delle fibre nel muscolo Soleo e nel Tibiale Anteriore sono in direzioni opposte, riflettendo il comportamento biomeccanico di questi muscoli complementari. Nella fase di flessione plantare, il muscolo Soleo si contrae e si accorcia, mentre il muscolo Tibiale Anteriore si allunga. Al contrario, nella dorsiflessione, il muscolo Soleo si allunga, mentre il muscolo Tibiale Anteriore si accorcia. In confronto all'ecografia 3D, la fiber tractography basata su DTI è stata esplorata come un metodo per visualizzare le fibre muscolari e misurare le proprietà muscolari, come l'angolo di pennazione e la lunghezza delle fibre, in posizioni specifiche. Nel Capitolo 4, abbiamo confrontato le misurazioni dell'angolo di pennazione ottenute tramite la fiber tractography basata su DTI con le misurazioni ottenute dall'ecografia 3D nel muscolo Vasto Laterale. Abbiamo valutato gli angoli di pennazione e le stime della lunghezza.
I meccanismi sottostanti alle misure preventive di interventi fisici per gli infortuni agli ischiocrurali non sono ancora pienamente compresi. Nel Capitolo 5, abbiamo impiegato la DTI come metodo quantitativo per analizzare gli effetti di diversi programmi di intervento mediante esercizi volti a prevenire gli infortuni agli ischiocrurali nei giocatori di pallacanestro. Le tecniche presentate in questa tesi sono state utilizzate per stimare le lunghezze e le orientazioni delle fibre muscolari, che sono state ulteriormente utilizzate per quantificare le alterazioni derivanti dall'esercizio. Abbiamo osservato un aumento della lunghezza del fascio del muscolo semitendinoso a seguito dell'esercizio di Nordics e una diminuzione dell'orientamento del fascio muscolare nella testa lunga del muscolo bicipite femorale a seguito dell'intervento chiamato divers.

List of Publications

Journal Publications

1. Secondulfo L, Hooijmans MT, Suskens JJ, Mazzoli V, Maas M, Tol JL, Nederveen AJ, Strijkers GJ. A diffusion tensor-based method facilitating volumetric assessment of fiber orientations in skeletal muscle. PLoS One. 2022 Jan 27;17(1):e0261777. doi: 10.1371/journal.pone.0261777. PMID: 35085267; PMCID: PMC8794095.

2. Secondulfo L, Ogier AC, Monte JR, Aengevaeren VL, Bendahan D, Nederveen AJ, Strijkers GJ, Hooijmans MT. Supervised segmentation framework for evaluation of diffusion tensor imaging indices in skeletal muscle. NMR Biomed. 2021 Jan;34(1):e4406. doi: 10.1002/nbm.4406. Epub 2020 Oct 1. PMID: 33001508; PMCID: PMC7757256.

3. Suskens JJM, Secondulfo L, Kiliç Ö, Hooijmans MT, Reurink G, Froeling M, Nederveen AJ, Strijkers GJ, Tol JL. Effect of two eccentric hamstring exercises on muscle architectural characteristics assessed with diffusion tensor MRI. Scand J Med Sci Sports. 2023 Apr;33(4):393-406. doi: 10.1111/sms.14283. Epub 2022 Dec 23. PMID: 36514886.

Portfolio

Name PhD student: Laura Secondulfo
PhD period: December 2017- March 2022
Department: Department of Biomedical Engineering and Physics, Amsterdam UMC, location AMC
Promotors: prof. dr. Gustav J. Strijkers, prof. dr. Aart J. Nederveen
Copromotor: dr. Melissa T. Hooijmans

PhD Training

Courses

Oral presentation in English (2018), 0.8 ECTS
Project management (2018), 0.8 ECTS
In-vivo NMR (2019), 1.4 ECTS
Data analysis in MATLAB (2018), 1.0 ECTS
Research Data Management (2018), 1.0 ECTS
3T MRI scan qualification- Safety Training (2018), 0.5 ECTS
Mathematica Principles of Wolfram Research (2019), 0.8 ECTS

Seminars and workshops

Weekly MRI Physics Seminars (2017-2022), 4 ECTS
Organizing committee weekly MRI Physics Seminars (2018-2020), 4 ECTS
PhD days (2018, 0.6 ECTS)
Monthly Muscle research Seminars (2018-2021), 3 ECTS

Attended conferences and symposia.

Amsterdam Movement Sciences (AMS) Annual research meeting (2018-2020), 1.8 ECTS
MYO-MRI (2019-2021), 2.4 ECTS
European Society for Magnetic Resonance in Medicine and Biology
(ESMRMB) (2019-2022), 2.4 ECTS
International Society for Magnetic Resonance in Medicine (ISMRM) (2018,2020-2022), 4 ECTS
ISMRM Benelux (2018-2021), 6 ECTS

Conference proceedings

Oral presentation

A comparison of muscle pennation angles measured with DTI fiber tractography and 3D-ultrasound

- Joint ISMRM-ESMRMB 2022 in London, UK (Virtual Environment), 1.5 ECTS
- ISMRM Benelux 2022 in Maastricht, The Netherlands, 1.5 ECTS

A method for quantification of changes in leg muscle fiber orientations

- ISMRM Benelux 2020 in Arnhem, The Netherlands, 1.5 ECTS

A novel DTI method for quantification of skeletal muscle pennation angles

- ESMRMB 2019 in Rotterdam, The Netherlands, 1.5 ECTS

Poster presentation

A comparison of muscle pennation angles measured with DTI fiber tractography and 3D-ultrasound

- Joint ISMRM-ESMRMB 2022 in London, UK (Virtual Environment), 0.5 ECTS

Comparison of the pennation angle measurement between 3DUS and fibertractography.

- MYO-MRI 2021, Virtual meeting, 0.5 ECTS

A method for quantification of changes in leg muscle fiber orientations

- ISMRM 2020 in Sydney, Australia (Virtual meeting), 0.5 ECTS

A novel DTI method for quantification of skeletal muscle pennation angles

- MYO-MRI 2019 in Berlin, Germany, 0.5 ECTS

Recognitions

EDITOR'S PICK- Secondulfo L, Ogier AC, Monte JR, Aengevaeren VL, Bendahan D, Nederveen AJ, Strijkers GJ, Hooijmans MT. Supervised segmentation framework for evaluation of diffusion tensor imaging indices in skeletal muscle. NMR Biomed. 2021 Jan;34(1)
AMS Outstanding Paper Award- Suskens JJM, Secondulfo L, Kiliç Ö, Hooijmans MT, Reurink G, Froeling M, Nederveen AJ, Strijkers GJ, Tol JL. Effect of two eccentric hamstring exercises on muscle architectural characteristics assessed with diffusion tensor MRI. Scand J Med Sci Sports. 2023 Apr;33(4)
ISMRM Educational stipend (2020)

Teaching

Supervising

Bachelor student – Biomedical Engineering, Polytech Marseille (2021), 2 ECTS
Master student – Medical Imaging & Interventions, Technical Medicine, University of Twente (2020), 1 ECTS
Master student – Medicine, Vrije Universiteit (2019), 1 ECTS

International journal reviewing

Scientific Reports (2023)
BMC Medical Imaging (2023)

Acknowledgements

First of all, I would like to thank all the people attending my defense. I have prepared a few words of thanks.

Eight years ago, I relocated to the Netherlands to pursue my master's degree. After a master, 3 jobs, now it appears that I am on the verge of obtaining a PhD in Amsterdam, my home. Without a doubt, I wouldn't have reached this point without the assistance and encouragement of numerous individuals.

Therefore, I would like to take this opportunity to express my heartfelt gratitude to all of you who have played a pivotal role in making this achievement possible.

I want to extend my appreciation to all my colleagues at the Amsterdam UMC, a group of remarkable, intelligent, and passionate individuals. Thank you for creating a supportive environment for PhD students. I consider myself extremely fortunate to have had the opportunity to pursue my PhD in the Biomedical Engineering and Physics Department, the Radiology department and the Orthopedics department.

A special thanks to my promotors, Gustav and Aart, and co-promotor, Melissa as well as to the MSK team.

Gustav, I appreciate everything you have done for me. Thank you for welcoming me to the Biomedical Engineering and Physics Department during my master's thesis and for entrusting me with a PhD position thereafter. Your willingness to engage in chats and scientific discussions, and your constant presence and support are truly appreciated. Your positive attitude, exceptional problem-solving skills, and effectiveness have been truly invaluable.

Aart, I am grateful for the time I spent in your Z0 group at the AMC in Amsterdam and I am thankfull for the opportunity to have had you as my promotor. Thank you for welcoming me to the Radiology Department and for entrusting me with a PhD position. Your willingness to engage in scientific discussions and your support for the department are highly valued. Your social elegance has been an example for me.

Melissa, your passion for your work, boundless enthusiasm for research and self-discipline have been truly inspiring. I want to express my sincere gratitude for introducing me to the captivating world of musculoskeletal MRI. Thank you for your valuable input, critical review of my manuscripts, and your ideas to highlight the clinical aspects.

Hans, having you involved in my research from the very start has been great. I have highly valued your ideas and suggestions.
Mario, I am grateful for the opportunity to work with you. Your expertise and leadership have been truly inspiring. Gustaaf, thank you for utilizing your expertise in sports medicine to benefit our team.

I would like to thank NWO and the user committee members of the DIMASK project for their input and fruitful discussions during the half-yearly progress meetings. Specifically: Wieke Haakma (NWO), Kamiel Maase (NOC*NSF), Maarten Moen (NOC*NSF), Ruud de Boer (Philips Healthcare), Josien van den Noort (Amsterdam UMC, MIQC), Chiel den Harder (Amsterdam UMC, MIQC).

David, it has been an honor to collaborate with someone of your caliber abroad. Rob, thank you for your creativity and proactivity in science and ability to connect different subjects.

I would like to extend my gratitude to Gustaaf, Martijn, Melissa and Valentina, whose PhD theses have served as invaluable references for me throughout these years.
Valentina and Martijn, thank you for the encouraging and knowledgeable exchanges. Cristina, thanks for your presence at the AMC and your consistent dedication to research.

Joep, thank you for the hard work and enthusiasm in our joint project. Jithsa, thank you for sharing with me our scienKfic journey to Marseille. Özgür, thank you for our collaboration in our joint project. Moritz, thank you for the dedication and perseverance in our joint project. Augustine, thank you for our collaboration in our joint international project.

A special thanks to Carla, Sandra, Raschel, Paul and Richard who made sure all administrative and technical issues would always be solved quickly, and who provided invaluable support.

To my roommates Mariah, Hugo and Susi, thank you so much. I thoroughly enjoyed all the years spent with you in the room. Mariah, thanks for being by my side the entire time. It means a lot to me to have you as a paranymph. Good luck with the very last bits of your PhD thesis, with all the great adventures in Wageningen and your future life. Hugo, thank you for your pearls of wisdom. Good luck with your future! Susi, you are so determined and ambitious. It was a fortunate choice to dedicate yourself full time to physics. We had nice research exchanges, bbq and sailing experiences together. Shine on in Leiden!

Thanks to the past Z0 group for: Carmen, Bobby, Koen, Sophie, Marieke, Tony, Jasper, Lukas, Eva, Kerry and the senior scientists.
Thanks to the past L0 group for the daily good Kmes: Praneeta, Henk, Nerea, Riaan, Lucas, Ricardo, Marcela, Marit, Daphne, Sissy, Giuliana, Roosje Ruis, Xavier, Inge, Laura, Louis, Meagan, Marteen, Daisy.

A special thanks to my friends in Amsterdam, in Italy, in Sweden and around the world that always supported me during the past years:

Alessia, Floriana, Maria, Vicktorija, Francesco, Giorgia, Serena, Luis e *gli amici romagnoli*, Stefano, Manuel, Lorenzo, Andrea, Gül, Defne, Eléna, Elif, Parants, Elena, Chiara, Cameron, Jordache, Niels, Naaz, Kasia, Wenwen, Célia, Guenola, Olya, Nicola, Leonardo and the friends at Easy laughs, Nev, Rabie, Jennifer, Paulo, Pedro, Basilio, Viviana, Marco *e gli amici di Eindhoven*, Diego, Frabrizio, Sylwia, Suzan and Mathijs, and the #goteamamra, especially the Clinical and the Imaging Science teams. In Latina: Martina, Fiorenza, Roberta, Luca, Stefano, Valeria, Martina, Ilaria *e le amiche dell'Anfiteatro Academy ASD*, Susanna, Luciana, Gabriele, Daniele, Marco, Elisa, Alessia, Serena e *tutti gli amici del Sunrisebay.*

Thank you, Carmina, for being a paranymph at my PhD defense. Our friendship since the traineeship in Eindhoven has been a blessing for me. I am glad you found your new dimension even though we live far apart now.

"*Specialmente, grazie al dottor Ermanno Notarianni, la dottoressa Maria Paola Gallinari, la dottoressa Margarita Petrova, Pubmed, la dottoressa Maddalena Ionata, Tiziana che che sono stati essenziali per il mio benessere*. *Infine, vorrei ringraziare la mia super estesa famiglia per supportarmi lungo questo percorso, il Circeo e la mia terra Pontina per la forza. In particolare, grazie ai miei genitori, i maggiori investitori, per il lavoro che svolgono dal primo giorno, per sopportarmi e supportarmi. A nonno Sandro, zia Rita, nonna Laura, nonna Tilde e zia Marialisa che ci hanno lasciati ma sono sempre presenti nei miei gesti."*

About the author

Laura Secondulfo was born on December 28th, 1990, in Latina, Italy. In 2009 she obtained her high school diploma at Liceo Scientifico G.B. Grassi, Latina. Between 2006 and 2009 she received three scholarships.
In 2013, she earned a Biomedical Engineering degree from the 'Guglielmo Marconi' Department of Electrical Energy and Information Engineering (DEI) at the University of Bologna's Cesena campus, Italy. Between 2009 and 2013 she received two scholarships.
The next year, she relocated to Amsterdam, Netherlands, for a combined MSc program in Medical Natural Sciences and Physics of Life and Health, with a focus on Physics, offered jointly by Vrije University and the University of Amsterdam.
During her Master's studies, she completed a minor project at Philips in Eindhoven, focusing on enhancing energy expenditure estimation algorithms using heart rate and motion data within the Health and Wellness division. This project was supervised by Dr. Alberto Bonomi, Dr. Francesco Sartor, and Dr. Gabriele Papini. This internship was supported by Philips' scholarship.
Additionally, she undertook a major project for her Master's at the Academic Medical Center of Amsterdam (AMC), in the Biomedical Engineering and Physics department. Under the guidance of Prof. Gustav J. Strijkers, Dr. Bram Coolen, and Dr. Jasper Schoormans, her project investigated the potential improvement of image quality for low-SNR 3D brain MRI acquisitions using compressed sensing with 3D Cartesian k-space undersampling, with which she received her Master degree in 2016.
Following her master's program, she gained brief experience working as a validation engineer at Vicentra, in Utrecht, before pausing her career in industry to begin a Ph.D.
In late 2017, she initiated a Ph.D. project led by Prof. Dr. Ir. Gustav J. Strijkers (Biomedical Engineering and Physics department, Amsterdam UMC, Location AMC), Prof. Dr. Ir. Aart J. Nederveen (Department of Radiology, Amsterdam UMC, Location AMC), and Dr. Melissa T. Hooijmans (Amsterdam University Medical Center, Amsterdam, The Netherlands). This thesis presents the outcomes of Laura's Ph.D. research. The project was financed by the Dutch Research Council (NWO).
From March 2022 to July 2023, Laura worked with the Clinical Science team at Amra Medical in Linköping, Sweden on the application of MRI-based body composition biomarkers in clinical trials.